

# Hypervelocity Impact Testing of Aluminum Foam Core Sandwich Panels

*Dr. Shannon Ryan*  
*USRA Lunar and Planetary Institute*  
*Johnson Space Center, Houston*

*Eric L. Christiansen*  
*Johnson Space Center, Houston*

National Aeronautics and  
Space Administration

Johnson Space Center  
Houston, TX 77058

---

November 2015

## THE NASA STI PROGRAM OFFICE . . . IN PROFILE

Since its founding, NASA has been dedicated to the advancement of aeronautics and space science. The NASA Scientific and Technical Information (STI) Program Office plays a key part in helping NASA maintain this important role.

The NASA STI Program Office is operated by Langley Research Center, the lead center for NASA's scientific and technical information. The NASA STI Program Office provides access to the NASA STI Database, the largest collection of aeronautical and space science STI in the world. The Program Office is also NASA's institutional mechanism for disseminating the results of its research and development activities. These results are published by NASA in the NASA STI Report Series, which includes the following report types:

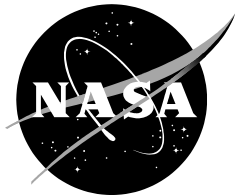
- **TECHNICAL PUBLICATION.** Reports of completed research or a major significant phase of research that present the results of NASA programs and include extensive data or theoretical analysis. Includes compilations of significant scientific and technical data and information deemed to be of continuing reference value. NASA's counterpart of peer-reviewed formal professional papers but has less stringent limitations on manuscript length and extent of graphic presentations.
- **TECHNICAL MEMORANDUM.** Scientific and technical findings that are preliminary or of specialized interest, eg, quick release reports, working papers, and bibliographies that contain minimal annotation. Does not contain extensive analysis.
- **CONTRACTOR REPORT.** Scientific and technical findings by NASA-sponsored contractors and grantees.

- **CONFERENCE PUBLICATION.** Collected papers from scientific and technical conferences, symposia, seminars, or other meetings sponsored or cosponsored by NASA.
- **SPECIAL PUBLICATION.** Scientific, technical, or historical information from NASA programs, projects, and mission, often concerned with subjects having substantial public interest.
- **TECHNICAL TRANSLATION.** English-language translations of foreign scientific and technical material pertinent to NASA's mission.

Specialized services that complement the STI Program Office's diverse offerings include creating custom thesauri, building customized databases, organizing and publishing research results . . . even providing videos.

For more information about the NASA STI Program Office, see the following:

- Access the NASA STI Program Home Page at <http://www.sti.nasa.gov>
- E-mail your question via the Internet to [help@sti.nasa.gov](mailto:help@sti.nasa.gov)
- Fax your question to the NASA Access Help Desk at (301) 621-0134
- Telephone the NASA Access Help Desk at (301) 621-0390
- Write to:  
NASA Access Help Desk  
NASA Center for AeroSpace  
Information  
7115 Standard  
Hanover, MD 21076-1320



# Hypervelocity Impact Testing of Aluminum Foam Core Sandwich Panels

*Dr. Shannon Ryan*  
*USRA Lunar and Planetary Institute*  
*Johnson Space Center, Houston*

*Eric L. Christiansen*  
*Johnson Space Center, Houston*

National Aeronautics and  
Space Administration

Johnson Space Center  
Houston, TX 77058

---

November 2015

## **Acknowledgments**

Impact testing was performed at the NASA Johnson Space Center (JSC) White Sands Test Facility in Las Cruces, N.M. as directed by the authors of the JSC Hypervelocity Impact Technology Facility.

Available from:

NASA Center for AeroSpace Information  
7115 Standard Drive  
Hanover, MD 21076-1320

National Technical Information Service  
5301 Shawnee Road  
Alexandria, VA 22312

Available in electric form at <http://ston.jsc.nasa.gov/collections/TRS>

## Contents

<b>Introduction.....</b>	<b>1</b>
<b>Background .....</b>	<b>2</b>
Existing Research .....	3
Aluminum Open-Cell Foam .....	12
<b>Test Articles and Target Setup .....</b>	<b>13</b>
Phase 1 Articles and Setup .....	13
1.0" Al F10 (ERG) .....	13
1.0" Al F20 (ERG) .....	14
1.0" Al F20 (NASA) .....	15
1.0" Al F40 (ERG) .....	15
1.0" Al F40 (NASA) .....	16
1.0" Al F40 (3%-5%) .....	17
Summary of Phase 1 targets .....	17
Phase 2 Articles and Setup .....	18
0.5" Al F40 .....	18
2.0" Al F40 .....	19
Phase 3 Articles and Setup .....	19
1.0" Al F40 B1W2.....	19
1.0" Al F40 B2W2.....	20
1.0" Al F40 B3W2.....	20
1.0" Al F40 B3W3.....	21
Summary of Phase 3 targets .....	22
Phase 4 Articles and Setup .....	22
2.0" Al HC .....	22
1.0" Trussgrid®.....	23
2.0" PN2 HC.....	24
2.0" Al F-var.....	25
2.0" Al F-var (Kevlar/epoxy composite (K/E)).....	26
2.0" Al F-var (Nextel/epoxy compsite (N/E)) .....	28
Summary of Phase 4 targets .....	29
<b>Test Facility .....</b>	<b>29</b>
<b>Test Results.....</b>	<b>29</b>
Assessment of Experimental Scatter .....	31

Phase 1 Test Results .....	32
Effect of facesheet temper and adhesive type.....	32
Effect of Pore Density (PPI).....	37
Effect of Relative Density .....	44
Summary	48
Phase 2 Test Results .....	48
Phase 3 Test Results .....	50
Phase 4 Test Results .....	51
<b>A Ballistic Limit Equation for Foam Core Sandwich Panels.....</b>	<b>64</b>
Comparison with Other Shield Types .....	72
<b>Concluding Remarks .....</b>	<b>74</b>
<b>References.....</b>	<b>76</b>
<b>Appendix A .....</b>	<b>77</b>

## Figures

Figure 1: Whipple shield concept .....	1
Figure 2: Predicted performance of a dual-wall shield at hypervelocity with and without a honeycomb core. ....	2
Figure 3: Open-cell (left) and closed-cell (right) metallic foam. ....	3
Figure 4: Alternate Columbus MMOD shield configuration incorporating metallic open-cell foam [8]. ....	4
Figure 5: AB2Mod rear wall following impact of 15.0 mm diameter Al2017-T4 spheres at no. 6.4 km/s with normal incidence. Left: m-pore foam bumper; right: Duocel foam bumper [9]. ....	4
Figure 6: m-pore (left) and Duocel (right) appearance microscopic appearance [9]. ....	5
Figure 7: Comparison of damages in an open-cell foam core (left) and honeycomb core (right) sandwich panel structures impacted by a 3.6 mm Al-sphere at $6.49 \pm 0.27$ km/s ( $0^\circ$ ). Upper: front facesheet damage; Middle: core damage (sectioned); Bottom: rear facesheet damage.....	6
Figure 8: Schematic of the double layer honeycomb (left) and modified double layer foam (right) shields. ....	7
Figure 9. Ballistic limit curves for the double-layer honeycomb (DL-H) and foam (DL-F) shields. ....	7
Figure 10: Top left to bottom right: 40 PPI Al foam, 100 PPI Cu foam, 100 PPI Ti foam, 60 PPI SS foam, 90 PPI Ni/Cr foam, 90 PPI Ni foam, 60 PPI Ag foam, 80 PPI RVC foam, 80 PPI silicon carbide foam. ....	8
Figure 11: Impact damages to double-foam bumper targets impacted by 0.317-cm diameter Al2017-T4 projectiles at nom. 6.80 km/s with normal incidence. ....	9
Figure 12: Definition of open-cell foam pore and cell size (left) and variation of ligament cross section with relative density (right) (©ERG Aerospace). ....	12
Figure 13: Characterization of the 10 PPI foam structure. Cell size (1) = 3.95 mm, pore size (3) = 2.33 mm, ligament width (2) = 382 $\mu\text{m}$ . ....	13
Figure 14: Schematic (left) and photograph (right) of target 1.0" Al F10. ....	14
Figure 15: Characterization of the 20 PPI foam structure. Cell size (1) = 3.28, pore size (3) = 1.78 mm, ligament width (2) = 329 $\mu\text{m}$ .....	14
Figure 16: Schematic (left) and photograph (right) of target 1.0" Al F20. ....	15
Figure 17: Characterization of the 40 PPI foam structure. Cell size (1) = 2.63 mm, pore size (3) = 1.59 mm, ligament width (2) = 251 $\mu\text{m}$ .....	16
Figure 18: Schematic (left) and photograph (right) of target 1.0" Al F40. ....	16
Figure 19: Characterization of the 40 PPI ( $\rho_{\text{rel}} = 3\% - 5\%$ ) foam structure. Cell size (1) = 2.68 mm, pore size (3) = 1.34 mm, ligament width (2) = 210 $\mu\text{m}$ .....	17
Figure 20: Foam core structure ( $\times 20$ magnification). From left to right: F10, F20, F40. ....	17
Figure 21: Schematic (left) and photograph (right) of the 0.5" Al F40 target. ....	18
Figure 22: Schematic (left) and photograph (right) of the 2.0" Al F40 target. ....	19
Figure 23: Schematic of the 1.0" Al F40 B1W2 target.....	20
Figure 24: Schematic of the 1.0" Al F40 B2W2 target.....	20
Figure 25: Schematic (left) and photograph (right) of the 1.0" Al F40 B3W2 target. ....	21
Figure 26: Schematic (left) and photograph (right) of the 1.0" Al F40 B3W3 target. ....	22
Figure 27: Schematic (left) and photograph (right) of the 2.0" Al HC target. ....	23
Figure 28: Trussgrid 3-D honeycomb.....	23
Figure 29: Schematic (left) and photograph (right) of the 1.0" Trussgrid target. ....	24
Figure 30: Nomex PN2 honeycomb core from Plascore, Inc. ....	24
Figure 31: Schematic (left) and photograph (right) of the 2.0" PN2 HC target. ....	25

Figure 32: Schematic (left) and photograph (right) of the 2.0" Al F-var (40/20/5) target.....	26
Figure 33: Schematic (left) and photograph (right) of the 2.0" Al F-var (5/20/40) target.....	26
Figure 34: X-ray of impact damage in an AETB-8 thermal tile demonstrating a large open cavity and multiple "finger" craters from intact projectile fragments.....	27
Figure 35: Schematic (left) and photograph (right) of the 2.0" Al F-var (K/E) target.....	27
Figure 36: Schematic (left) and photograph (right) of the reversed 2.0" Al F-var (K/E) target.....	28
Figure 37: Schematic (left) and photograph (right) of the 2.0" Al F-var (N/E) target.....	28
Figure 38: Sandwich panel damage measurement schematics.....	30
Figure 39: Sandwich panel damage measurement schematics (cont.).....	30
Figure 40: Comparison of foam core damage in five targets impacted at nominally identical conditions (2.7 mm diameter projectile, 45°, 6.8 km/s).....	31
Figure 41: Comparison of damages in the 1.0" Al F40 NASA (left) and ERG (right) panels induced by impact of 2.0 mm diameter projectiles at nom. 6.8 km/s with normal incidence (0°). From top to bottom: front facesheet, rear facesheet, sectioned core.....	35
Figure 42: Comparison of damages in the 1.0" Al F40 NASA (left) and ERG (right) panels induced by impact of 2.7 mm diameter projectiles at nom. 6.8 km/s with oblique incidence (45°). From top to bottom: front facesheet, rear facesheet, sectioned core.....	36
Figure 43: Comparison of damage in 10 PPI (left), 20 PPI (middle), and 40 PPI (right) foam core sandwich panels impacted by 2.1 mm diameter Al2017-T4 spheres at $2.32 \pm 0.14$ km/s and 0°.....	38
Figure 44: Comparison of damage in 10 PPI (left), 20 PPI (middle), and 40 PPI (right) foam core sandwich panels impacted by 2.5 mm diameter Al2017-T4 spheres at $6.62 \pm 0.16$ km/s and 45°.....	39
Figure 45: Comparison of damage in 10 PPI (left), 20 PPI (middle), and 40 PPI (right) foam core sandwich panels impacted by 2.0 mm diameter Al2017-T4 spheres at $6.69 \pm 0.18$ km/s and 0°.....	41
Figure 46: Comparison of damage in 10 PPI (left), 20 PPI (middle), and 40 PPI (right) foam core sandwich panels impacted by 3.2 mm diameter Al2017-T4 spheres at $6.63 \pm 0.07$ km/s and 60°.....	43
Figure 47: Tests used to evaluate the effect of foam relative density on shielding performance.....	44
Figure 48: Comparison of damages in HITF08263 ( $\rho_{rel} = 6\%-8\%$ ) and HITF08574 ( $\rho_{rel} = 3\%-5\%$ ).....	45
Figure 49: Comparison of damages in HITF09007 ( $\rho_{rel} = 6\%-8\%$ ) and HITF08575 ( $\rho_{rel} = 3\%-5\%$ ).....	46
Figure 50: Comparison of damages in HITF08423 ( $\rho_{rel} = 6\%-8\%$ ) and HITF08583 ( $\rho_{rel} = 3\%-5\%$ ).....	47
Figure 51: Failure limits of the 0.5", 1.0", and 2.0" thick Al F40 targets at approx. 6.8 km/s normalized in terms of: Left: 1.0" F40 KE <sub>crit</sub> ; right: KE <sub>crit</sub> ( $\theta=0^\circ$ ).....	49
Figure 52: Variation of high-speed failure limits with increasing panel thickness and areal density.....	50
Figure 53: Two instances of minimal failure in Phase 3 tests useful for definition of ballistic limits.....	51
Figure 54: Comparison of impact damage in the 1.0" Al F40 (NASA) foam (left) and 1.0" Trussgrid (right) panels impacted by 2.0 mm diameter Al2017-T4 spheres at ~6.8 km/s with normal incidence.....	54
Figure 55: Comparison of impact damage in the 1.0" Al F40 (NASA) foam (left) and 1.0" Trussgrid (right) panels impacted by 2.1 mm diameter Al2017-T4 spheres at ~2.5 km/s with normal incidence.....	55
Figure 56: Comparison of impact damage in the 1.0" Al F40 (NASA) foam (left) and 1.0" Trussgrid (right) panels impacted by 3.4 mm diameter Al2017-T4 spheres at ~6.8 km/s with oblique incidence (60°).....	56
Figure 57: Comparison of the 2.0" Al F40 [10], F-var, F-var (K/E), and F-var (N/E) panels impacted by 4.0" mm diameter projectiles at ~6.8 km/s with 0°.....	57
Figure 58: Al HC target damage following normal impact of a 2.5 mm diameter projectile at 6.91 km/s.....	58
Figure 59: Comparison of the 2.0" Al F40 [10], Al HC [10], and PN2 HC panels impacted by 3.6 mm diameter projectiles at ~6.8 km/s with 0°.....	59

Figure 60: Comparison of the 2.0" Al F40, Al HC, and PN2 HC panels impacted by 6.0 mm diameter projectiles at ~6.8 km/s with 60°.....	60
Figure 61: Comparison of the F-var original (left) and reversed (right) configurations impacted by 4.0 mm diameter projectiles at ~6.8 km/s with normal incidence (0°).....	62
Figure 62: Comparison of the F-var (K/E) original (left) and reversed (right) configurations impacted by 4.0 mm diameter projectiles at ~6.8 km/s with normal incidence (0°) .....	63
Figure 63: Evidence of decreased cratering depth with increasing velocity between 2.2 km/s and 5.0 km/s: HITF08423 (left) and HITF08424 (right).....	64
Figure 64: Evidence of decreased cratering depth with increasing velocity between 2.2 km/s and 5.0 km/s: HITF08420 (left) and HITF08427 (right).....	65
Figure 65: Ballistic limit curve for the baseline 1.0" Al foam sandwich panel at 0° plotted with test data.....	67
Figure 66: Ballistic limit curve for the baseline 1.0" Al foam sandwich panel at 45° plotted with test data.....	68
Figure 67: Ballistic limit curve for the baseline 1.0" Al foam sandwich panel at 60° plotted with test data.....	68
Figure 68: Ballistic limit curve for the 0.5" Al foam sandwich panel at 0° plotted against test data (including data from [10]). .....	69
Figure 69: Ballistic limit curve for the 0.5" Al foam sandwich panel at 45° plotted against test data (including data from [10]). .....	69
Figure 70: Ballistic limit curve for the 0.5" Al foam sandwich panel at 60° plotted against test data. ....	70
Figure 71: Ballistic limit curve for the 2.0" Al foam sandwich panel at 0° plotted against test data (including data from [10]). .....	70
Figure 72: Ballistic limit curve for the 2.0" Al foam sandwich panel at 45° plotted against test data (including data from [10]). .....	71
Figure 73: Ballistic limit curve for the 2.0" Al foam sandwich panel at 60° plotted against test data. ....	71
Figure 74: Evaluating the accuracy of the foam ballistic limit equation. ....	72
Figure 75: Comparison of ballistic limit curves for the 1.0" Al F40 foam panel, flight-representative Whipple shield, and honeycomb core sandwich panel (normal impact (top), 60° impact (bottom)).....	73

## Tables

Table 1: Characteristic measurements of the foam cores .....	17
Table 2: Summary of Phase 1 target configurations .....	18
Table 3: Summary of Phase 3 target configurations .....	22
Table 4: Summary of Phase 3 target configurations .....	29
Table 5: Damage measurement notation and indices.....	30
Table 6: Experimental scatter assessment test details and results.....	31
Table 7: Phase 1 test results.....	33
Table 8: Details of impact tests used to evaluate difference between the NASA and ERG panels.....	34
Table 9: Comparison of performance for varying PPI foam core panels at nominally identical impact conditions....	37
Table 10: Summary of 1.0" foam core panel failure limits ( $V \approx 6.8$ km/s). ....	48
Table 11: Phase 2 test results.....	48
Table 12: Phase 3 test results.....	50
Table 13: Phase 4 test results.....	52
Table A-1: Phase 1 test results.....	77
Table A-2: Phase 2 test results.....	79
Table A-3: Phase 3 test results.....	79
Table A-4: Phase 4 test results.....	80

## **Glossary of Terms and Acronyms**

AD	areal density
Al	aluminum
bumper	outermost shield layer used to break up MMOD particles
FOM	figure of merit
HC	honeycomb
HITF	Hypervelocity Impact Technology Facility
ISS	International Space Station
JSC	Johnson Space Center
KE	Kinetic energy
K/E	Kevlar/epoxy composite
MMOD	micrometeoroid and orbital debris
NASA	National Aeronautics and Space Administration
N/E	Nextel/epoxy composite
NNO	new non-optimum
PPI	pores per (linear) inch
RVC	reticulated vitreous carbon
SEM	Scanning Electron Microscope
SP	sandwich panel

## Notations

d	projectile diameter (cm)
S	target spacing (cm)
$\rho$	density ( $\text{g}/\text{cm}^3$ )
$\sigma$	rear wall yield stress (MPa)
t	thickness (cm)
$\theta$	impact angle measured from normal to surface (degrees)
V	projectile velocity (km/s)

## Subscripts

b	bumper
c	critical
f	foam
HV	high velocity
LV	low velocity
n	normal
p	projectile
rel	relative
w	rear wall

## Introduction

Spacecraft weight and/or volume restrictions often prevent the inclusion of a dedicated shield for protection against the impact of micrometeoroids and orbital debris (MMOD). In such circumstances, shielding is provided by the vehicle's primary structure – commonly constructed of honeycomb core sandwich panels (HC SPs). Although their high specific strength and stiffness are ideal for structural requirements, the protective capability of HC SPs is rather poor. For the majority of impact conditions relevant to MMOD, pressures generated during impact are sufficient to induce projectile fragmentation. Common MMOD shielding configurations such as the Whipple shield [1] and stuffed Whipple shield [2] utilize this effect by locating a thin, sacrificial plate (aka bumper plate) ahead of the vehicle pressure hull. Expanding projectile and bumper fragments disperse as they propagate through the shield, spreading the load over an area of the pressure hull significantly larger than that of the original projectile. The Whipple shield concept is illustrated in Figure 1.

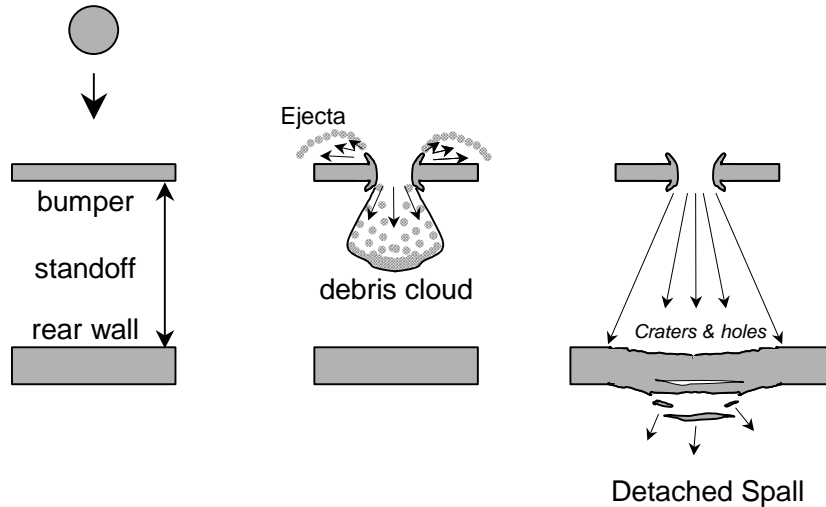


**Figure 1:** Whipple shield concept.

For impact on HC SPs, expansion of the projectile and facesheet debris cloud is restricted by the presence of honeycomb cell walls. Considering impact at normal incidence (i.e. projectile velocity vector perpendicular to the target front facesheet), fragments with a high radial expansion angle and kinetic energy (KE) are able to penetrate the thin cell foils and propagate into adjacent honeycomb cells. The remaining fragments ricochet off the cell walls, remaining within the initial honeycomb core cell/s. The fragment cloud is subsequently concentrated over a significantly smaller area, resulting in a more lethal impact upon the rear facesheet (relative to an equivalent Whipple shield). Taylor et al. [3] quantified the degradation in performance of a dual-wall structure due to the presence of honeycomb cells as a 50% reduction in effective rear wall thickness (at hypervelocities, i.e. molten and/or vaporized debris cloud). Ryan et al. [4] defined a degradation in shielding performance due to the presence of a honeycomb cell core equal to a ~46% reduction in shielding capability at normal incidence, reducing with increased obliquity (i.e. for impact at 60°, an ~18% reduction in performance is defined). Sennett and Lathrop [5] also quantified the effect of the honeycomb core, stating that once the panel thickness increases above 2 times the honeycomb cell size, no increase in shielding capability is achieved with an increase in shield thickness (for molten and/or vaporized ejecta). For solid fragment ejecta, the effect was not nearly as severe.

In Figure 2, a comparison between the predicted performance of dual-wall shields with and without a honeycomb core is made at 7 km/s (normal incidence). For the Whipple shield configuration (i.e. no honeycomb core), the new non-optimum (NNO) equation [2] is used. It should be noted that the NNO, Sennett and Lathrop, and Taylor approaches may provide non-conservative predictions for projectile diameter to shield spacing ratios less than 15 (i.e.  $d_p/S < 15$ ).

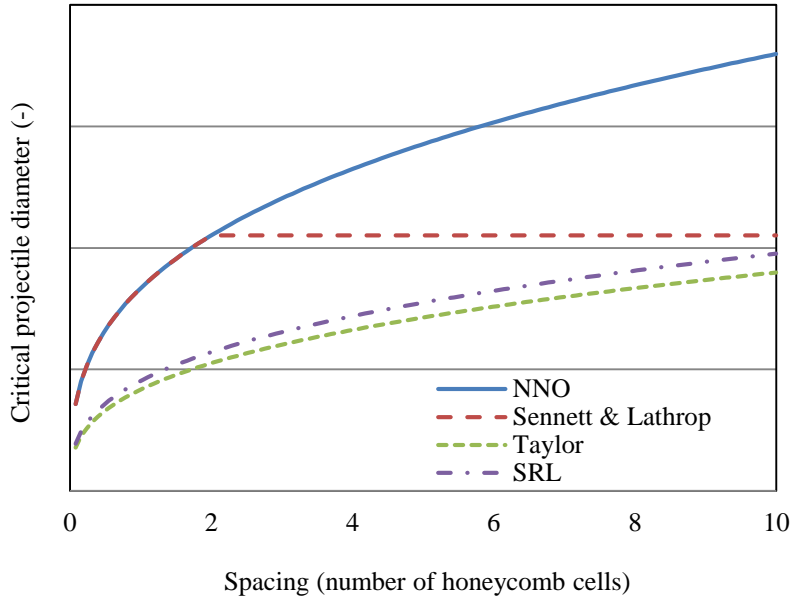


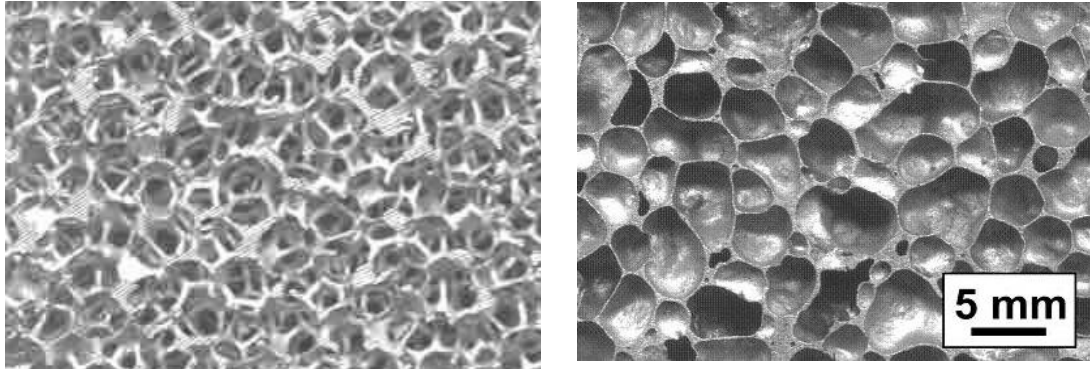
**Figure 2:** Predicted performance of a dual-wall shield at hypervelocity with and without a honeycomb core.

Metallic foams are a promising new material for spacecraft primary structures as they provide comparative mechanical performance to metallic honeycombs without the presence of channeling cells detrimental to MMOD shielding. The objective of this study was to characterize the shielding performance of sandwich panel structures with open-cell metallic foam cores. The test program was divided into four phases, each with a different objective:

- Phase 1: The effect of foam parameters on shielding performance
- Phase 2: The effect of core thickness on shielding performance
- Phase 3: The effect of facesheet thickness on shielding performance
- Phase 4: Comparison with alternate structural panels

## Background

Metallic foams are a relatively new class of materials with low density and novel physical, mechanical, thermal, electrical and acoustic properties. Although incompletely characterized, they offer significant performance gains in light, stiff structures, for the efficient absorption of energy, for thermal management, for acoustic control, etc. [6]. There are two competing types of metallic foams: open cell and closed cell. Although closed-cell foams are capable of retaining some residual atmosphere, which may aid in debris shielding through deceleration of penetrating fragments via drag, open-cell foams are considered the more promising technology. Open-cell foams are generally of lower weight, and provide a higher degree of homogeneity than low-density closed-cell metallic foams.



© ERG Aerospace

© Shinko Wire

**Figure 3:** Open-cell (left) and closed-cell (right) metallic foam.

## Existing Research

A number of preliminary studies have investigated the performance of metal foams in hypervelocity impact. Alternative configurations for the International Space Station (ISS) Columbus module shielding were evaluated [7]. One of the configurations considered included a panel of open-cell aluminum foam (referred to in [7] as configuration AB2Mod). A schematic of AB2Mod shield is provided in Figure 4. Testing found that the AB2Mod configuration provided increased protection over the reference Columbus stuffed Whipple shield at high velocities ( $> 6 \text{ km/s}$ ) and normal incidence. At oblique incidence, the performance of the reference stuffed Whipple shield and foam-modified configuration were comparable (at high velocity). For low-velocity testing, the performance of the AB2Mod configuration was clearly worse than that of the reference Columbus shield. The authors concluded that the foam configuration was vulnerable to impact of large projectiles (above 1 cm in diameter) at low velocities, as the shield was unable to induce projectile fragmentation.

While the AB2Mod configuration was found to provide a similar level of protection to the reference stuffed Whipple shield, the primary advantages of the configuration are related to: increased coverage of the pressure hull volume (due to a concentration of mass in the outer layer), and; other design aspects such as a reduction in non-ballistic mass (stiffeners, local reinforcements, etc.).

The AB2Mod shield was configured with two different types of open-cell aluminum foam bumpers: m-pore (base alloy Al356.0, 20 pores per linear inch (PPI), areal density (AD) =  $0.619 \text{ g/cm}^2$ , manufactured by m-pore GmbH) and Duocel (base alloy Al6101-T6, 20 PPI, AD =  $0.690 \text{ g/cm}^2$ , manufactured by ERG Aerospace). Despite minor differences in target specification and impact conditions, significant variations in performance occurred (see Figure 5). The m-pore foam was found to have broader ligaments, larger pores, and a less-regular surface appearance. Scanning Electron Microscope (SEM) images of the two foam types are shown in Figure 6. The grains on the surface of the m-pore foam were considered to be silicon deposits resulting from impurities in the manufacturing process.

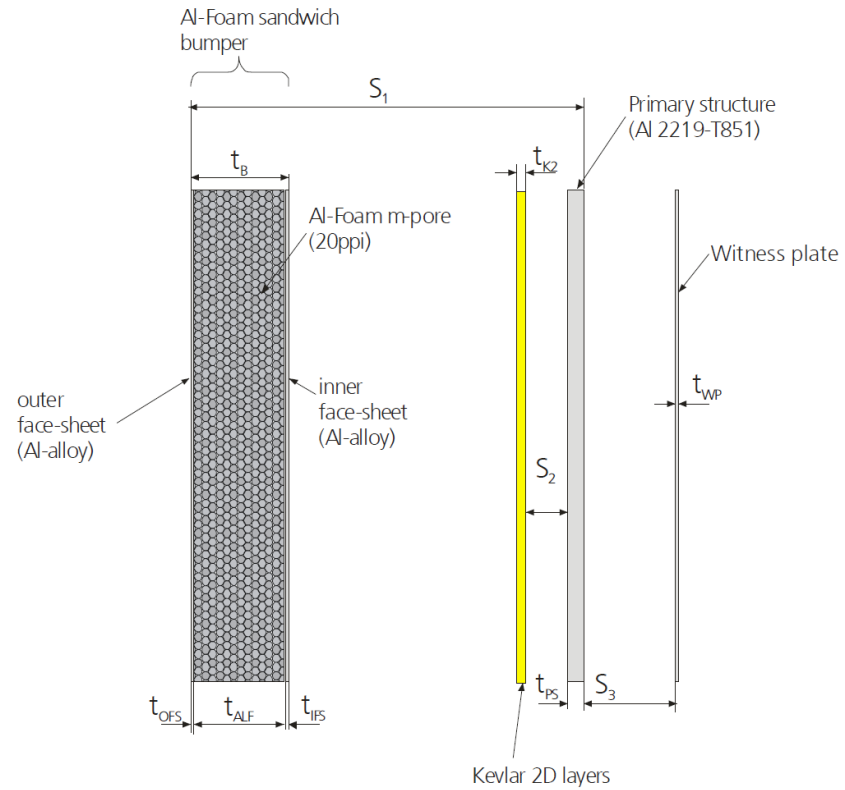
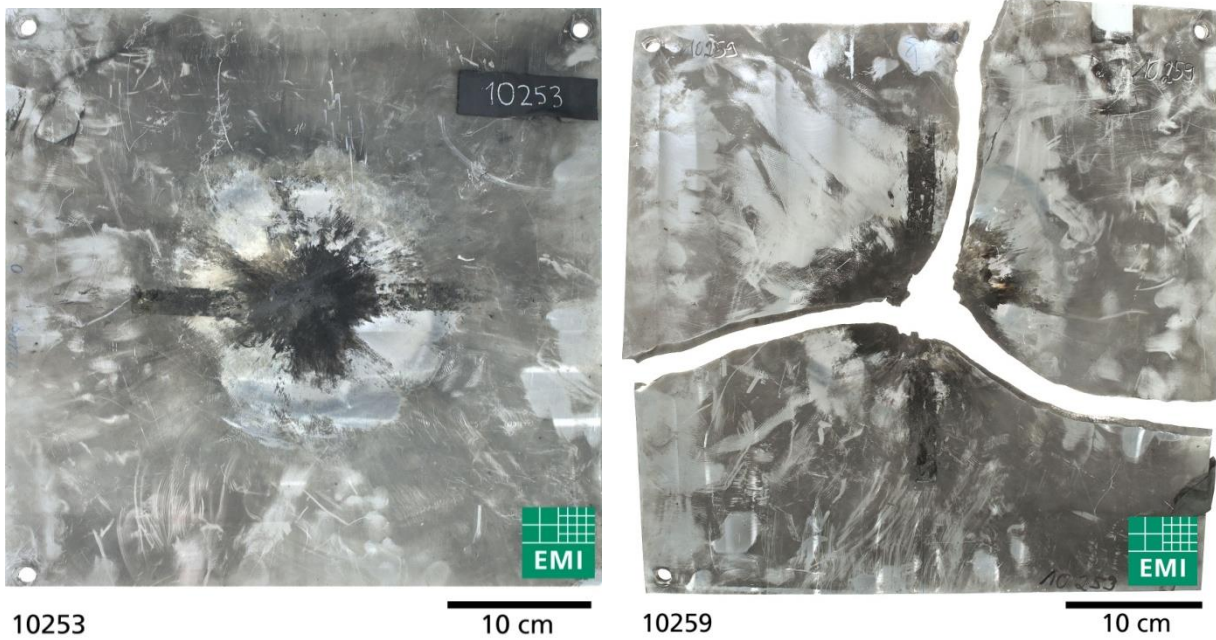


**Figure 4:** Alternate Columbus MMOD shield configuration incorporating metallic open-cell foam [8].



10253

10 cm

10259

10 cm

**Figure 5:** AB2Mod rear wall following impact of 15.0 mm diameter Al2017-T4 spheres at no. 6.4 km/s with normal incidence. Left: m-pore bumper; right: Duocel foam bumper [9].

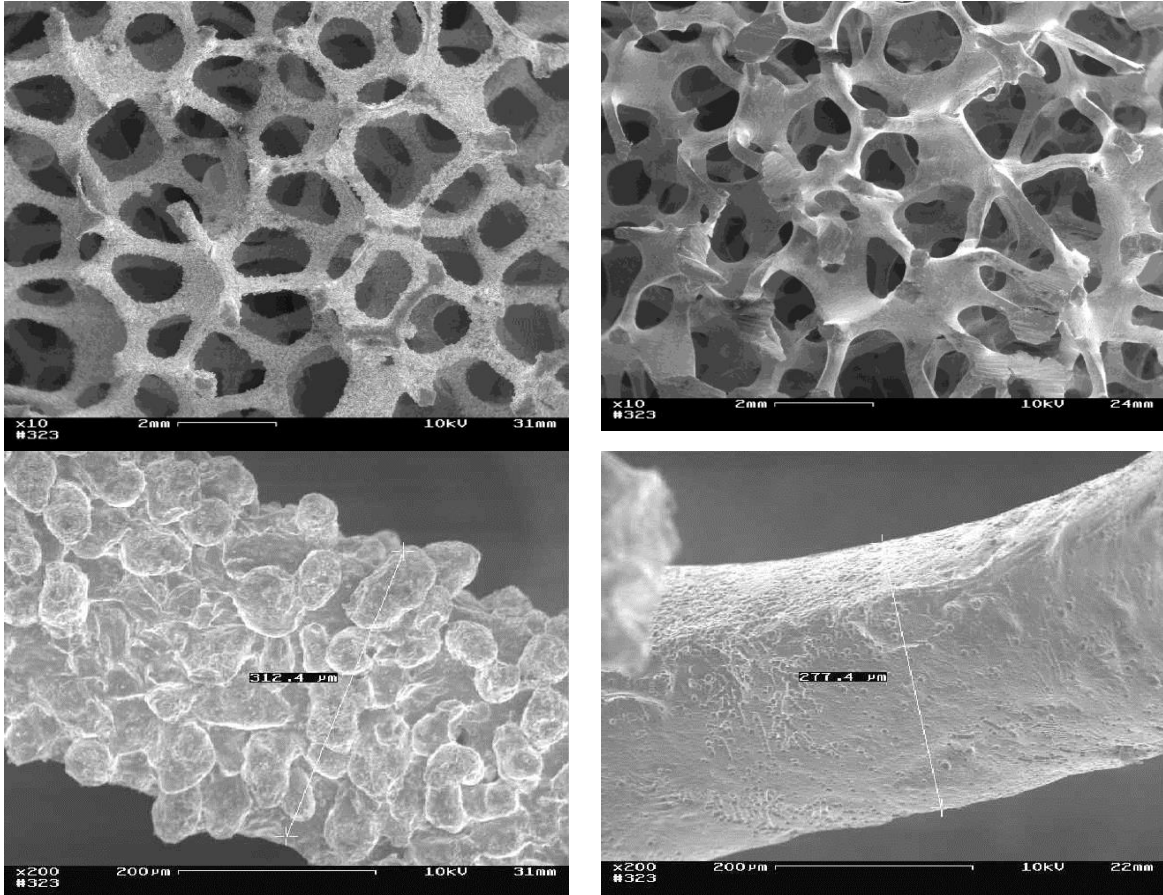


**Figure 6:** m-pore (left) and Duocel (right) appearance microscopic appearance [9].

The shielding performance of sandwich panel structures with open-cell aluminum foam cores was evaluated in Yasensky, Christiansen, Prior [10] against that of aluminum (Al) HC SPs. In this study, 5.08 cm and 1.27 cm thick sandwich panel configurations were subject to nominally identical impact conditions, and a direct comparison between impact damages and failure limits was made. A 10 PPI Duocel 6101-T6 aluminum foam from ERG Aerospace with a nominal relative density of 6%-8% was used for the foam panel, with 0.0254 cm thick Al6061-T6 facesheets. The honeycomb sandwich panel had a 1/8-5052-.003 designation core from Hexcel and 0.127/0.041 cm thick Al6061-T6 facesheets for the 5.08 cm thick and 1.27 cm thick sandwich panels respectively. A comparison between the damage induced by the impact of a 3.6 mm Al 2017-T4 sphere at normal incidence with a velocity of  $\sim 6.49 \pm 0.27$  km/s on the 5.08 cm thick sandwich panels is shown in Figure 7. Although the facesheet of the honeycomb sandwich panel was significantly thicker (0.127 cm vs. 0.0254 cm for the foam sandwich panel), the foam sandwich panel was able to successfully defeat the projectile, while a clear perforation hole ( $7.8 \times 4.9$  mm) was observed in the honeycomb sandwich panel rear facesheet.

The performance of foam-constituent panels was again compared to that of honeycomb configurations [11]; however, this time the materials were part of multi-layer shields representative of those used onboard the ISS. The baseline configuration consisted of two 12.7 mm thick aluminum honeycomb sandwich panels, with a double outer layer of aluminum mesh, and a monolithic aluminum rear wall (see Figure 8). The modified configuration replaced the honeycomb cores with 10 PPI Duocel 6101-T6 aluminum foams (6%-8% relative density). As the foam core was slightly heavier than the honeycomb, the facesheets of the second sandwich panel were removed in the foam configuration.

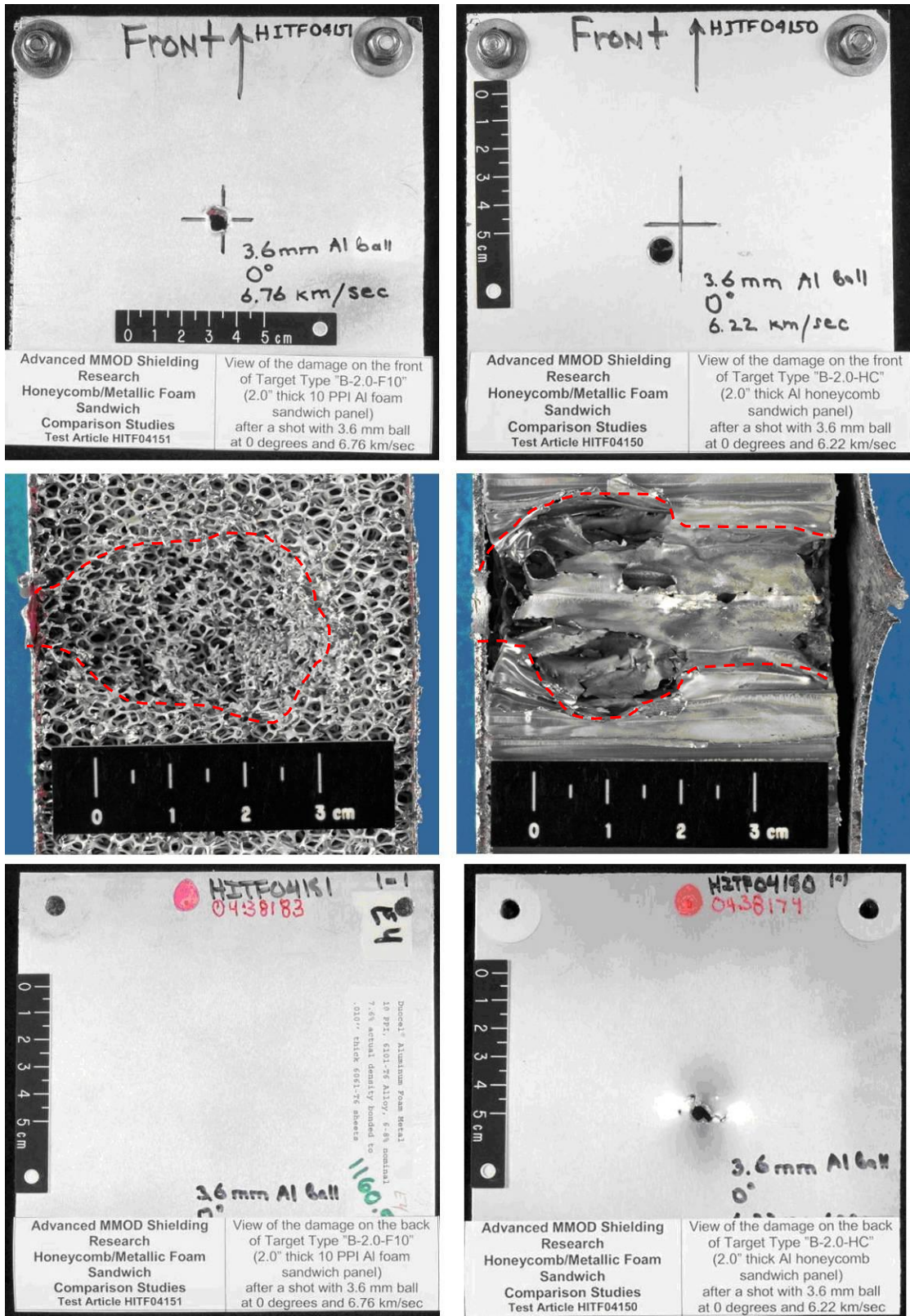


**Figure 7:** Comparison of damages in an open-cell foam core (left) and honeycomb core (right) sandwich panel structures impacted by a 3.6 mm Al-sphere at  $6.49 \pm 0.27$  km/s ( $0^\circ$ ). Upper: front facesheet damage; Middle: core damage (sectioned); Bottom: rear facesheet damage.

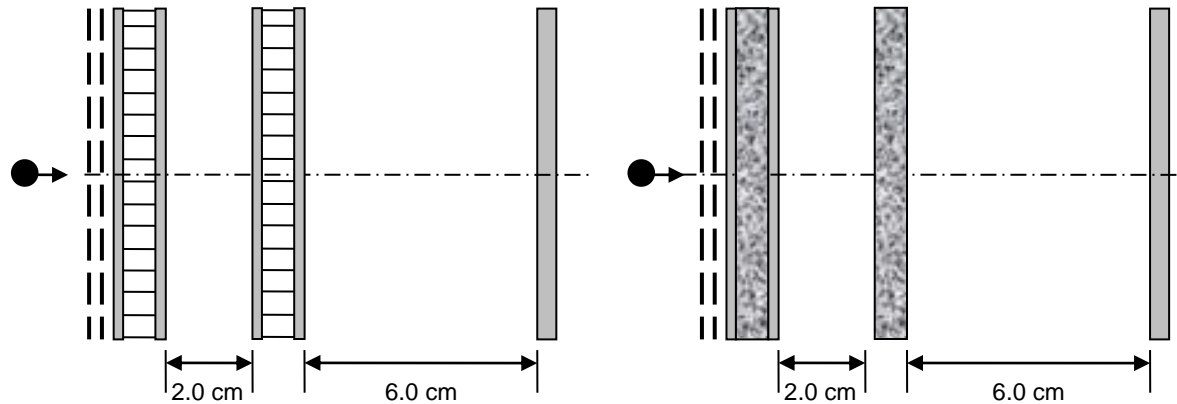


**Figure 8:** Schematic of the double layer honeycomb (left) and modified double layer foam (right) shields.

Ballistic limit equations derived for the two configurations predicted a 15% increase in protective capability at low velocity (i.e. 3 km/s) for the foam modification, and a 3% increase at high velocity (i.e. 7 km/s). Furthermore, with higher obliquities, the performance enhancement from the foam was predicted to increase up to 29% (at 60°, 6.0 km/s). A comparison of the ballistic limit curves for the baseline honeycomb and modified foam shields is shown in Figure 9.

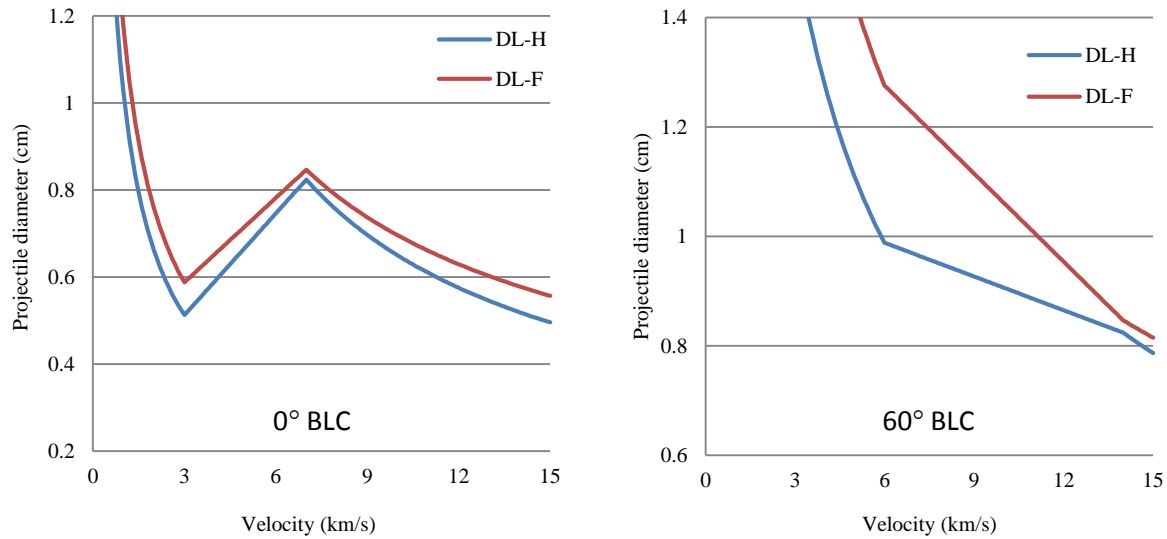


**Figure 9.** Ballistic limit curves for the double-layer honeycomb (DL-H) and foam (DL-F) shields.

The performance of metallic, ceramic, and amorphous foams was investigated as components of multi-layer shielding configurations [12]. Images of the different foam materials tested are shown in Figure 10.

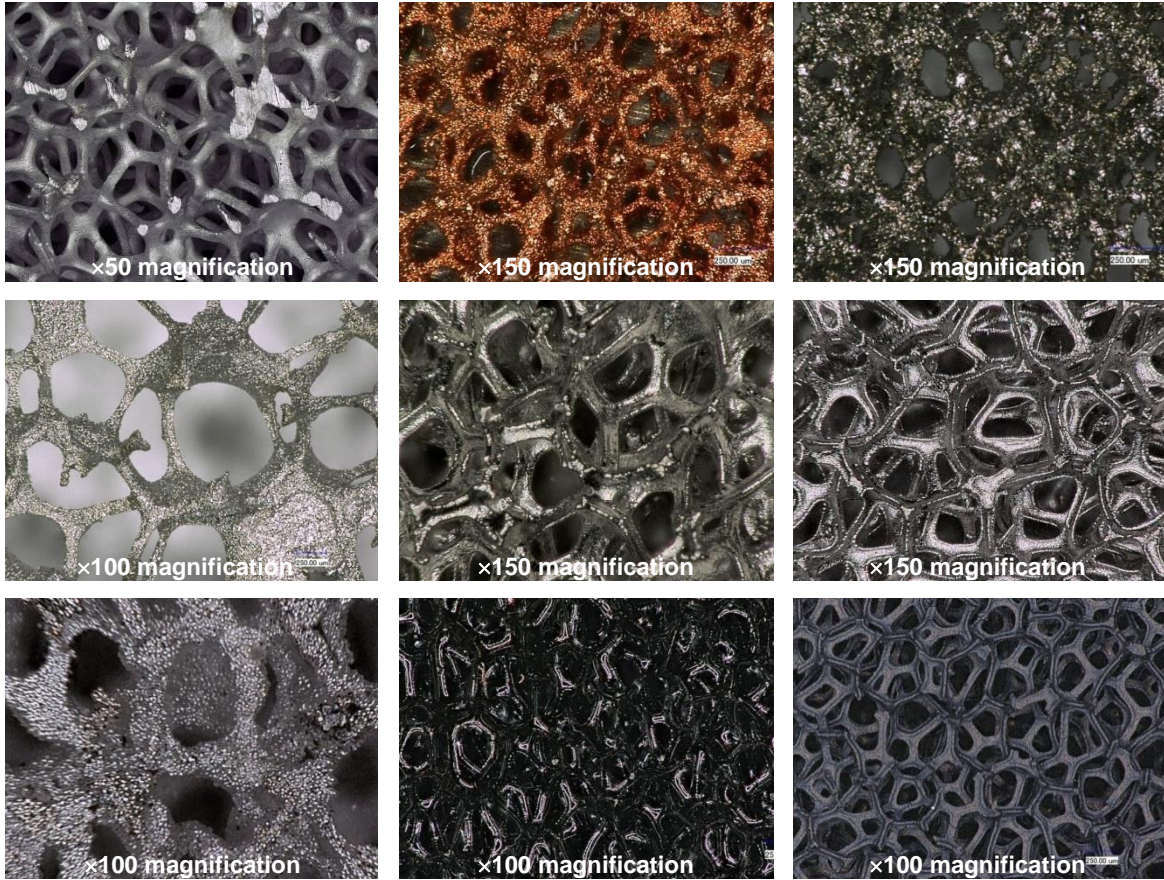


**Figure 10:** Top left to bottom right: 40 PPI Al foam, 100 PPI Cu foam, 100 PPI Ti foam, 60 PPI SS foam, 90 PPI Ni/Cr foam, 90 PPI Ni foam, 60 PPI Ag foam, 80 PPI RVC foam, 80 PPI silicon carbide foam.

The targets were evaluated using a figure of merit (FOM) based on rear wall failure modes (impulsive and cratering). A statistical analysis was used to rank the shielding capability of the various foam materials, which provided the following results (from best-to-worst):

titanium > stainless steel > copper > aluminum > reticulated vitreous carbon (RVC) > silicon carbide  
> chromized nickel/chromium > nickel

These results are preliminary, as additional evaluation is underway of the large number of tests performed in this study using a variety of target configurations and parameters. A number of nominally identical hypervelocity impact tests were performed on double-bumper configurations that maintained constant spacing, rear-wall material and thickness, while varying the foam material used for the outer and inner bumper plates. A comparison of the target damages is provided in Figure 11.

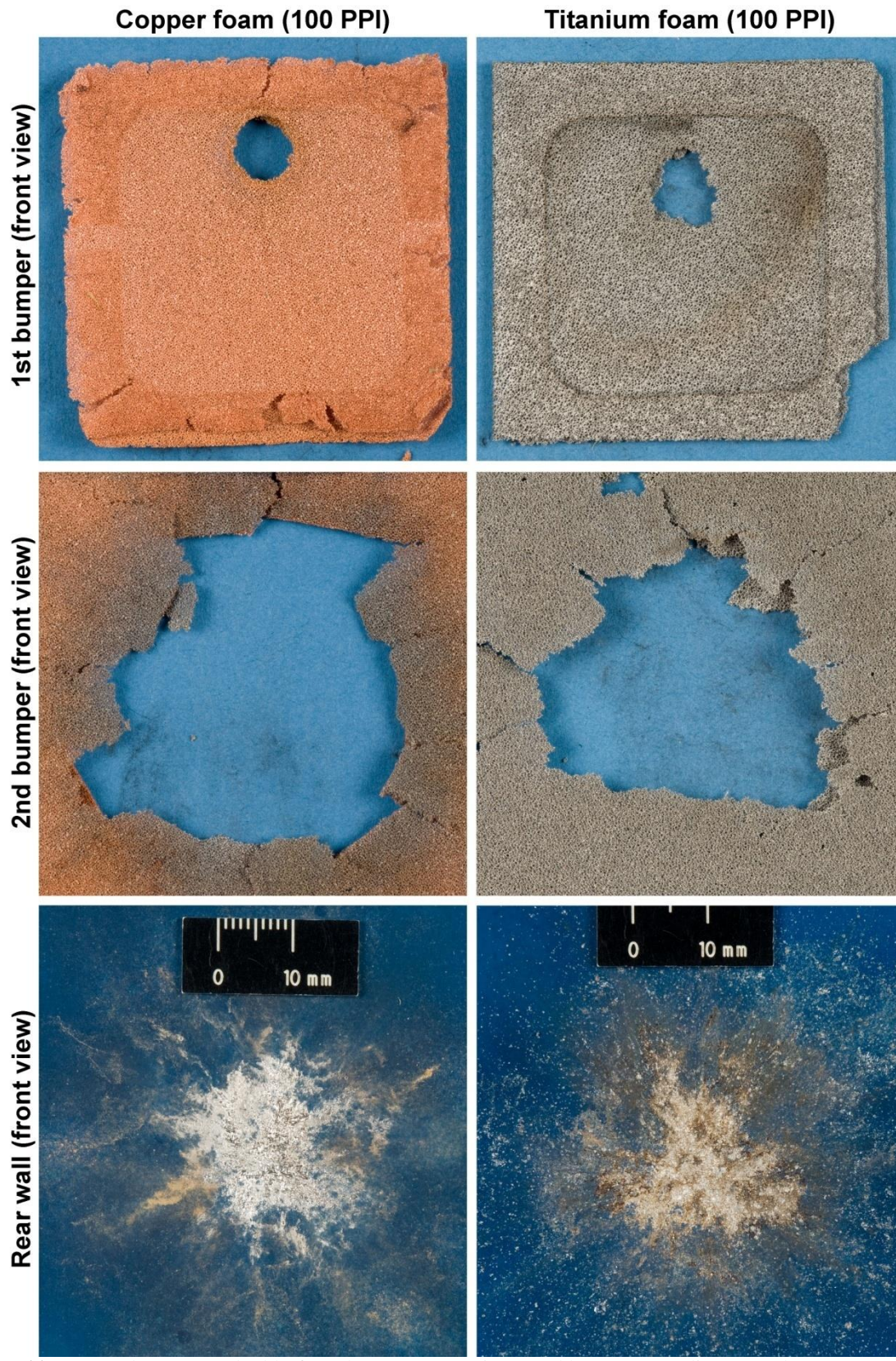


**Figure 11:** Impact damages to double-foam bumper targets impacted by 0.317-cm diameter Al2017-T4 projectiles at nom. 6.80 km/s with normal incidence.

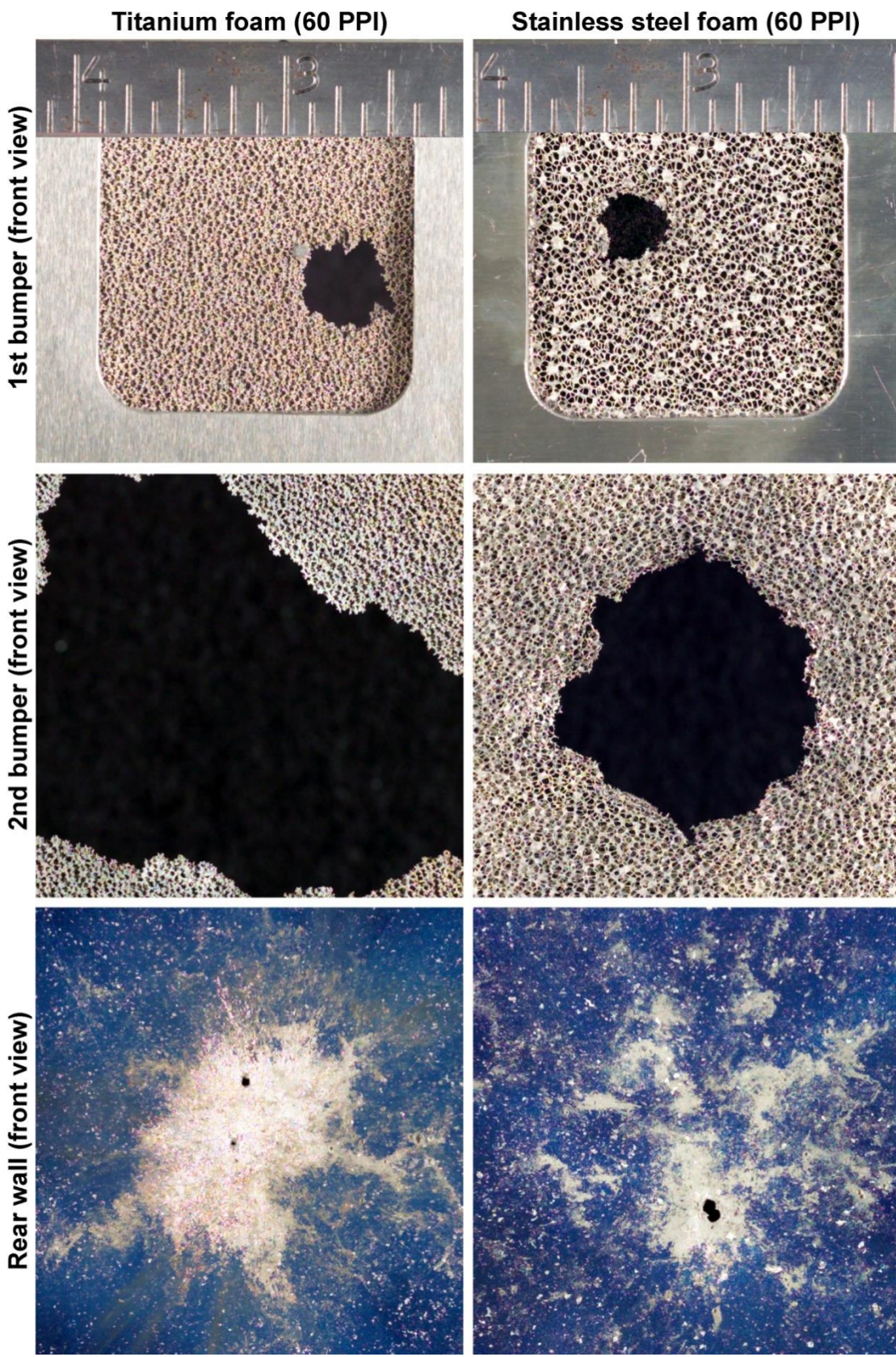


**Figure 11 (cont.):** Impact damages to double-foam bumper targets impacted by 0.3175-cm diameter Al2017-T4 projectiles at nom. 6.80 km/s with normal incidence.

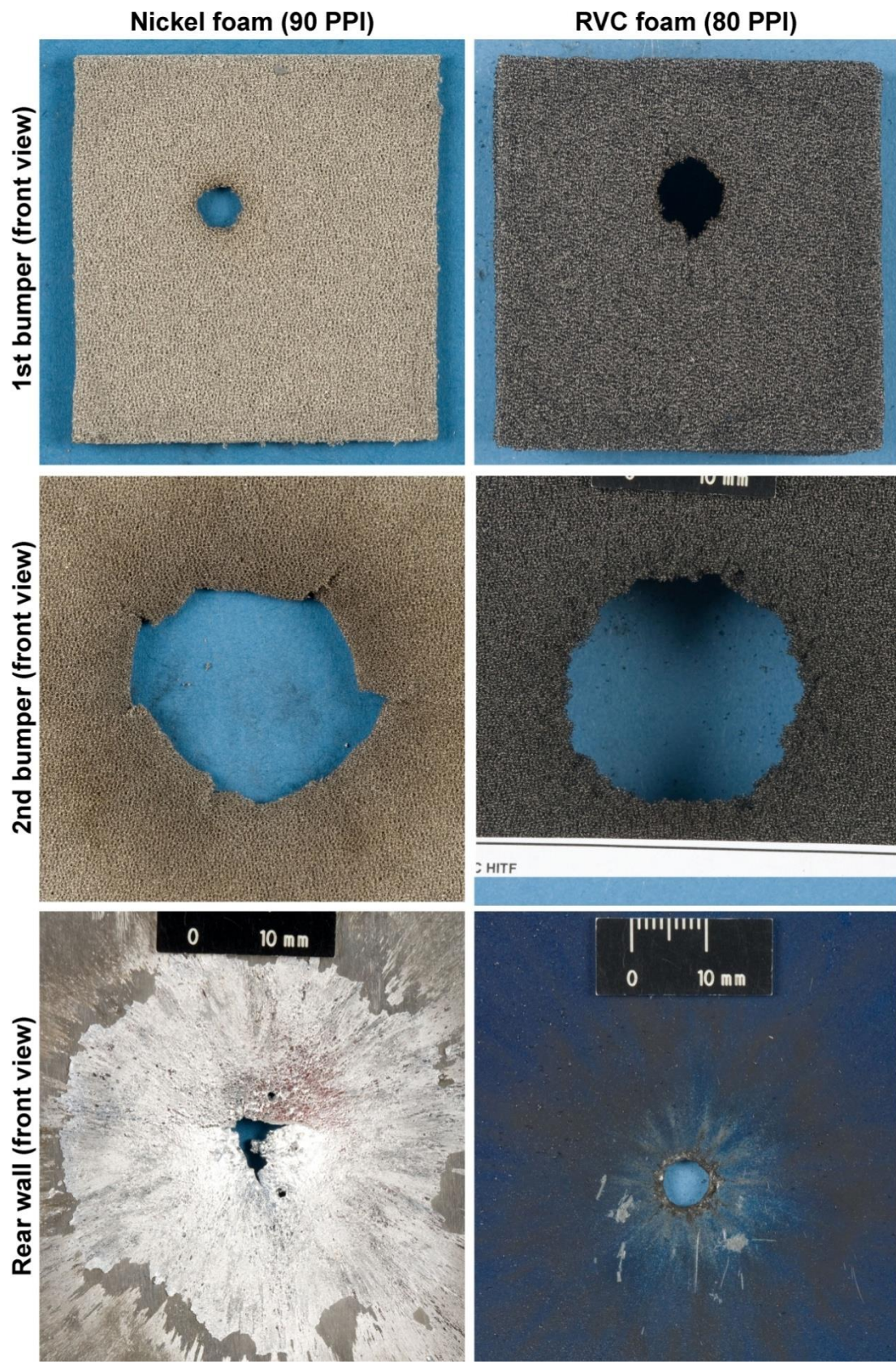


**Figure 11 (cont.):** Impact damages to double-foam bumper targets impacted by 0.3175-cm diameter Al2017-T4 projectiles at nom. 6.80 km/s with normal incidence.

## Aluminum Open-Cell Foam

A number of different manufacturing techniques exist for metallic foams. These techniques can be categorized into four classes: formation from the vapor phase; electrodeposited from an aqueous solution; liquid-state processed; and solid-state processed. In this study, Duocel aluminum foams from ERG Aerospace were selected for testing. Duocel foams are formed through utilization of a solid negative-image ceramic mould, which is filled with a liquid aluminum alloy and allowed to cool. The individual cells are typically 14-faceted polyhedral or solid tetrakaidecahedrons. Once the foam has solidified, the thin membranes or windows are removed through a reticulation process, leaving behind only interconnected struts that form the open-cell foam structure. The tetrakaidecahedrons are referred to as cells, and the individual windows between the interconnected foam ligaments are the pores, shown in Figure 12. The pore size controls the number and nominal size of foam ligaments, while the relative density controls their cross-sectional form and actual size. Examples of ligament cross sections are also provided in Figure 12.

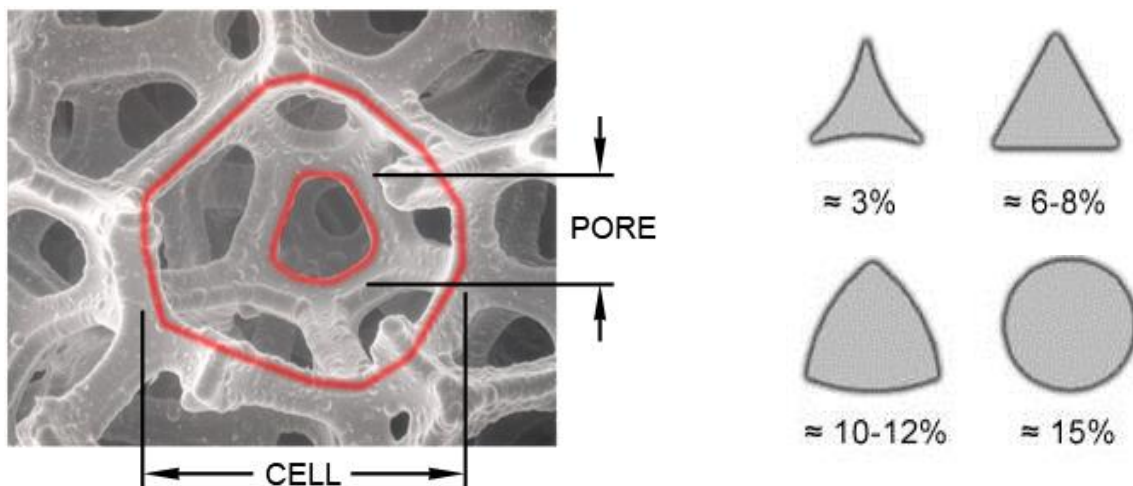


**Figure 12:** Definition of open-cell foam pore and cell size (left) and variation of ligament cross section with relative density (right) (©ERG Aerospace).

## Test Articles and Target Setup

### Phase 1 Articles and Setup

#### 1.0" Al F10 (ERG)

The 1.0" Al F10 (ERG) target consists of a 25.40 mm thick sandwich panel with an open-cell aluminum foam core and 0.254 mm thick Al6061-T6 facesheets, bonded using Scotch-Weld AF 163-2M (0.0095 in.) modified epoxy structural adhesive film. The foam core has a nominal density 6%-8% that of the base Al6101-T6 material ( $\rho = 2.70 \text{ g/cm}^3$ ) and is manufactured by ERG Aerospace (Oakland). F10 indicates the pore density of the foam is 10 PPI, details of which are shown in Figure 13. ERG Aerospace performed the assembly of the structural panel. The areal density of the target is measured as  $0.79 \text{ g/cm}^2$ .

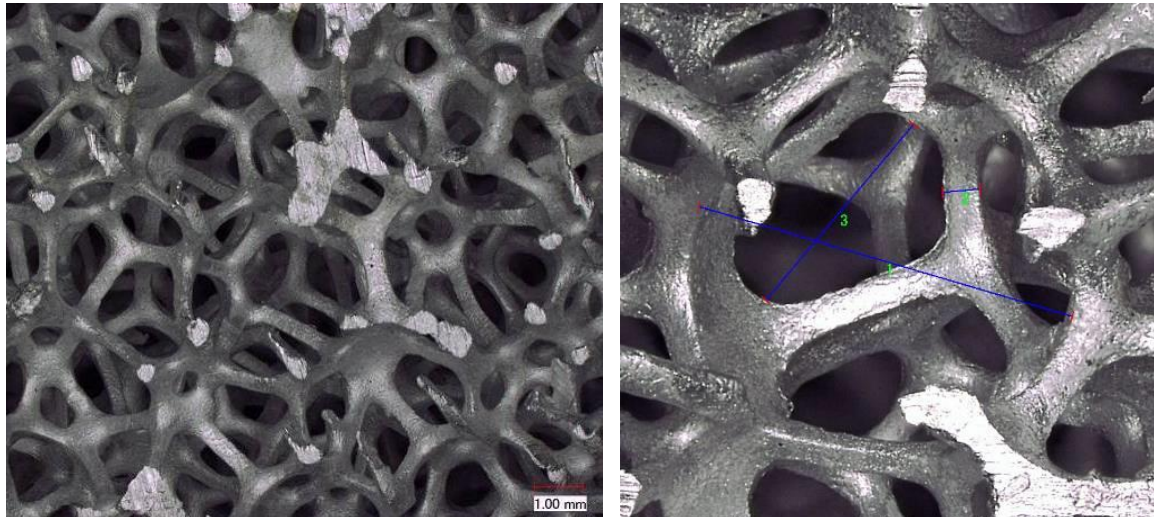


**Figure 13:** Characterization of the 10 PPI foam structure. Cell size (1) = 3.95 mm, pore size (3) = 2.33 mm, ligament width (2) = 382  $\mu\text{m}$ .

For normal impact tests, a  $101.6 \times 101.6 \text{ mm}$  (4 × 4 in.) target is used, which is mounted in a target frame that exposes a  $76.2 \times 76.2 \text{ mm}$  (3 × 3 in.) area of the sandwich panel front and rear facesheets. For oblique impact tests, a larger  $152.4 \times 152.4 \text{ mm}$  (6 × 6 in.) target is used, mounted in a target frame that exposes a  $127.0 \times 127.0 \text{ mm}$  (5 × 5 in.) area of the target. A 1.016 mm (0.04 in.) thick Al6061-T6 witness plate is spaced 100 mm (3.94 in.) from the rear side of the sandwich panel, held in place via threaded rods. The witness plate is dusted with a thin coat of blue paint to enhance the visibility of ejecta deposits. The target configuration is shown in Figure 14.

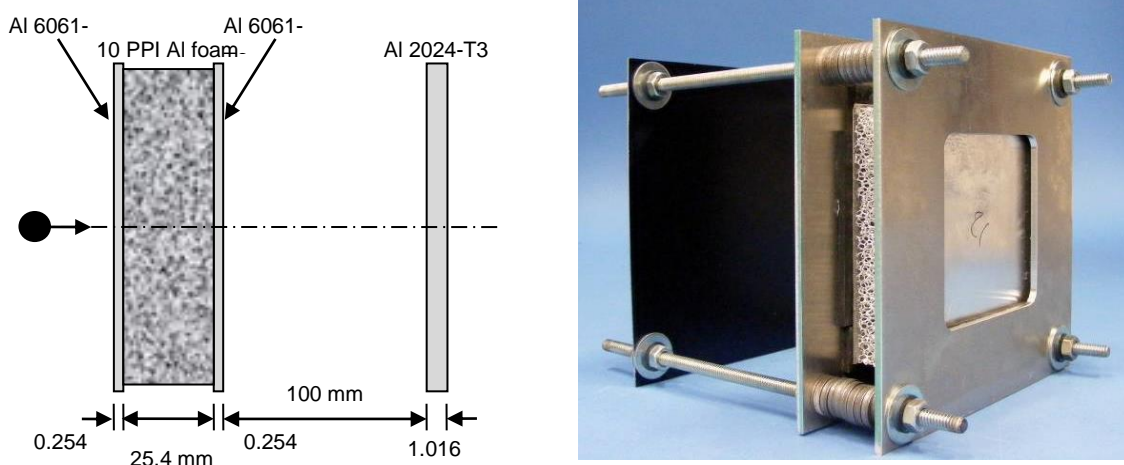


**Figure 14:** Schematic (left) and photograph (right) of target 1.0" Al F10.

### 1.0" Al F20 (ERG)

The 1.0" Al F20 (ERG) target consists of a 25.40 mm thick sandwich panel with an open-cell aluminum foam core and 0.254 mm thick Al6061-T6 facesheets, bonded using Scotch-Weld AF 163-2M (0.0095 in.) modified epoxy structural adhesive film.. The foam core has a nominal density of 6%-8% that of the base Al6101-T6 material ( $\rho = 2.70 \text{ g/cm}^3$ ) and is manufactured by ERG Aerospace. F20 indicates the pore density of the foam is 20 PPI, details of which are shown in Figure 15. Assembly of the structural panel was performed by ERG Aerospace. The areal density of the target is measured as  $0.77 \text{ g/cm}^2$ .

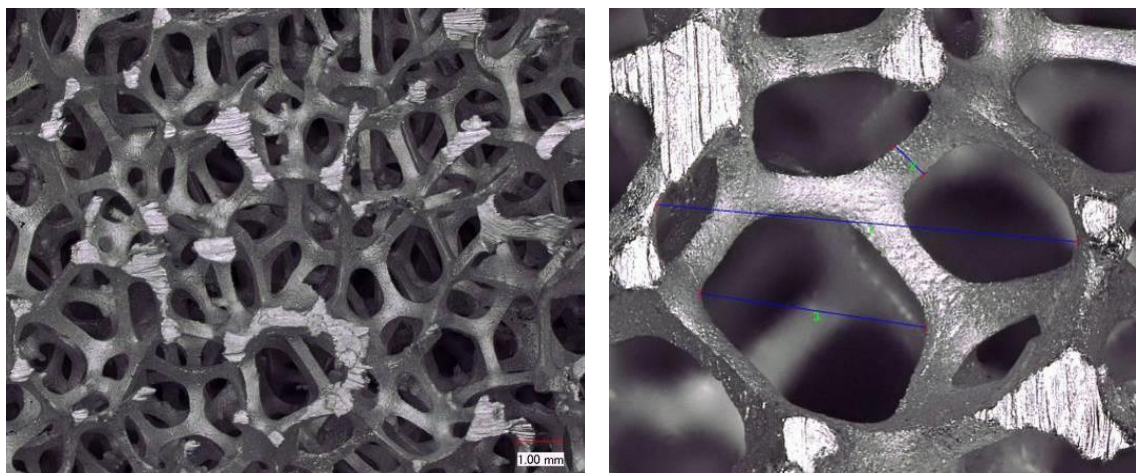


**Figure 15:** Characterization of the 20 PPI foam structure. Cell size (1) = 3.28, pore size (3) = 1.78 mm, ligament width (2) = 329  $\mu\text{m}$ .

For normal impact tests a  $101.6 \times 101.6 \text{ mm}$  (4× 4 in.) target is used, which is mounted in a target frame that exposes a  $76.2 \times 76.2 \text{ mm}$  (3 × 3 in.) area of the sandwich panel front and rear facesheets. For oblique impact tests, a larger  $152.4 \times 152.4 \text{ mm}$  (6 × 6 in.) target is used, mounted in a target frame that exposes a  $127.0 \times 127.0 \text{ mm}$  (5 × 5 in.) area of the target. A 1.016 mm (0.04 in.) thick Al6061-T6 witness plate is spaced 100 mm from the rear side of the sandwich panel, held in place via threaded rods. The

witness plate is dusted with a thin coat of blue paint to enhance the visibility of ejecta deposits. The target configuration is shown in Figure 16.

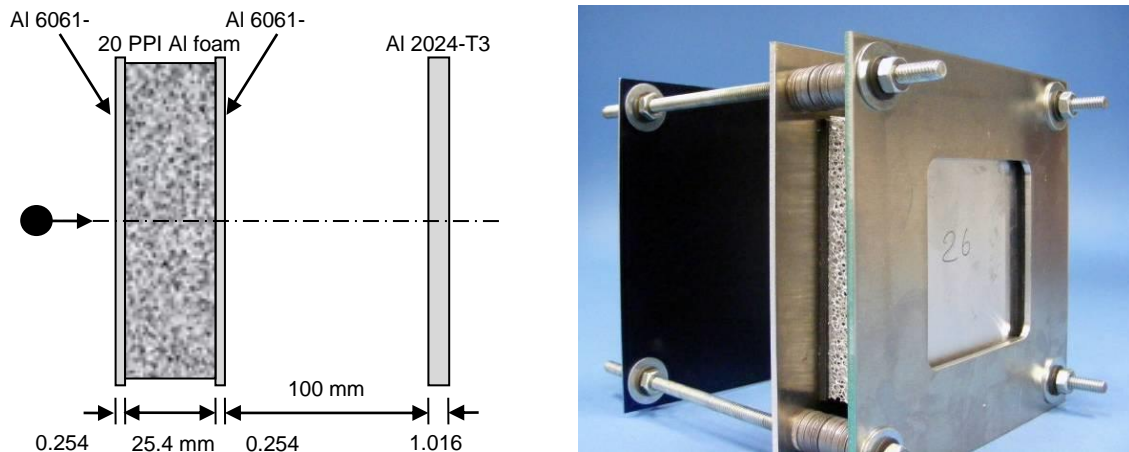


**Figure 16:** Schematic (left) and photograph (right) of target 1.0" Al F20.

### 1.0" Al F20 (NASA)

The 1.0" Al F20 (NASA) target consists of a 25.40 mm thick sandwich panel with an open-cell aluminum foam core and 0.254 mm thick Al6061-O facesheets, bonded using HYSOL EA-934NA epoxy paste adhesive. The foam core has a nominal density 6%-8% that of the base Al6101-T6 material ( $\rho = 2.70 \text{ g/cm}^3$ ) and is manufactured by ERG Aerospace (Oakland). F20 indicates the pore density of the foam is 20 PPI. Assembly of the structural panel was performed by NASA Johnson Space Center (JSC). Target assembly is identical to that of the 1.0" Al F20 (ERG) panel. The areal density of the target is measured as  $0.77 \text{ g/cm}^2$ .

### 1.0" Al F40 (ERG)

The 1.0" Al F40 target consists of a 25.40 mm thick sandwich panel with an open-cell aluminum foam core and 0.254 mm thick Al6061-T6 facesheets, bonded using Scotch-Weld AF 163-2M (0.0095 in.) modified epoxy structural adhesive film. The foam core has a nominal density of 6%-8% that of the base Al6101-T6 material ( $\rho = 2.70 \text{ g/cm}^3$ ) and is manufactured by ERG Aerospace. F40 indicates the pore density of the foam is 40 PPI, details of which are shown in Figure 17. Assembly of the structural panel was performed by ERG Aerospace. The areal density of the target is measured as  $0.81 \text{ g/cm}^2$ .

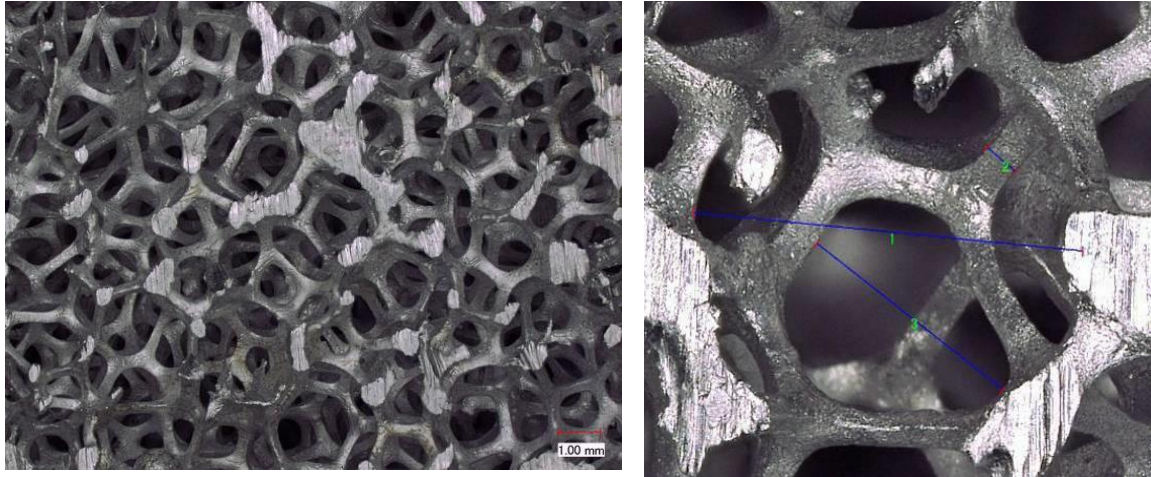


**Figure 17:** Characterization of the 40 PPI foam structure. Cell size (1) = 2.63 mm, pore size (3) = 1.59 mm, ligament width (2) = 251  $\mu\text{m}$ .

For normal impact tests a  $101.6 \times 101.6$  mm ( $4 \times 4$  in.) target is used, which is mounted in a target frame that exposes a  $76.2 \times 76.2$  mm ( $3 \times 3$  in.) area of the sandwich panel front and rear facesheets. For oblique impact tests, a larger  $152.4 \times 152.4$  mm ( $6 \times 6$  in.) target is used, mounted in a target frame that exposes a  $127.0 \times 127.0$  mm ( $5 \times 5$  in.) area of the target. A 1.016 mm (0.04 in.) thick Al6061-T6 witness plate is spaced 100 mm from the rear side of the sandwich panel, held in place via threaded rods. The witness plate is dusted with a thin coat of blue paint to enhance the visibility of ejecta deposits. The target configuration is shown in Figure 18.

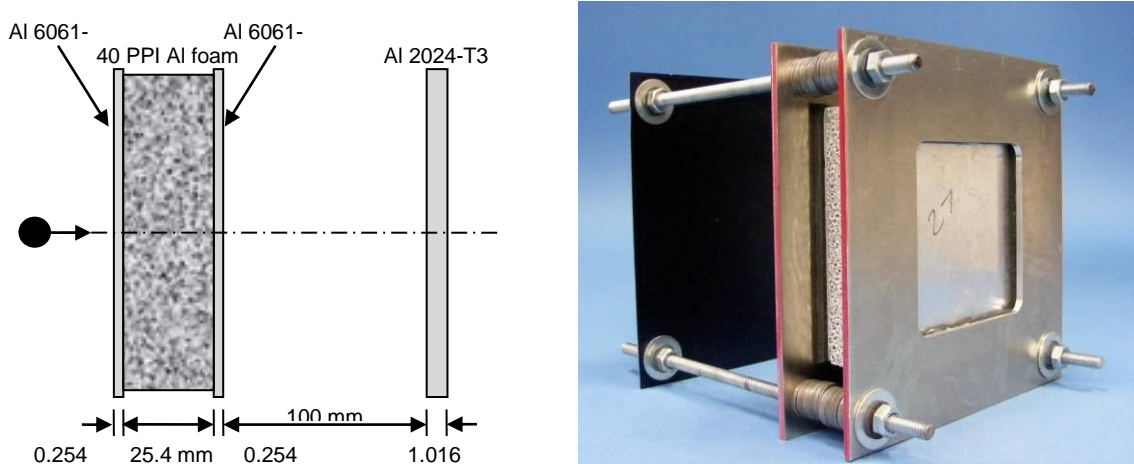


**Figure 18:** Schematic (left) and photograph (right) of target 1.0" Al F40.

### 1.0" Al F40 (NASA)

The 1.0" Al F40 (NASA) target consists of a 25.40 mm thick sandwich panel with an open-cell aluminum foam core and 0.254 mm thick Al6061-O facesheets, bonded using HYSOL EA-934NA epoxy paste adhesive. The foam core has a nominal density 6%-8% that of the base Al6101-T6 material ( $\rho = 2.70$  g/cm $^3$ ) and is manufactured by ERG Aerospace (Oakland). F20 indicates the pore density of the foam is 40 PPI. Assembly of the structural panel was performed by NASA JSC. Target assembly is identical to that of the 1.0" Al F40 (ERG) panel. The areal density of the target is measured as 0.77 g/cm $^2$ .

### 1.0" Al F40 (3%-5%)

The 1.0" Al F40 (3%-5%) target consists of a 25.40 mm thick sandwich panel with an open-cell aluminum foam core and 0.254 mm thick Al6061-T6 facesheets, bonded using Scotch-Weld AF 163-2M (0.0095 in.) modified epoxy structural adhesive film. The foam core has a nominal density 3%-5% that of the base Al6101-T6 material ( $\rho = 2.70 \text{ g/cm}^3$ ) and is manufactured by ERG Aerospace (Oakland). F40 indicates the pore density of the foam is 40 PPI, details of which are shown in Figure 19. The areal density of the 1.0" Al F40 (3%-5%) target is measured as  $0.66 \text{ g/cm}^2$ . Target assembly is identical to the 1.0" Al F40 (ERG) panel.

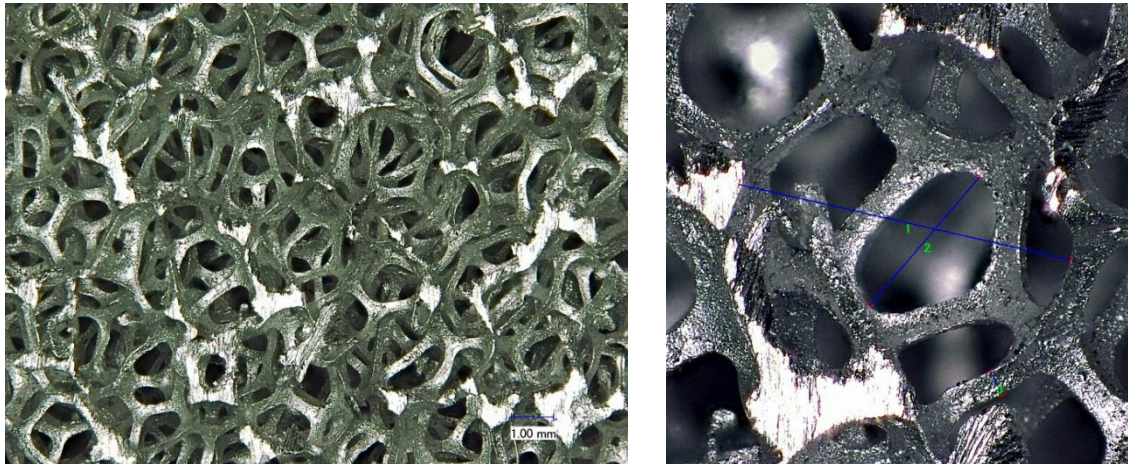


**Figure 19:** Characterization of the 40 PPI ( $\rho_{\text{rel}} = 3\%-5\%$ ) foam structure. Cell size (1) = 2.68 mm, pore size (3) = 1.34 mm, ligament width (2) = 210  $\mu\text{m}$ .

### Summary of Phase 1 targets

A comparison of the three foam cores considered during Phase 1 of this study is made in Figure 20 and Table 1. An overview of the target configurations for Phase 1 is made in Table 2.

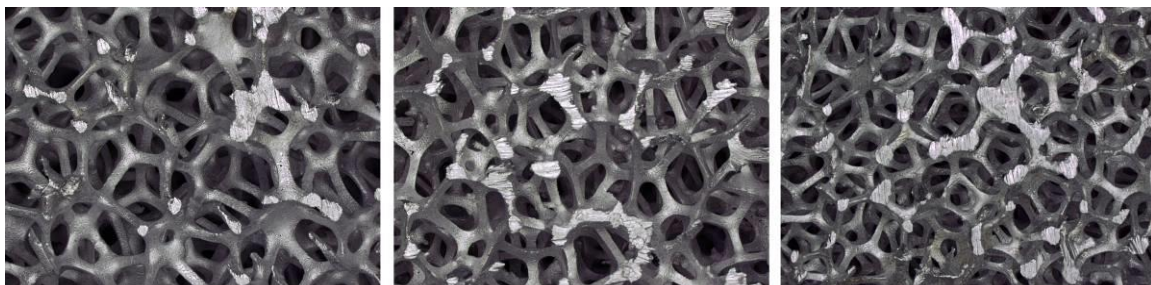


**Figure 20:** Foam core structure ( $\times 20$  magnification). From left to right: F10, F20, F40.

**Table 1:** Characteristic measurements of the foam cores.

Pore density	Cell size (mm)	Pore size (mm)	Ligament width ( $\mu\text{m}$ )
10 PPI ( $\rho_{\text{rel}} = 6\%-8\%$ )	3.95	2.33	382
20 PPI ( $\rho_{\text{rel}} = 6\%-8\%$ )	3.28	1.78	329
40 PPI ( $\rho_{\text{rel}} = 6\%-8\%$ )	2.63	1.59	251
40 PPI ( $\rho_{\text{rel}} = 3\%-5\%$ )	2.68	1.34	210

**Table 2:** Summary of Phase 1 target configurations

Target	Core			Facesheet		Adhesive type (-)	Areal density (g/cm <sup>2</sup> )
	Material (-)	Thickness (mm)	PPI	Material (-)	Thickness (mm)		
1.0" Al F10 (ERG)	Al6101-T6	25.4	10	Al6061-T6	0.254	AF 163-2M	0.794
1.0" Al F10 (NASA)	Al6101-T6	25.4	10	Al6061-O	0.254	EA-934NA	0.781
1.0" Al F20 (ERG)	Al6101-T6	25.4	20	Al6061-T6	0.254	AF 163-2M	0.767
1.0" Al F20 (NASA)	Al6101-T6	25.4	20	Al6061-O	0.254	EA-934NA	0.769
1.0" Al F40 (ERG)	Al6101-T6	25.4	40	Al6061-T6	0.254	AF 163-2M	0.807
1.0" Al F40 (NASA)	Al6101-T6	25.4	40	Al6061-O	0.254	EA-934NA	0.768
1.0" Al F40 (3%-5%)	Al6101-T6	25.4	40	Al6061-T6	0.254	AF 163-2M	0.664

## Phase 2 Articles and Setup

### 0.5" Al F40

The 0.5" Al F10 target consists of a 12.70 mm thick sandwich panel with an open-cell aluminum foam core and 0.254 mm thick Al6061-T6 facesheets, bonded using Scotch-Weld AF 163-2M (0.0095 in.) modified epoxy structural adhesive film. The foam core has a nominal density 6%-8% that of the base Al6101-T6 material ( $\rho = 2.70 \text{ g/cm}^3$ ) and is manufactured by ERG Aerospace (Oakland). F40 indicates the pore density of the foam is 40 PPI, details of which are shown in previously in Figure 17. The areal density of the target was measured as 0.50 g/cm<sup>2</sup>.

A 1.016 mm thick Al6061-T6 witness plate is attached to the rear of the target via threaded rods that maintain a spacing of 100 mm (measured from the rear facesheet surface). The lateral dimensions of both the sandwich panel and witness plate are 152.4 × 152.4 mm (6 × 6 in.). The target configuration is shown in Figure 21.

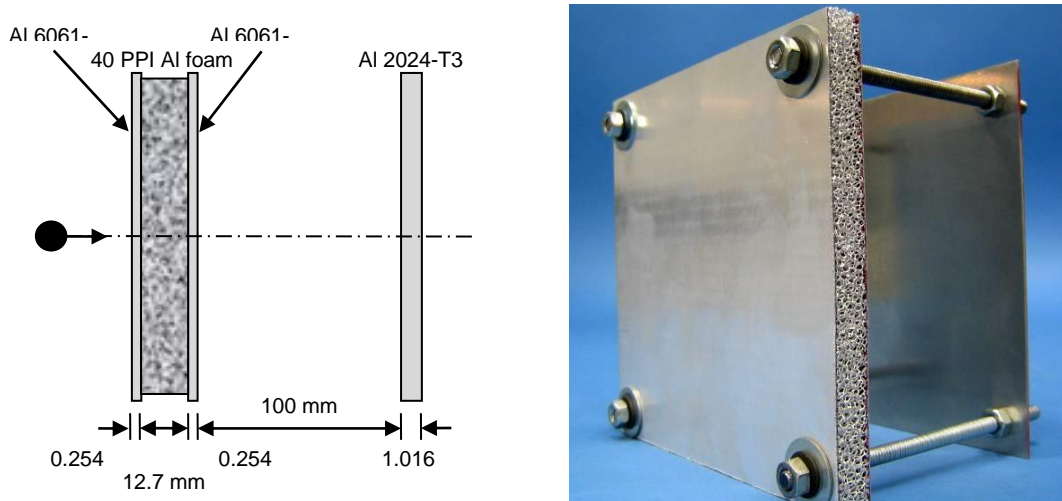


**Figure 21:** Schematic (left) and photograph (right) of the 0.5" Al F40 target.

## 2.0" Al F40

The 2.0" Al F10 target consists of a 50.80 mm thick sandwich panel with an open-cell aluminum foam core and 0.254 mm thick Al6061-T6 facesheets, bonded using Scotch-Weld AF 163-2M (0.0095 in.) modified epoxy structural adhesive film. The foam core is nominally identical to that used in the 0.5" Al F40 panel, details of which are shown previously in Figure 17. The areal density of the target was measured as 1.32 g/cm<sup>2</sup>.

A 1.016 mm thick Al6061-T6 witness plate is attached to the rear of the target via threaded rods that maintain a spacing of 100 mm (measured from the rear facesheet surface). The lateral dimensions of both the sandwich panel and witness plate are 152.4 × 152.4 mm (6 × 6 in.). The target configuration is shown in Figure 22.

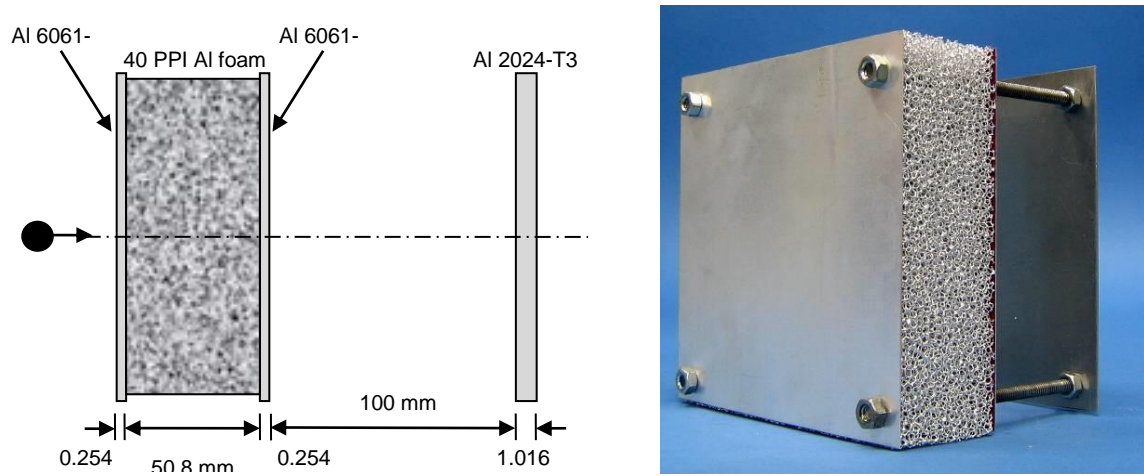


**Figure 22:** Schematic (left) and photograph (right) of the 2.0" Al F40 target.

## Phase 3 Articles and Setup

### 1.0" Al F40 B1W2

The 1.0" Al F40 B1W2 target consists of a 25.40 mm thick sandwich panel with an open-cell aluminum foam core and Al6061-T6 facesheet facesheets, bonded using Scotch-Weld AF 163-2M (0.0095 in.) modified epoxy structural adhesive film. The front facesheet is 0.254 mm thick, and the rear facesheet is 0.508 mm thick. The foam core has a nominal density 6%-8% that of the base Al6101-T6 material ( $\rho = 2.70 \text{ g/cm}^3$ ) and is manufactured by ERG Aerospace (Oakland). F40 indicates the pore density of the foam is 40 PPI, details of which are shown previously in Figure 17. The areal density of the 1.0" Al F40 B1W2 target was measured as 0.80 g/cm<sup>2</sup>.

A 1.016 mm thick Al6061-T6 witness plate is attached to the rear of the target via threaded rods that maintain a spacing of 100 mm (measured from the rear facesheet surface). The lateral dimensions of both the sandwich panel and witness plate are 152.4 × 152.4 mm (6 × 6 in.). A target schematic is shown in Figure 23.

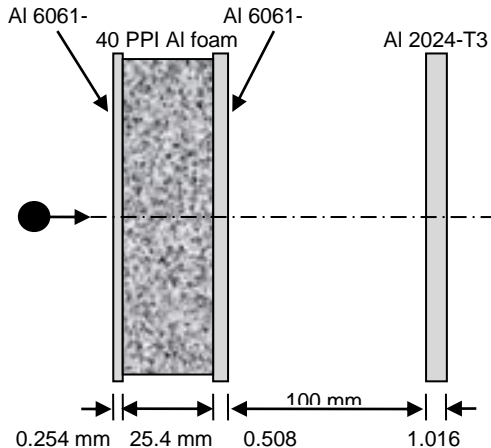


**Figure 23:** Schematic of the 1.0" Al F40 B1W2 target.

### 1.0" Al F40 B2W2

The 1.0" Al F40 B2W2 target consists of a 25.40 mm thick sandwich panel with an open-cell aluminum foam core and Al6061-T6 facesheets, bonded using Scotch-Weld AF 163-2M (0.0095 in.) modified epoxy structural adhesive film. The front facesheet is 0.4064 mm thick, and the rear facesheet is 0.508 mm thick. The foam core has a nominal density 6%-8% that of the base Al6101-T6 material ( $\rho = 2.70 \text{ g/cm}^3$ ) and is manufactured by ERG Aerospace (Oakland). F40 indicates the pore density of the foam is 40 PPI, details of which are shown previously in Figure 17. The areal density of the 1.0" Al F40 B2W2 target was measured as  $0.82 \text{ g/cm}^2$ .

A 1.016 mm thick Al6061-T6 witness plate is attached to the rear of the target via threaded rods that maintain a spacing of 100 mm (measured from the rear facesheet surface). The lateral dimensions of both the sandwich panel and witness plate are  $152.4 \times 152.4 \text{ mm}$  (6 × 6 in.). A target schematic is shown in Figure 24.

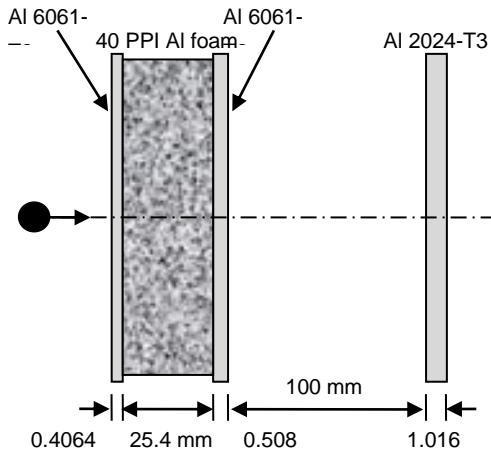


**Figure 24:** Schematic of the 1.0" Al F40 B2W2 target.

### 1.0" Al F40 B3W2

The 1.0" Al F40 B3W2 target consists of a 25.40 mm thick sandwich panel with an open-cell aluminum foam core and Al6061-T6 facesheets, bonded using Scotch-Weld AF 163-2M (0.0095 in.) modified epoxy structural adhesive film. The front facesheet is 0.508 mm thick, and the rear facesheet is

0.508 mm thick. The foam core has a nominal density 6%-8% that of the base Al6101-T6 material ( $\rho = 2.70 \text{ g/cm}^3$ ) and is manufactured by ERG Aerospace (Oakland). F40 indicates the pore density of the foam is 40 PPI, details of which are shown previously in Figure 17. The areal density of the 1.0" Al F40 B3W2 target was measured as  $0.85 \text{ g/cm}^2$ .

A 1.016 mm thick Al6061-T6 witness plate is attached to the rear of the target via threaded rods that maintain a spacing of 100 mm (measured from the rear facesheet surface). The lateral dimensions of both the sandwich panel and witness plate are  $152.4 \times 152.4 \text{ mm}$  ( $6 \times 6 \text{ in.}$ ). A target schematic is shown in Figure 25.

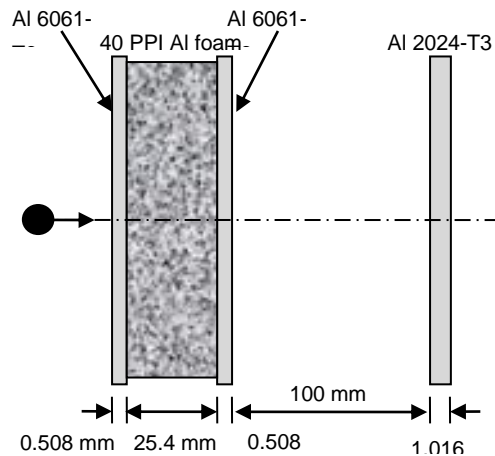


**Figure 25:** Schematic (left) and photograph (right) of the 1.0" Al F40 B3W2 target.

### 1.0" Al F40 B3W3

The 1.0" Al F40 B3W3 target consists of a 25.40 mm thick sandwich panel with an open-cell aluminum foam core and Al6061-T6 facesheets, bonded using Scotch-Weld AF 163-2M (0.0095 in.) modified epoxy structural adhesive film. The front facesheet is 0.508 mm thick, and the rear facesheet is 0.8128 mm thick. The foam core has a nominal density 6%-8% that of the base Al6101-T6 material ( $\rho = 2.70 \text{ g/cm}^3$ ) and is manufactured by ERG Aerospace (Oakland). F40 indicates the pore density of the foam is 40 PPI, details of which are shown previously in Figure 17. The areal density of the 1.0" Al F40 B3W3 target was measured as  $0.92 \text{ g/cm}^2$ .

A 1.016 mm thick Al6061-T6 witness plate is attached to the rear of the target via threaded rods that maintain a spacing of 100 mm (measured from the rear facesheet surface). The lateral dimensions of both the sandwich panel and witness plate are  $152.4 \times 152.4 \text{ mm}$  ( $6 \times 6 \text{ in.}$ ). A target schematic is shown in Figure 26.

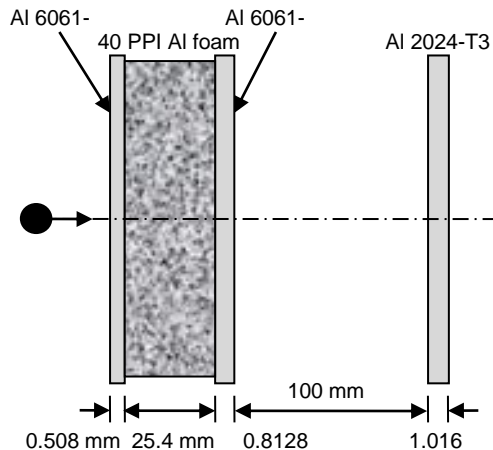


**Figure 26:** Schematic (left) and photograph (right) of the 1.0" Al F40 B3W3 target.

### Summary of Phase 3 targets

An overview of the Phase 3 targets is given in Table 3.

**Table 3:** Summary of Phase 3 target configurations

Target	Core		Front Facesheet		Rear Facesheet		Areal density (g/cm <sup>2</sup> )	
	Material (-)	Thickness (mm)	PPI	Material (-)	Thickness (mm)	Material (-)	Thickness (mm)	
1.0" Al F40 B1W2	Al6101-T6	25.4	40	Al6061-T6	0.254	Al6061-T6	0.508	0.802
1.0" Al F40 B2W2	Al6101-T6	25.4	40	Al6061-T6	0.4064	Al6061-T6	0.508	0.821
1.0" Al F40 B3W2	Al6101-T6	25.4	40	Al6061-T6	0.508	Al6061-T6	0.508	0.850
1.0" Al F40 B3W3	Al6101-T6	25.4	40	Al6061-T6	0.508	Al6061-T6	0.8128	0.922

## Phase 4 Articles and Setup

In Phase 4, a number of alternate sandwich panels were selected for comparison with the foam core configuration.

### 2.0" Al HC

Aluminum honeycomb sandwich panels (Al HC SPs) are considered the benchmark configuration for this study. The panels selected for testing are 5.08 cm thick, with 0.127 cm thick Al6061-T6 facesheets and a 1/8-5052-.003-12.0 type honeycomb core ( $\rho_{vol} = 0.192 \text{ g/cm}^3$ ) manufactured by Teklam Corp. The Al HC SPs have a total areal density of 1.43 g/cm<sup>2</sup> (measured), approximately 20% above that of the 40 PPI panel. A schematic and photograph of the 2.0" Al HC target is provided in Figure 27.

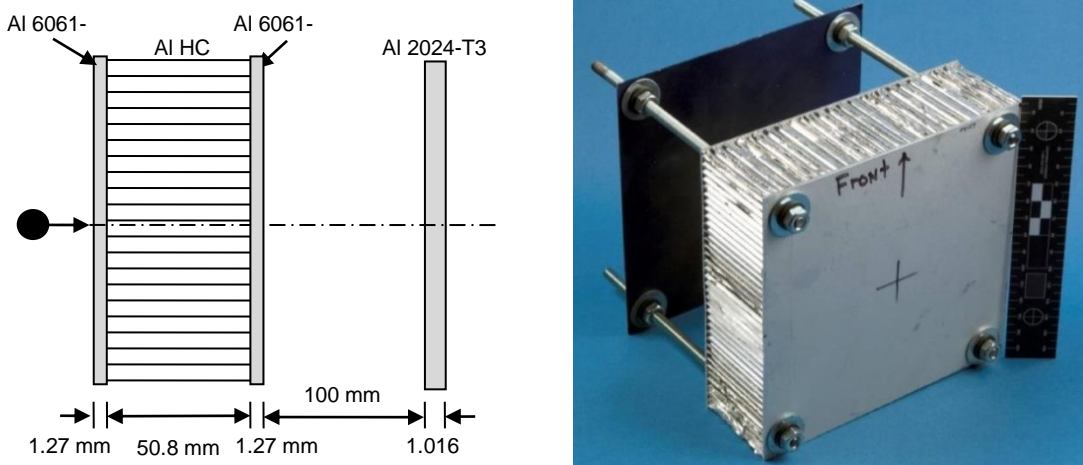


**Figure 27:** Schematic (left) and photograph (right) of the 2.0" Al HC target.

### 1.0" Trussgrid®

Trussgrid is a three-dimensional (3-D) honeycomb made of cross-laminated ( $\pm 45^\circ$ ) aluminum foil corrugations manufactured by Alcore (Edgewood, MD). By cross laminating the honeycomb foils, Trusscore provides excellent energy absorption and crush efficiency in all three dimensions. For MMOD shielding, it provides an alternative to conventional honeycomb cores without the detrimental through-thickness cell channels. The Trusscore material is shown in Figure 28.

The 1.0" Trussgrid target consists of a 25.40 mm thick sandwich panel with a 7.9-1/4-5052-N Trussgrid aluminum core and 0.508 mm thick Al6061-T6 facesheets, bonded using HYSOL EA-934NA epoxy past adhesive. The areal density of the Trussgrid panel is 0.74 g/cm<sup>2</sup> (measured), directly comparable to that of the foam core panels. A 1.016 mm thick Al6061-T6 witness plate is attached to the rear of the target via threaded rods that maintain a spacing of 100 mm (measured from the rear facesheet surface). The lateral dimensions of both the sandwich panel and witness plate are 152.4 × 152.4 mm (6 × 6 in.). The target configuration is shown in Figure 29.

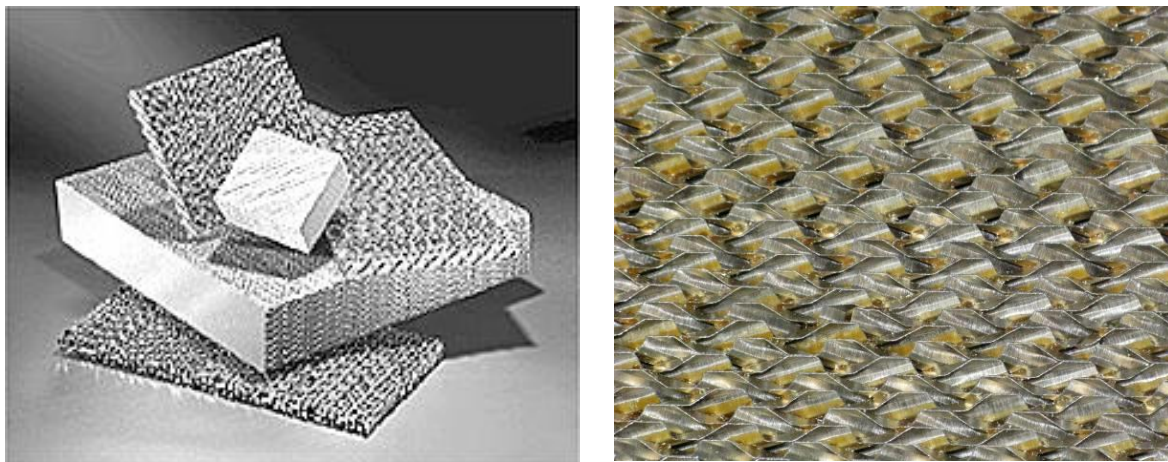


**Figure 28:** Trussgrid 3-D honeycomb

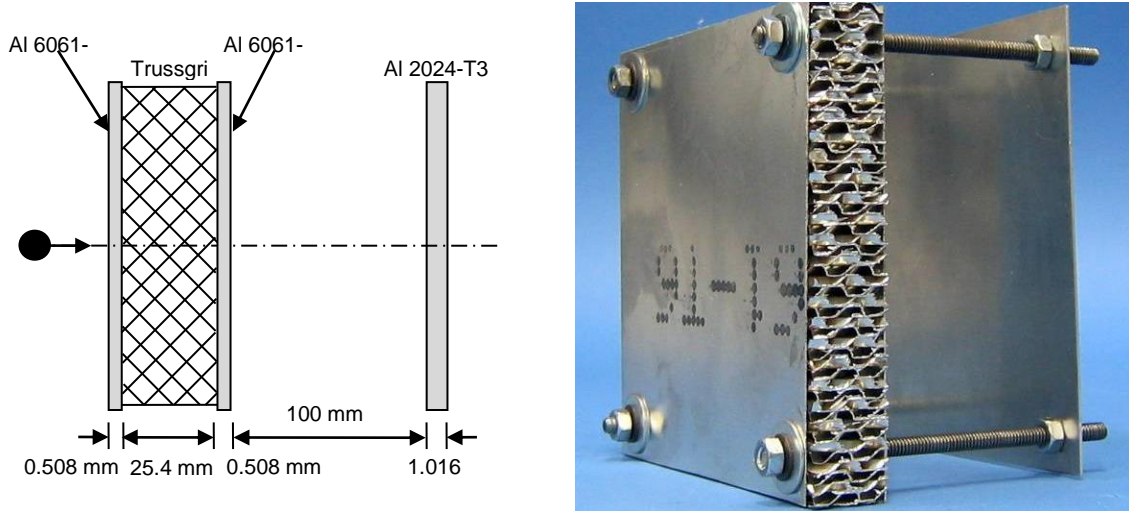


**Figure 29:** Schematic (left) and photograph (right) of the 1.0" Trussgrid target.

## 2.0" PN2 HC

Nomex is the standard for non-metallic honeycomb structures in the aerospace industry. For hypervelocity impact shielding, Nomex is of interest due to its higher ricochet angle ( $75^\circ$ - $80^\circ$ ) compared to that of aluminum alloys ( $60^\circ$ - $65^\circ$ ) as a result of lower surface hardness [13]. With a higher ricochet angle, the degree of fragment channeling within the honeycomb core should be reduced, lessening the detrimental effect of the honeycomb. An image of the Nomex honeycomb core material is shown in Figure 30.

The Nomex honeycomb targets are 5.08 cm thick, with 0.127 cm thick Al6061-T6 facesheets and a type PN2-1/8-4.0 honeycomb core ( $\rho_{vol} = 0.064 \text{ g/cm}^3$ ), manufactured by Plascore, Inc. The Nomex honeycomb panels have a total areal density of  $1.10 \text{ g/cm}^2$  (measured), approximately 8% less than that of the foam core panels. A schematic and photograph of the 2.0 PN2 HC target is provided in Figure 31.

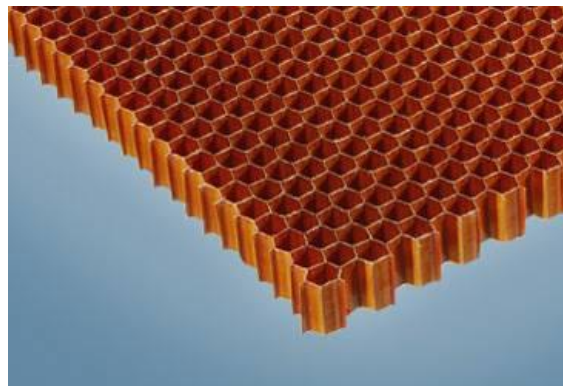


**Figure 30:** Nomex PN2 honeycomb core from Plascore, Inc.

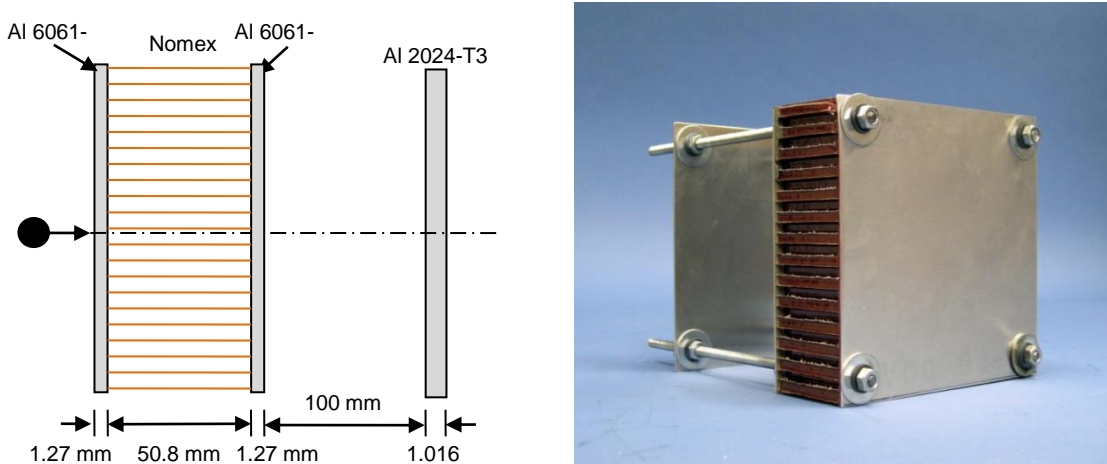


**Figure 31:** Schematic (left) and photograph (right) of the 2.0" PN2 HC target.

### 2.0" Al F-var

The F-var configuration utilizes a varying pore density foam core, consisting of 1.27 cm thick 40 PPI Al6101-T6 foam, 1.27 cm thick 20 PPI Al6101-T6 foam, and 2.54 cm thick 5 PPI Al6061-T6 foam. The individual foam layers are bonded together using Epibond 1210-A resin with hardener 9615A. The foam core is sandwiched with 0.0254 cm thick Al6061-T6 facesheets, bonded to the foam core using Scotch-Weld AF 163-2M (0.0095 in.) modified epoxy structural adhesive film.

The F-var panel is impacted at two orientations: (1) with the higher PPI sections impacted first (i.e. 40/20/5 PPI in order of impact); and (2) with the lower PPI sections impact first (i.e. 5/20/40 PPI). The underlying hypothesis for both panel orientations is given:

1. 40/20/5 configuration: Higher PPI foams are more capable of inducing projectile and front facesheet fragmentation due to an increased number of secondary impacts on foam ligaments. Following fragmentation, a lower PPI foam should permit a higher degree of lateral expansion (relative to higher PPI material), dispersing the debris cloud over a larger area of the panel rear facesheet.
2. 5/20/40 configuration: With increasing levels of fracture, the size of individual fragments decrease, and the probability of secondary impacts upon foam ligaments decreases. This configuration locates the larger pores at the outer edge of the core where the fragment cloud is concentrated in a small volume and consists of larger individual bodies. As the fragments propagate through the core thickness, the size of foam cells decreases, maximizing the probability of secondary impacts.

The 2.0" Al F-var panels have a total areal density of 1.31 g/cm<sup>2</sup>, approximately 10% greater than the baseline 40 PPI panel. Schematics and photographs of the two target setups are provided in Figure 32 and Figure 33.

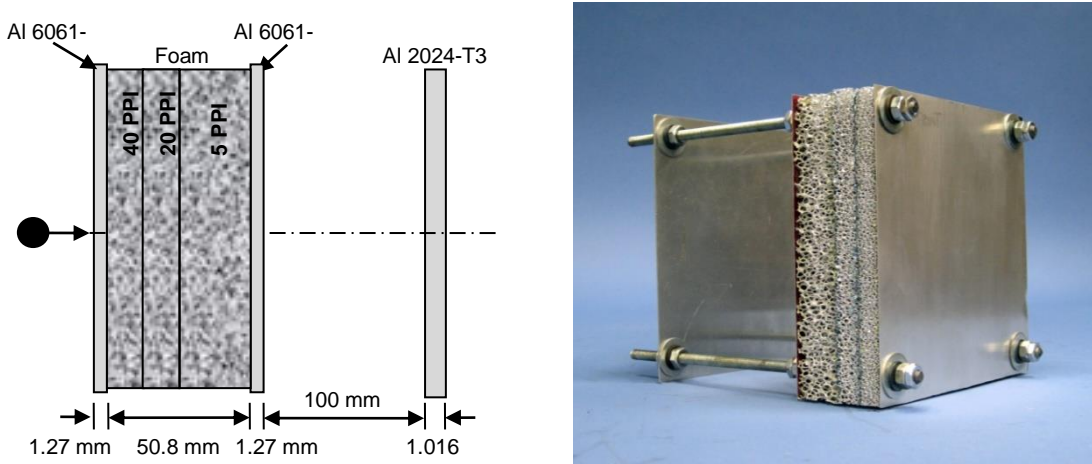


**Figure 32:** Schematic (left) and photograph (right) of the 2.0" Al F-var (40/20/5) target.

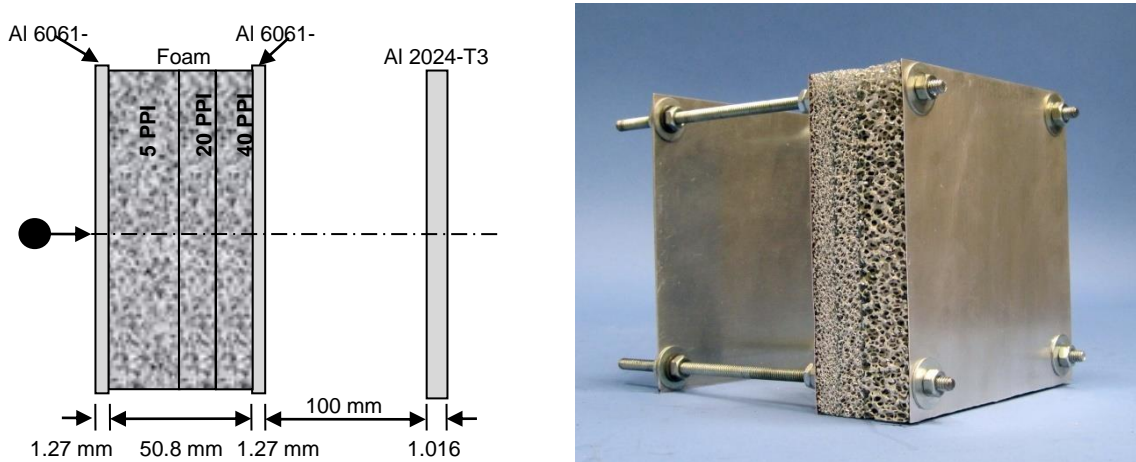


**Figure 33:** Schematic (left) and photograph (right) of the 2.0" Al F-var (5/20/40) target.

### 2.0" Al F-var (Kevlar/epoxy composite (K/E))

Typical damage features in thick porous targets include a large open cavity and deeper, narrow craters formed by individual fragments (herein referred to as "fingers"), shown in Figure 34. In preliminary investigations (e.g. [10]) it can be noted that the failure threshold of foam core sandwich panels with thin rear facesheets (relative to core thickness) is commonly exceeded by individual fragments that penetrate substantially deeper than the large open cavity. In advanced multi-wall shields – e.g. stuffed Whipple shield – intermediate layers of Kevlar fabric are added to impede the progress of residual projectile and bumper fragments.

The 2.0" Al F-var (K/E) configuration incorporates a layer of K/E within the sandwich panel foam core, intended to slow or stop the penetration of intact fragments. The panel core is 5.08 cm thick, consisting of 2.45 cm thick 40 PPI Al6101-T6 foam, and 2.45 cm 5 PPI Al6101-T6 foam separated by a 0.18 cm thick K/E, bonded together using Epibond 1210-A resin with hardener 9615A. The composite consists of four layers of Kevlar 710 plain weave fabric, impregnated with Pro-set 125/229 epoxy. The foam core is sandwiched between 0.0254 cm thick Al6061-T6 facesheets, bonded to the foam core using Scotch-Weld AF 163-2M (0.0095 in.) modified epoxy structural adhesive film.

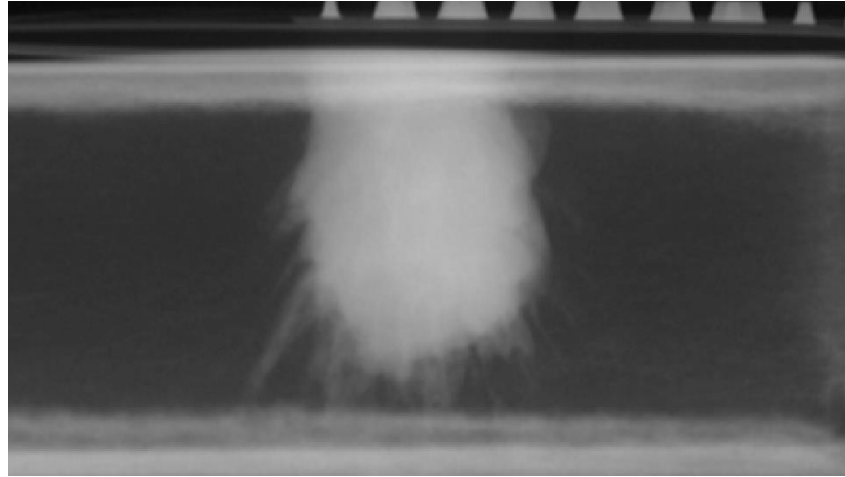


**Figure 34:** X-ray of impact damage in an AETB-8 thermal tile demonstrating a large open cavity and multiple “finger” craters from intact projectile fragments.

The 2.0" Al F-var (K/E) panels are impacted at two orientations: (1) with the 40 PPI foam layer impacted first; and (2) with the 5 PPI foam layer impacted first. The panels have a total areal density of  $1.12 \text{ g/cm}^2$ , approximately 6% less than that of the baseline 40 PPI panel. Schematics and photographs of the two target setups are provided in Figure 35 and Figure 36.

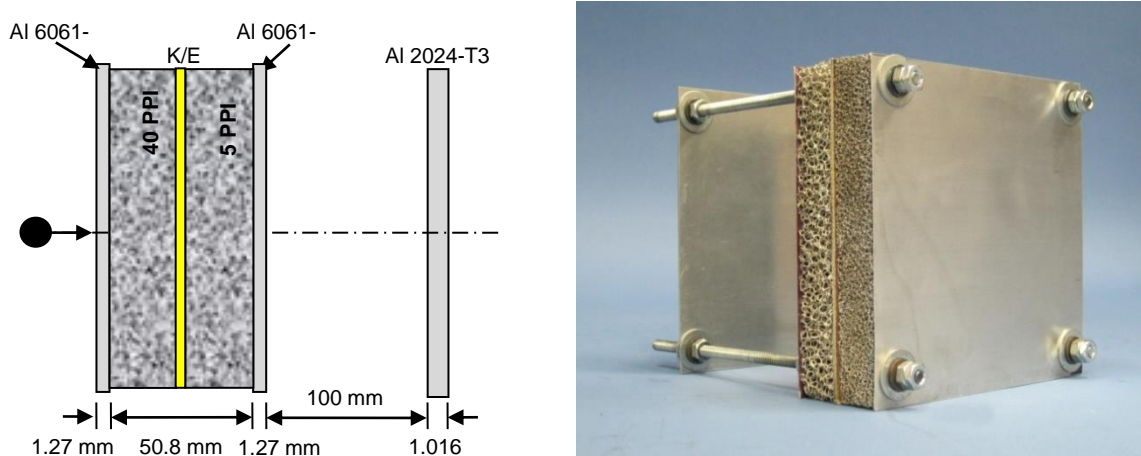


**Figure 35:** Schematic (left) and photograph (right) of the 2.0" Al F-var (K/E) target.

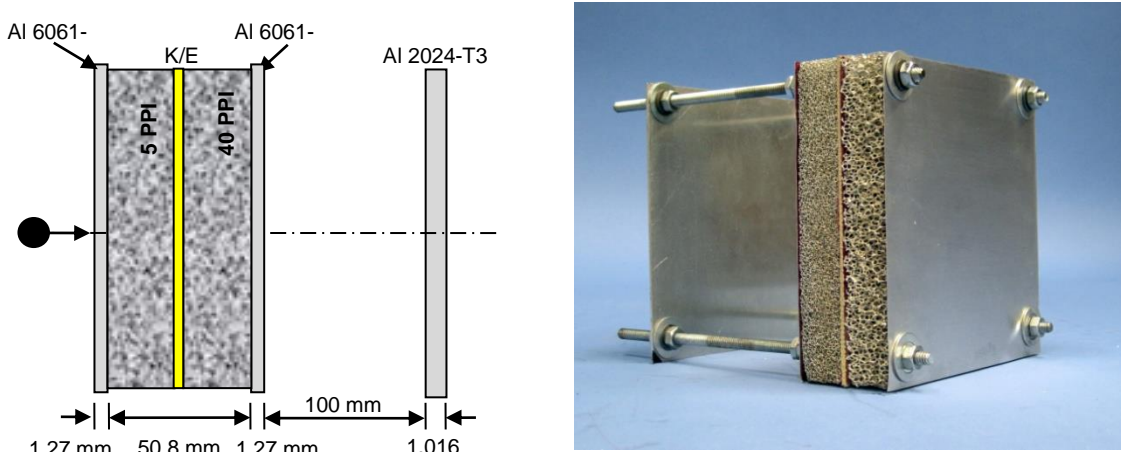


**Figure 36:** Schematic (left) and photograph (right) of the reversed 2.0" Al F-var (K/E) target.

### 2.0" Al F-var (Nextel/epoxy composite (N/E))

Similar to the Kevlar/epoxy insert configuration, the 2.0" Al F-var (N/E) target includes an intermediate composite reinforcement. Unlike the high-strength K/E composite, which is expected to slow or capture solid fragments, the role of the N/E layer is to disrupt the remnant fragments through induced shocks, leading to particle melt/vaporization. Molten/vaporized fragments have a considerably reduced capability, compared to solid fragments, of penetrating the rear facesheet.

The 2.0" Al F-var (N/E) panels are 5.08 cm thick, consisting of 2.46 cm thick 40 PPI Al6101-T6 foam, and 2.46 cm 5 PPI Al6101-T6 foam separated by a 0.16 cm thick N/E, bonded together using Epibond 1210-A resin with hardener 9615A. The composite consists of four layers of Nextel AF10 5 harness satin weave fabric, impregnated with Pro-set 125/229 epoxy. The foam core is sandwiched between 0.0254 cm thick Al6061-T6 facesheets, bonded to the foam core using Scotch-Weld AF 163-2M (0.0095 in.) modified epoxy structural adhesive film.

The 2.0" Al F-var (N/E) panel is aligned so that the 40 PPI foam is impacted first. The panel has a total areal density of 1.11 g/cm<sup>2</sup>, approximately 7% less than that of the baseline 40 PPI panel. A schematic and photograph of the target setup is provided in Figure 35.

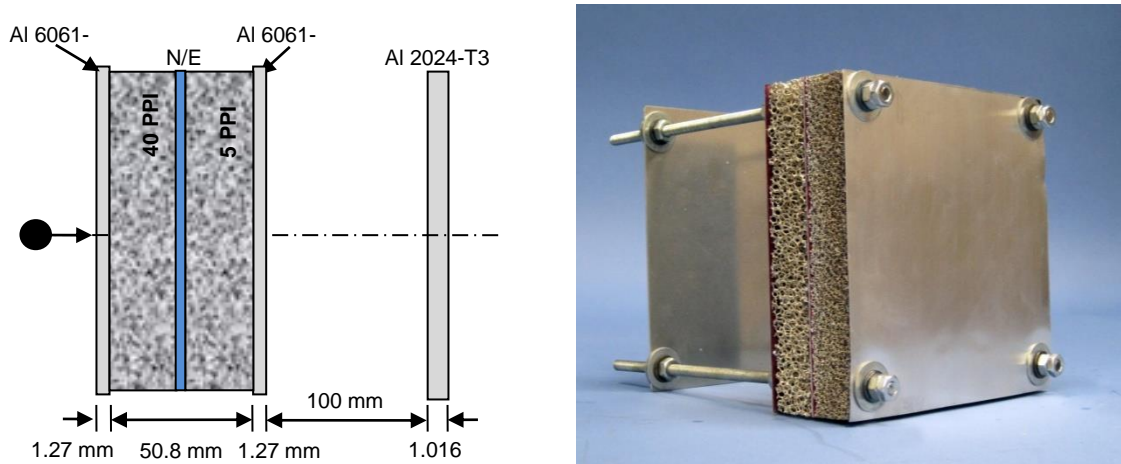


**Figure 37:** Schematic (left) and photograph (right) of the 2.0" Al F-var (N/E) target.

### **Summary of Phase 4 targets**

An overview of the Phase 4 targets is given in Table 4.

**Table 4:** Summary of Phase 3 target configurations.

Target	Core		Front Facesheet		Rear Facesheet		Areal density (g/cm <sup>2</sup> )
	Thickness (mm)	Type	Material (-)	Thickness (mm)	Material (-)	Thickness (mm)	
2.0" Al HC	50.8	1/8-5052-003-12.0	Al6061-T6	1.27	Al6061-T6	1.27	1.43
1.0" Trussgrid	25.4	7.9-1/4-5052-N	Al6061-T6	0.508	Al6061-T6	0.508	0.742
2.0" PN2 HC	50.8	PN2-1/8-4.0	Al6061-T6	1.27	Al6061-T6	1.27	1.10
2.0" Al F-var	50.8	5/20/40 PPI foam	Al6061-T6	0.254	Al6061-T6	0.254	1.31
2.0" Al F-var (K/E)	50.8	5/40 PPI foam, K/E	Al6061-T6	0.254	Al6061-T6	0.254	1.12
2.0" Al F-var (N/E)	50.8	5/40 PPI foam, K/E	Al6061-T6	0.254	Al6061-T6	0.254	1.11

## **Test Facility**

All tests have been performed at the NASA JSC White Sands Test Facility in Las Cruces, New Mexico. For projectiles smaller than 3.40 mm in diameter, testing has been performed in the facility 0.17-cal launcher [14]. For larger projectiles, the facility 0.50-cal launcher was used [15]. The flight range and target chamber of the 0.17-cal launcher was maintained at 2.5 Torr or less during testing. Projectile velocity was obtained by laser stations/intervelometers with a conservative measurement error of 0.7% or ~50 m/s. Photo diode impact flash detectors on the stripper plate and target are used as a secondary velocity measurement device (generally within ±0.02 km/s of the laser measurement). The flight range and target chamber of the 0.50-cal launcher was maintained at 6-7 Torr or less during testing. Projectile velocity was obtained by laser stations/intervelometers with a conservative measurement error of 0.3% or ~15 m/s. Photo diode impact flash detectors on the stripper plate and target are used as a secondary velocity measurement device (generally within ±0.02 km/s of the laser measurement).

## **Test Results**

For all tests, the failure threshold was defined as the onset of material ejection from the sandwich panel rear facesheet (i.e. detached spallation). Clear hole perforation and through-cracks are considered more comprehensive failures. Post-test damage measurements are made to allow a comprehensive evaluation and comparison of shielding performance. An overview of target damage measurements is given in Table 5. Schematics of the measurements are shown in Figure 38 and Figure 39.

**Table 5:** Damage measurement notation and indices.

Symbol	Description
<i>Front facesheet</i>	
$d_{h,i}$	Entry hole diameter ( $i = 1,2$ )
$D_{\text{dam},i}$	Diameter of maximum facesheet damage ( $i = 1,2$ )
<i>Rear facesheet</i>	
$d_{h,i}$	(Largest) Exit hole diameter ( $i = 1,2$ )
$N_h$	Number of perforation holes in the rear facesheet
$D_{h,i}$	Extension of area containing perforation holes ( $i = 1,2$ ) (only if multiple holes are present)
$b_{\max}$	Maximum height of rear facesheet petal/bulge
$b_{d,i}$	Diameter of bulge on rear facesheet
<i>Core</i>	
$D_{HC,\max}$	Maximum diameter of core damage
$\Delta_{h,i}$	Offset of perforation hole center (front facesheet to rear facesheet) ( $i = 1,2$ )
<i>Subscript</i>	<i>Description</i>
f	Front facesheet
r	Rear facesheet
1	Horizontal
2	Vertical

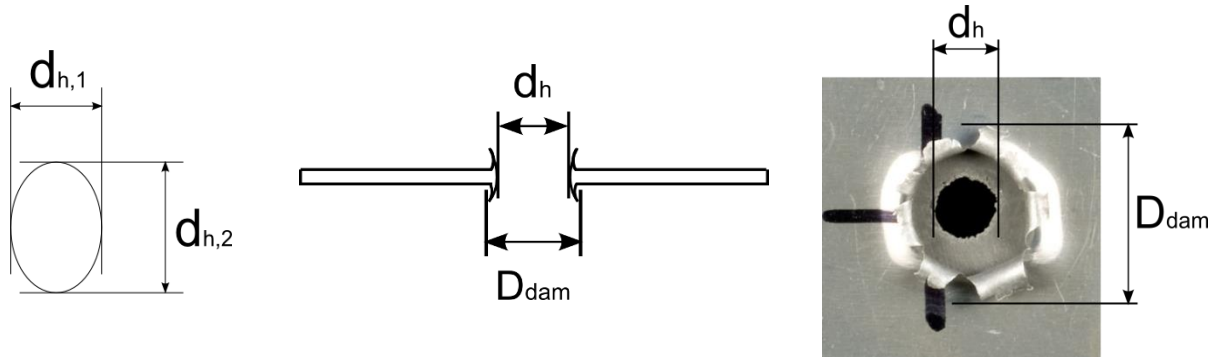


**Figure 38:** Sandwich panel damage measurement schematics.

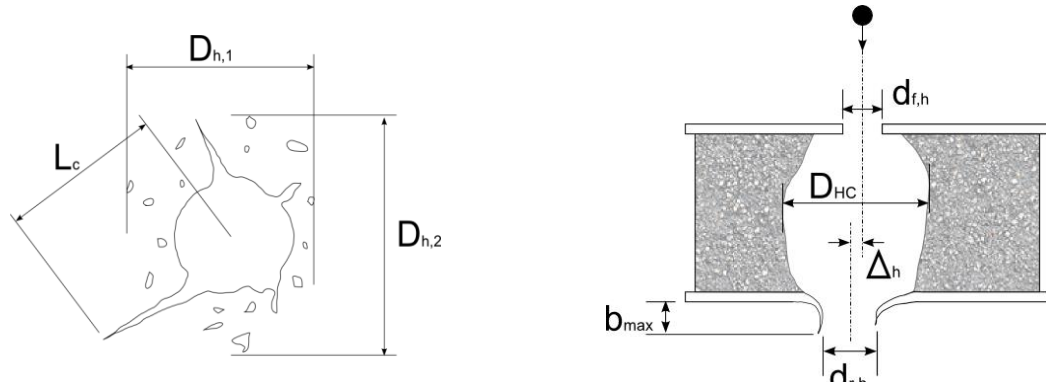


**Figure 39:** Sandwich panel damage measurement schematics (cont.).

## Assessment of Experimental Scatter

Due to the non-homogeneity of the foam microstructure, impacting projectiles or fragments may experience a significantly different shield profile during the penetration process. As such, the degree of scatter in the failure limits of foam core sandwich panels may be more significant than traditional monolithic plate-based configurations (e.g. Whipple shield). To assess scatter, a series of five nominally identical experiments were performed on the 1.0" Al F40 (ERG) target. Details of the impact tests are provided in Table 6.

**Table 6:** Experimental scatter assessment test details and results.

HITF No.	Target	Projectile		Impact conditions		Result	
		Material	Diameter r (-)	Angle (deg)	Velocity (km/s)	Coarse	Detailed
1 09065	1.0" Al F40 (ERG)	Al2017-T4	2.70	45	6.70	Pass	<
2 09066	1.0" Al F40 (ERG)	Al2017-T4	2.70	45	6.86	Pass	<
3 09067	1.0" Al F40 (ERG)	Al2017-T4	2.70	45	7.11	Pass	<
4 09068	1.0" Al F40 (ERG)	Al2017-T4	2.70	45	6.79	Pass	<
5 08569	1.0" Al F40 (ERG)	Al2017-T4	2.70	45	6.66	Perforated	>

A comparison of the core damage is shown in Figure 40. Of the five tests, one resulted in perforation of the rear facesheet (Hypervelocity Impact Technology Facility (HITF)08569), while the other four showed varying degrees of rear facesheet deformation. For the non-perforated targets, penetration depth varied from 78% (HITF09067) to 98% (HITF09066).

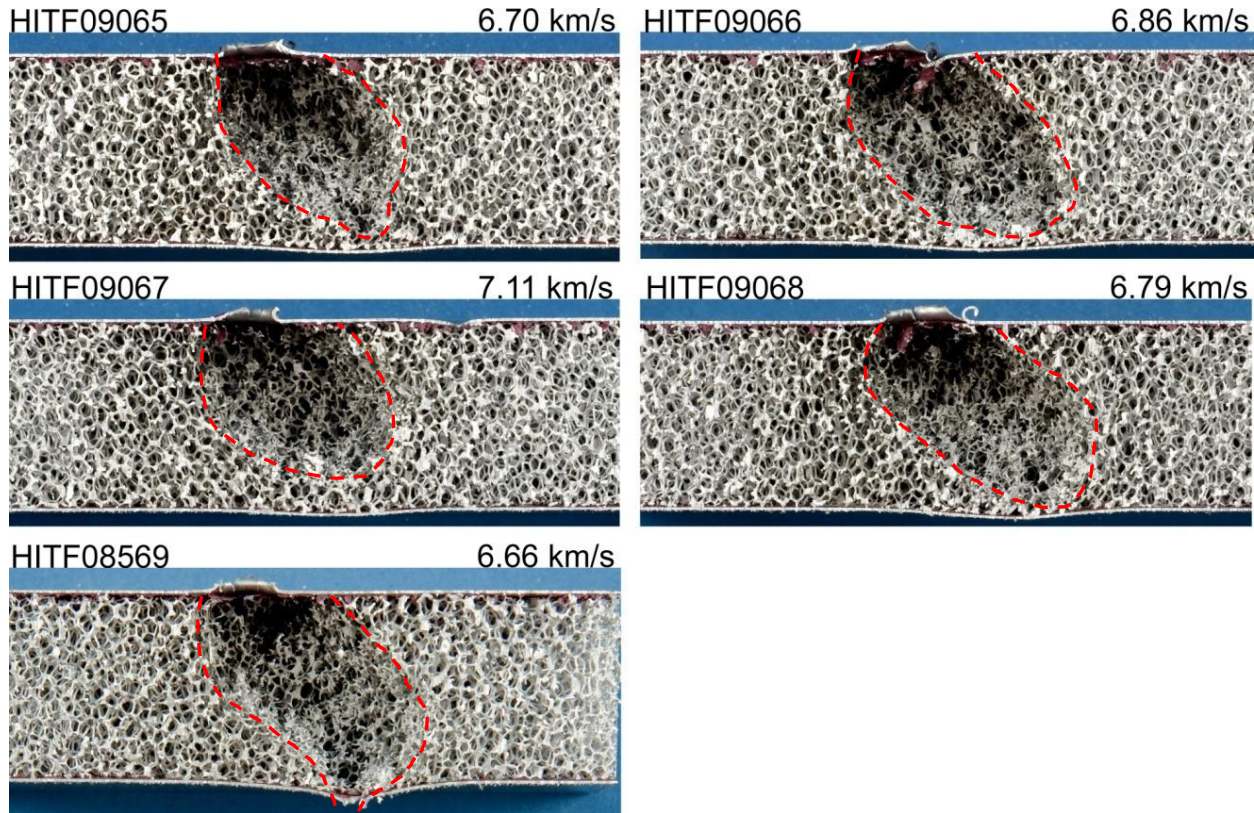


**Figure 40:** Comparison of foam core damage in five targets impacted at nominally identical conditions (2.7 mm diameter projectile, 45°, 6.8 km/s).

## **Phase 1 Test Results**

In Phase 1, there were 47 successful impact experiments performed on the 1.0" thick foam sandwich panels with cores possessing pore densities of 10, 20, and 40 PPI. An overview of the test conditions and results is given in Table 7. A complete summary of the damage measurements is provided in Appendix A.

### ***Effect of facesheet temper and adhesive type***

Two impact tests on the 1.0" Al F40 (NASA) panel were repeated at nominally identical conditions on the 1.0" Al F40 (ERG) panel to evaluate the effect of facesheet temper and adhesive type, details of which are shown in Table 8. Under impact of 2.0-mm projectiles at normal incidence, the performance of the ERG panel was superior to that of the NASA panel (see Figure 41). However, under oblique impact by 2.7-mm projectiles, the performance of the NASA panel was superior (see Figure 42).

**Table 7:** Phase 1 test results.

HITF No.	Target	Projectile		Impact conditions		Result	
		Material (-)	Diameter (mm)	Angle (deg)	Velocity (km/s)		
1	08252	1.0" Al F20 (NASA)	Al2017-T4	2.5	0	6.88	Perforated
2	08253	1.0" Al F20 (NASA)	Al2017-T4	2	0	6.85	Perforated
3	08254	1.0" Al F20 (NASA)	Al2017-T4	1.9	0	6.87	Pass
4	08255	1.0" Al F20 (ERG)	Al2017-T4	2.5	45	7.1	Perforated
5	08256	1.0" Al F20 (ERG)	Al2017-T4	2.3	45	6.88	Pass
6	08257	1.0" Al F20 (ERG)	Al2017-T4	2.5	45	6.46	Perforated
7	08258	1.0" Al F20 (ERG)	Al2017-T4	3	60	7.13	Pass
8	08259	1.0" Al F20 (ERG)	Al2017-T4	3.2	60	7.1	Perforated
9	08260	1.0" Al F20 (ERG)	Al2017-T4	3.2	60	6.68	Pass
10	08261	1.0" Al F10 (NASA)	Al2017-T4	2	0	6.87	Perforated
11	08263	1.0" Al F40 (NASA)	Al2017-T4	2	0	6.52	Perforated
12	08268	1.0" Al F10 (NASA)	Al2017-T4	2.5	45	6.62	Pass
13	08269	1.0" Al F10 (NASA)	Al2017-T4	2.7	45	7.04	Perforated
14	08270	1.0" Al F40 (NASA)	Al2017-T4	2.5	45	6.78	Pass
15	08271	1.0" Al F40 (NASA)	Al2017-T4	2.7	45	6.99	Pass
16	08272	1.0" Al F10 (ERG)	Al2017-T4	3.2	60	6.7	Perforated
17	08267	1.0" Al F40 (NASA)	Al2017-T4	3.2	60	6.57	Pass
18	09007	1.0" Al F40 (ERG)	Al2017-T4	3.4	60	6.91	Pass
19	08276	1.0" Al F20 (NASA)	Al2017-T4	2.1	0	2.46	Perforated
20	08279	1.0" Al F40 (NASA)	Al2017-T4	3.4	0	2.62	Perforated
21	08280	1.0" Al F10 (NASA)	Al2017-T4	2.1	0	2.18	Perforated
22	08420	1.0" Al F40 (ERG)	Al2017-T4	2.5	45	2.44	Perforated
23	08421	1.0" Al F40 (ERG)	Al2017-T4	2.2	45	2.68	Pass
24	08422	1.0" Al F40 (NASA)	Al2017-T4	2.5	0	2.75	Perforated
25	08424	1.0" Al F40 (ERG)	Al2017-T4	2.3	0	4.68	Perforated
26	08425	1.0" Al F20 (ERG)	Al2017-T4	2.3	0	4.71	Pass
27	08427	1.0" Al F40 (ERG)	Al2017-T4	2.6	45	4.78	Pass
28	08428	1.0" Al F40 (ERG)	Al2017-T4	2.8	45	4.76	Pass
29	08423	1.0" Al F40 (NASA)	Al2017-T4	2.1	0	2.34	Perforated
30	08567	1.0" Al F40 (NASA)	Al2017-T4	1.9	0	2.2	Pass
31	08568	1.0" Al F40 (ERG)	Al2017-T4	2	0	6.63	Pass
32	08569	1.0" Al F40 (ERG)	Al2017-T4	2.7	45	6.66	Perforated
33	08585	1.0" Al F40 (ERG)	Al2017-T4	2	0	4.43	Pass
34	09072	1.0" Al F40 (ERG)	Al2017-T4	2.2	0	3.11	Pass
35	09357	1.0" Al F40 (ERG)	Al2017-T4	2.4	0	3.25	Pass
36	09073	1.0" Al F40 (ERG)	Al2017-T4	2.2	0	5.36	Pass
37	09358	1.0" Al F40 (ERG)	Al2017-T4	2.5	0	5.48	Perforated
38	09074	1.0" Al F40 (ERG)	Al2017-T4	2.0	0	7.56	Pass
39	09359	1.0" Al F40 (ERG)	Al2017-T4	2.3	0	7.38	Perforated
40	09075	1.0" Al F40 (ERG)	Al2017-T4	2.5	45	3.76	Pass
41	09360	1.0" Al F40 (ERG)	Al2017-T4	2.8	45	3.52	Perforated
42	09362	1.0" Al F40 (ERG)	Al2017-T4	2.9	45	5.5	Pass
43	09363	1.0" Al F40 (ERG)	Al2017-T4	2.5	45	7.19	Pass
44	09364	1.0" Al F40 (ERG)	Al2017-T4	2.7	45	7.24	Pass
45	08574	1.0" Al F40 (3%-5%)	Al2017-T4	2.0	0	6.63	Perforated
46	08575	1.0" Al F40 (3%-5%)	Al2017-T4	3.4	60	6.88	Pass
47	08583	1.0" Al F40 (3%-5%)	Al2017-T4	2.1	0	2.35	Pass

**Table 8:** Details of impact tests used to evaluate difference between the NASA and ERG panels.

HITF No.	Target	Impact conditions			Result	
		Diameter (mm)	Angle (deg)	Velocity (km/s)	Coarse	Detailed
11	08263	1.0" Al F40 (NASA)	2.0	0	6.52	Perforated
31	08568	1.0" Al F40 (ERG)	2.0	0	6.63	Pass
15	08271	1.0" Al F40 (NASA)	2.7	45	6.99	Pass
32	08569	1.0" Al F40 (ERG)	2.7	45	6.66	Perforated

In both tests, the depth of penetration through the foam core is comparable for the NASA and ERG panels. The primary difference in target damage occurs on the front facesheet, where the untempered material of the NASA panel is shown to peel back around the entry hole, detaching from the foam core. The entry hole on the ERG panel is more irregular in shape, with minimal facesheet detachment. Shield performance is expected to vary with the rear wall yield strength; however, the facesheets may be insufficiently thick to capture this effect.

In test HITF08263, the foam core damage is shown to penetrate through only 80% of the total thickness. Perforation of the rear facesheet is caused by a single fragment, which propagates well beyond the depth of the main damage zone. This type of behavior is commonly observed for hypervelocity impact on porous media (e.g. silica heat insulation tiles). Although not captured in the scatter analysis, this type of behavior is responsible for the majority of uncertainty in defining the failure limits of these shields.

From the two tests performed, no clear effect of the different facesheet temper and adhesive type is discernable.

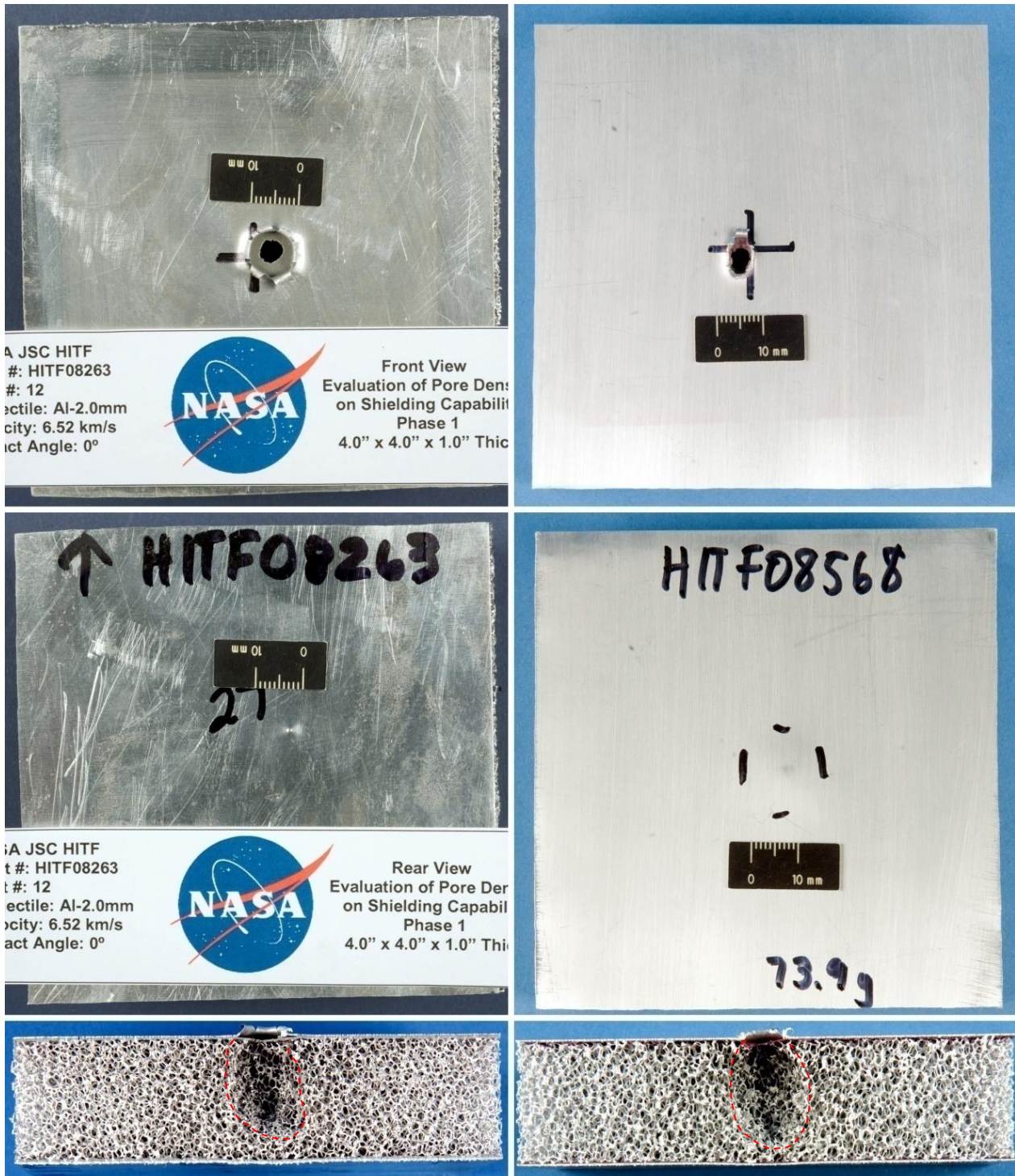


**Figure 41:** Comparison of damages in the 1.0" Al F40 NASA (left) and ERG (right) panels induced by impact of 2.0 mm diameter projectiles at nom. 6.8 km/s with normal incidence ( $0^\circ$ ). From top to bottom: front facesheet, rear facesheet, sectioned core.

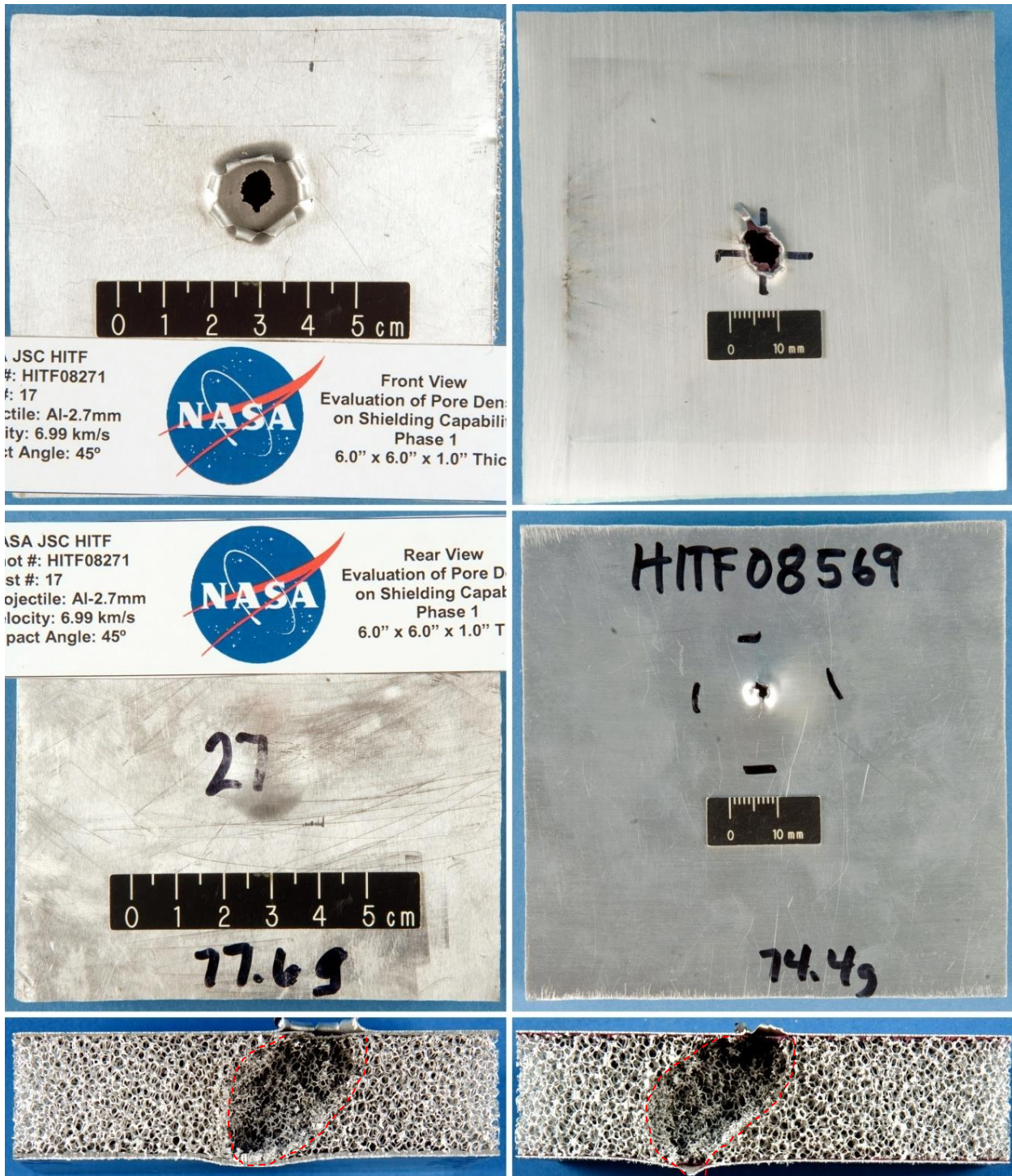


**Figure 42:** Comparison of damages in the 1.0" Al F40 NASA (left) and ERG (right) panels induced by impact of 2.7 mm diameter projectiles at nom. 6.8 km/s with oblique incidence (45°). From top to bottom: front facesheet, rear facesheet, sectioned core.

### **Effect of Pore Density (PPI)**

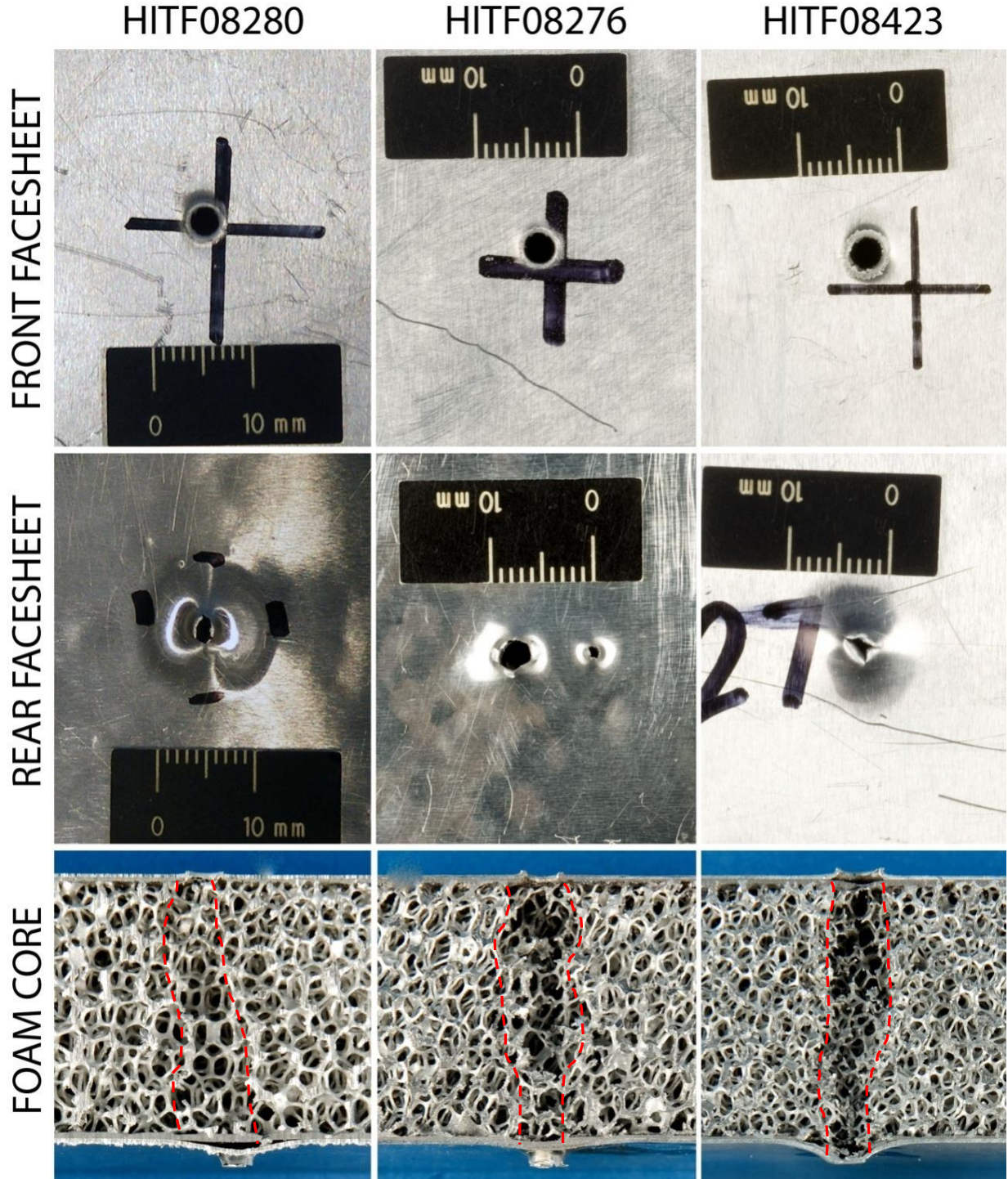
A series of four nominally identical impact tests were performed on the three variations of pore density (10, 20, 40 PPI), details of which are provided in Table 9. An additional set of five impact tests were performed on the 10 and 40 PPI panels in [10], details of which are also included in Table 9.

**Table 9:** Comparison of performance for varying PPI foam core panels at nominally identical impact conditions.

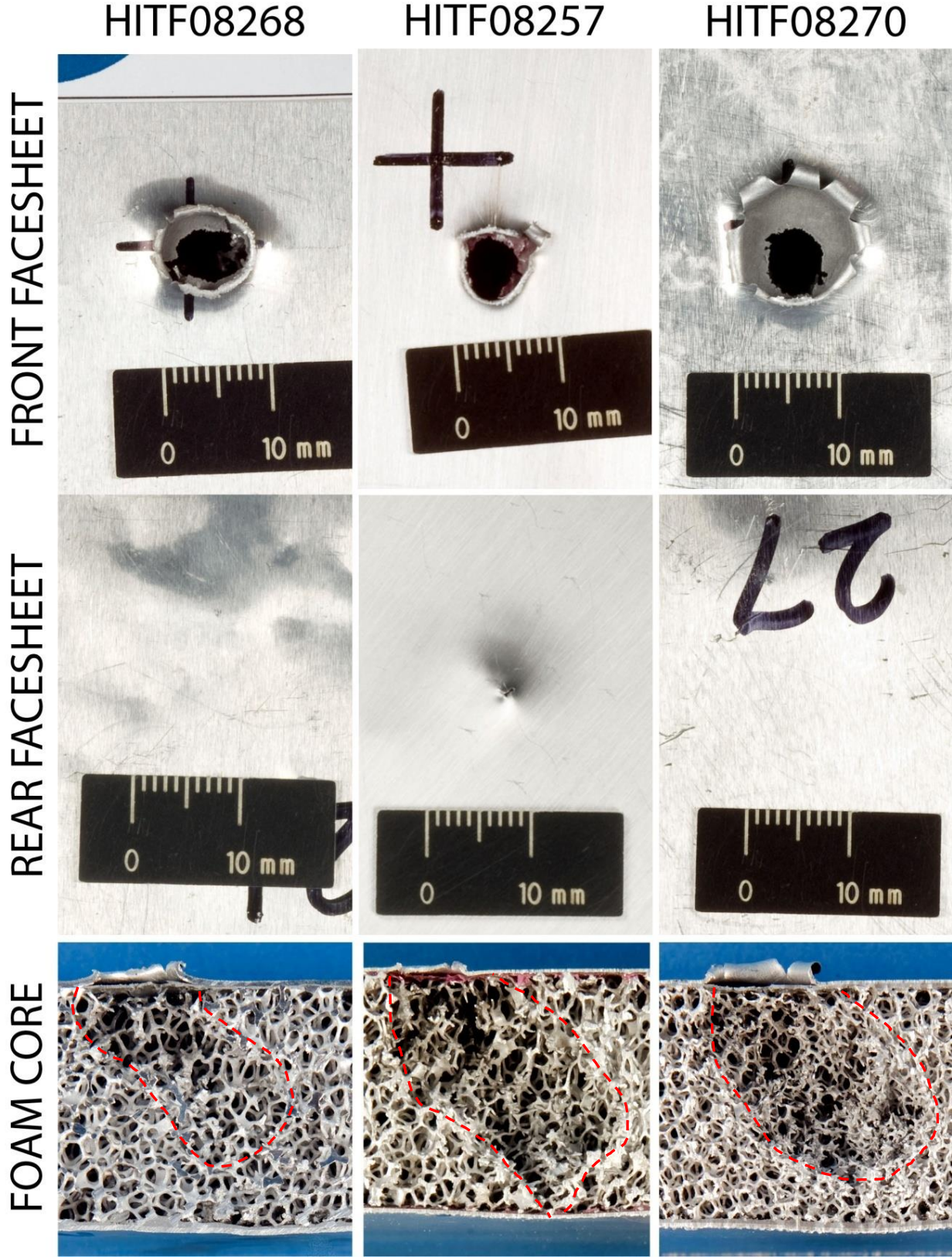
Test no. [10/20/40 PPI]	$\theta$ (deg)	Impact conditions		Result [10/20/40 PPI]	Comments
		V (km/s)	$d_p$ (mm)		
8280/8276/8423	0	2.18/2.46/2.34	2.1	>/>/>	All targets perforated with 1-2 small holes
8268/8257/8270	45	6.62/6.46/6.78	2.5	<</≥/≤<	No damage to 10/40 PPI target rear facesheets, single pin-sized perforation of 20 PPI panel
8261/8253/8263	0	6.87/6.85/6.52	2.0	≥/≥/≥	All targets with single small perforation hole
8272/8260/8267	60	6.70/6.68/6.57	3.2	>/<</<<	Small bulge on 20 and 40 PPI panel rear facesheets, single hole perforation of 10 PPI panel
3147-4/-/5036-2	0	6.87/-/6.90	1.2	>/-/-<	Perforation of 10 PPI panel, 40 PPI no damage
3148-1/-/5037-1	45	7.13/-/7.05	1.2	</-/-<	No damage to rear facesheet of 10 and 40 PPI panels
5045-1/-/8571	45	7.02/-/6.68	1.4	</-/-<	Small bulge on 40 PPI panel rear facesheet, no damage to 10 PPI panel rear facesheet
4151/-/4152	0	6.76/-/6.79	3.57	</-/-<	No damage to rear facesheet of 10 and 40 PPI panels
4161/-/4163	0	6.89/-/6.79	4.0	≥/ - / ≥	Two small perforation holes in 10 PPI panel rear facesheet, single small perforation of 40 PPI panel

Figure 43 compares the damage induced in the 10/20/40 PPI panels by impact of 2.1 mm diameter projectiles at low velocity with normal incidence. The three panels are all perforated, with similar-sized exit holes. The damage to the foam cores is comparable for the three panels, showing a roughly cylindrical progression with minor deviations. The diameter of the core damage is similar to that of the entry hole for all three panels.

In Figure 44, the performance of the 10/20/40 PPI foam core panels under oblique (45°) impact of 2.5 mm diameter projectiles at high velocity is compared. The 20 PPI panel is of type ERG, while the 10 and 40 PPI panels are type NASA. Subsequently, the entry hole in the front facesheet of the 20 PPI panel is different to that of the other two panels, showing minimal facesheet detachment from the foam core. The 40 PPI panel shows a larger degree of facesheet detachment and petalling than the 10 PPI panel. The 20 PPI panel is perforated, with a single small tear, while the rear facesheets of the 10 and 40 PPI panels are undamaged. Variations in the surface appearance of the 10 PPI rear facesheet are due to the bonding process, and are not a result of the impact test. The sectioned foam cores show the propagation of damage through to the rear facesheet of the 20 PPI panel, while damage in the 10 and 40 PPI cores only progresses through approximately 80% of their relative thicknesses.



**Figure 43:** Comparison of damage in 10 PPI (left), 20 PPI (middle), and 40 PPI (right) foam core sandwich panels impacted by 2.1 mm diameter Al2017-T4 spheres at  $2.32 \pm 0.14$  km/s and  $0^\circ$ .



**Figure 44:** Comparison of damage in 10 PPI (left), 20 PPI (middle), and 40 PPI (right) foam core sandwich panels impacted by 2.5 mm diameter Al2017-T4 spheres at  $6.62\pm0.16$  km/s and 45°.

In Figure 45, induced damages are compared following impact of 2.0 mm diameter projectiles at high velocity with normal incidence. All three panels are minimally above the ballistic limit, each with a single small perforation hole in the rear facesheet. Examination of the foam core damages show that perforation in these three tests is caused by individual fragments that penetrate well beyond the open cavity. Penetration depth of the open cavity is approximately 50%/70%/80% of the core thickness for the 10/20/40 PPI panels, respectively. Unlike the low speed tests, core damage in Figure 45 shows expansion of the debris cloud following perforation of the front facesheet.

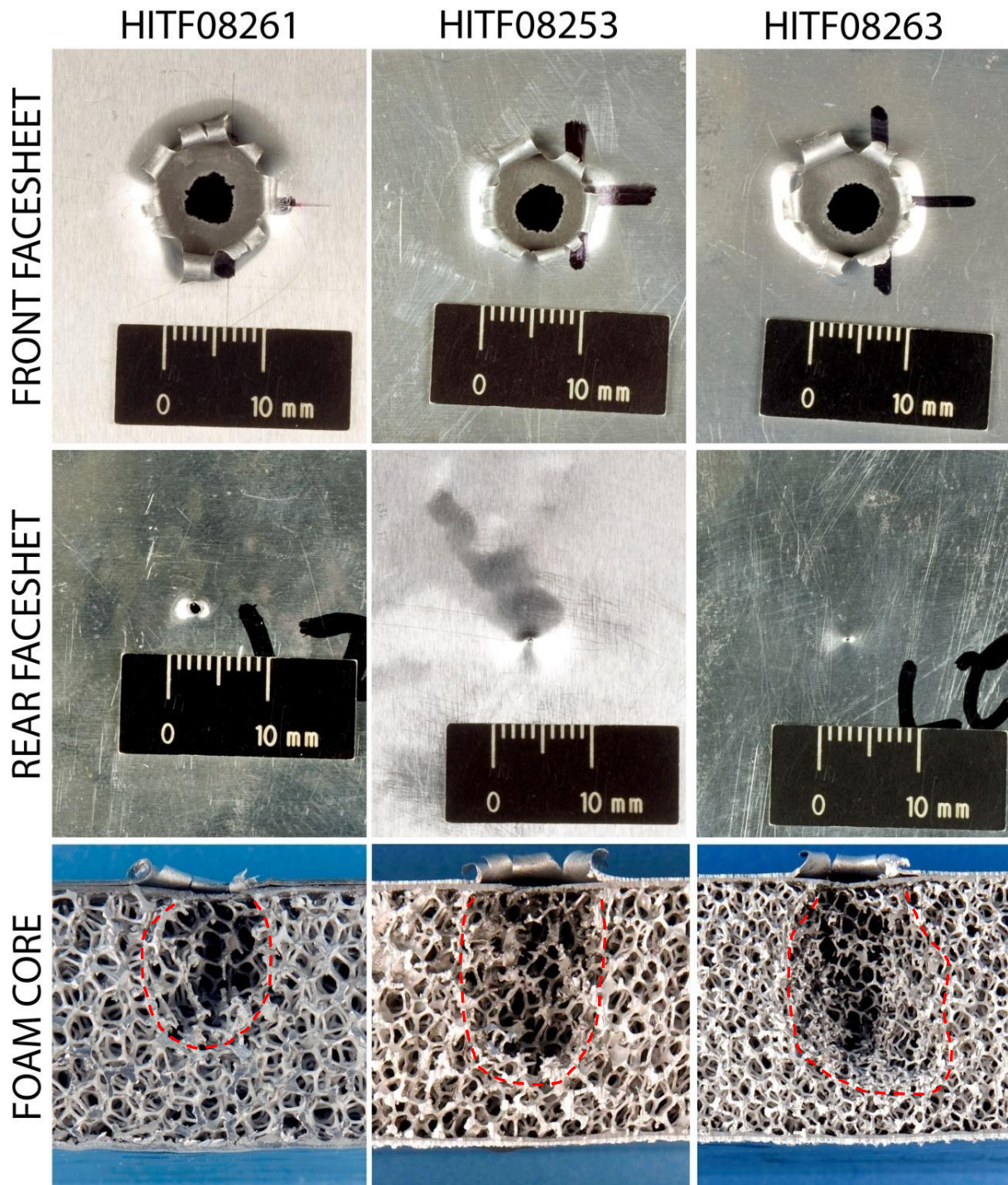


**Figure 45:** Comparison of damage in 10 PPI (left), 20 PPI (middle), and 40 PPI (right) foam core sandwich panels impacted by 2.0 mm diameter Al2017-T4 spheres at  $6.69 \pm 0.18$  km/s and  $0^\circ$ .

In Figure 46, damage induced by 3.2 mm diameter projectiles at 60° and high velocity on the three panels is compared. The 10 PPI and 20 PPI panels are type NASA, while the 40 PPI panel is of type ERG. The result of the different facesheet temper and adhesive is apparent on the front facesheets, which show facesheet detachment and petalling of the 40 PPI sample. Of the three targets, only the 10 PPI panel is perforated, with the 20 and 40 PPI panels showing only slight bulges on the rear facesheet. A comparison of the foam cores shows significantly larger lateral extension of damage within the 20 and 40 PPI cores than in the 10 PPI panel.

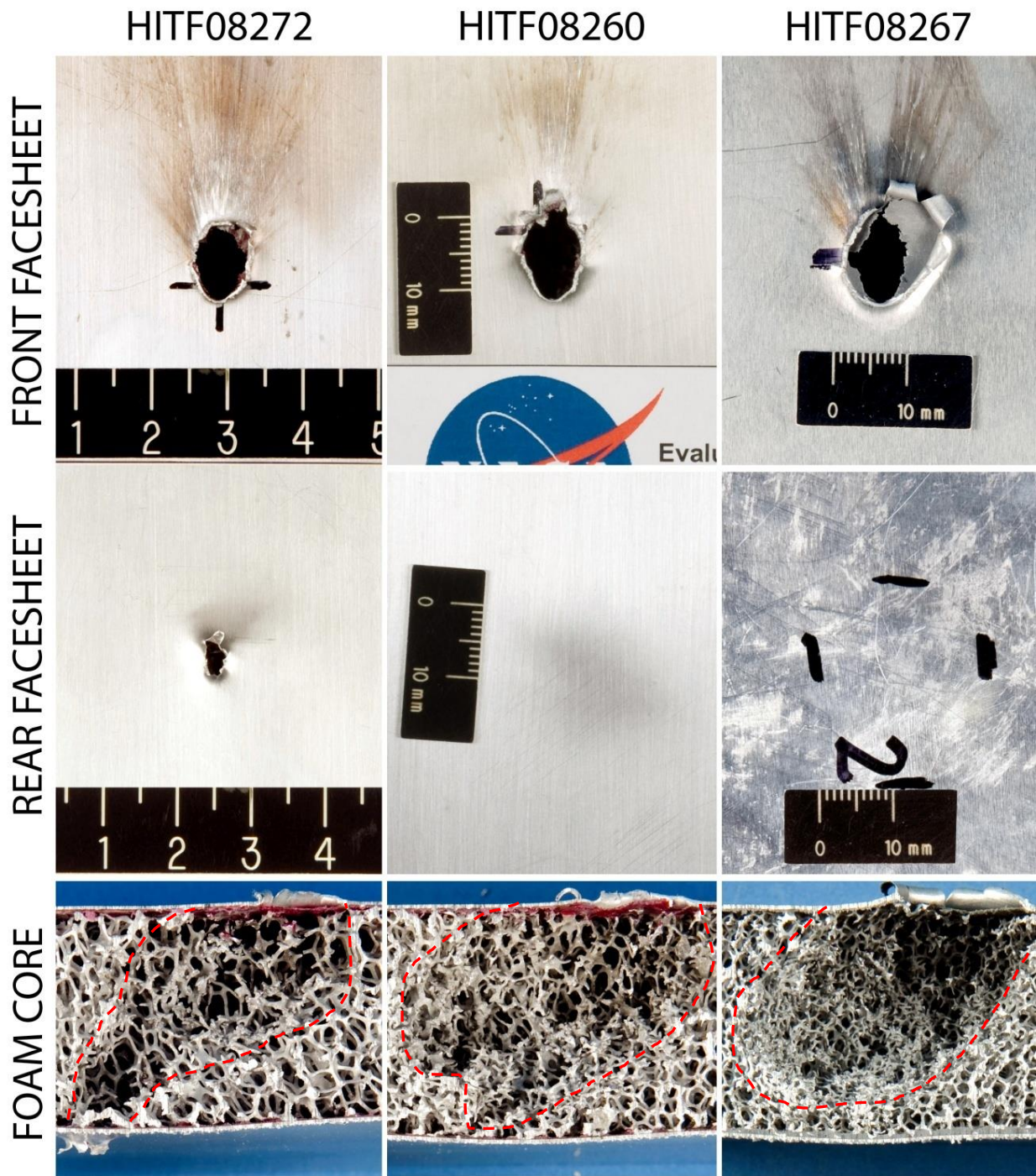


**Figure 46:** Comparison of damage in 10 PPI (left), 20 PPI (middle), and 40 PPI (right) foam core sandwich panels impacted by 3.2 mm diameter Al2017-T4 spheres at  $6.63 \pm 0.07$  km/s and  $60^\circ$ .

### **Effect of Relative Density**

Relative density controls the cross-sectional form of the foam ligaments (see Figure 12). Characterization of the foam microstructure found that a reduction in relative density from 6%-8% to 3%-5% resulted in a 30% decrease in ligament cross-sectional area, while the cell and pore size were relatively constant (within common variation). To investigate the effect of relative density on shielding performance, nominally identical impact tests were performed on the 1.0" Al F40 and 1.0" Al F40 (3%-5%) targets, an overview of which is given in Figure 47.

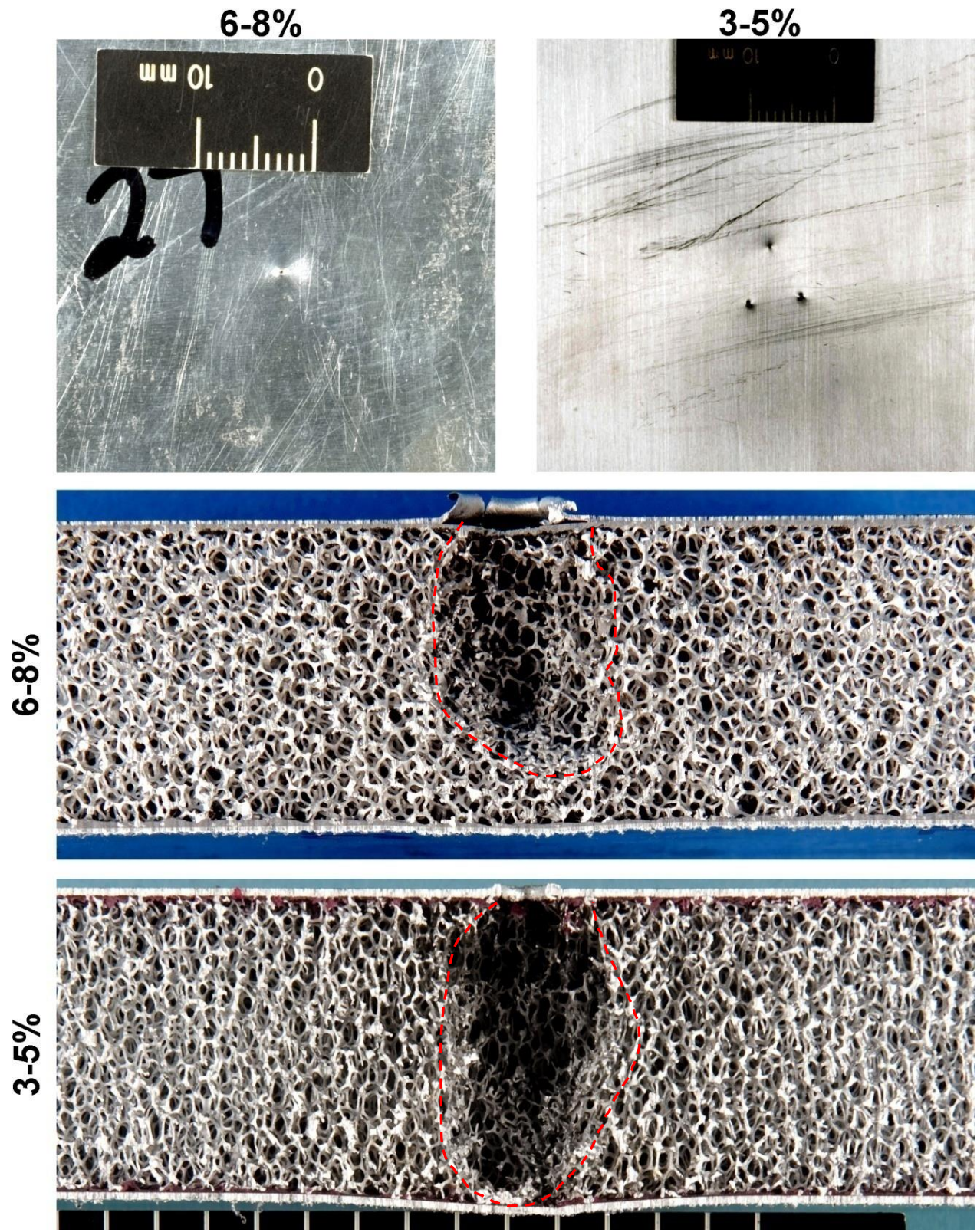
**Figure 47:** Tests used to evaluate the effect of foam relative density on shielding performance.

Test no. [6%-8% / 3%-5%]	Impact conditions $\theta$ (deg)	V (km/s)	$d_p$ (mm)	Result [6%-8% / 3%-5%]	Comments
8263/8574	0	6.52 / 6.63	2.0	$\geq / \geq$	Both panels minimally perforated with 1/2 small hole/s, respectively
9007/8575	60	6.91 / 6.88	3.4	$< / <$	Single bulge on both panels, no dimpling of rear surface
8423/8583	0	2.10 / 2.35	2.1	$> / \leq$	Baseline panel perforated, exit hole looks more like a tear than blowout. 3%-5% panel has three dimples, no spall or perforation

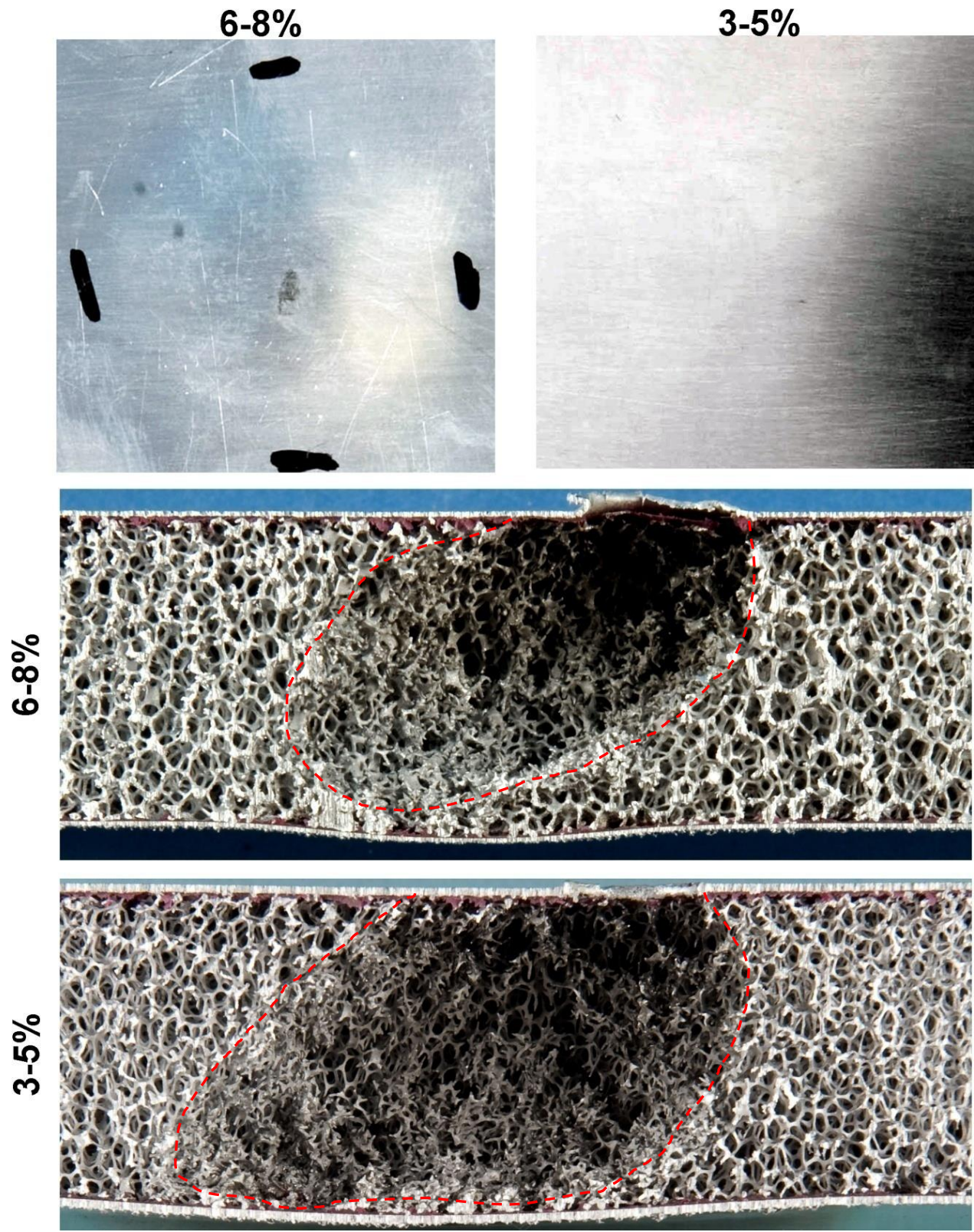
A comparison of impact induced damages in the 6%-8% and 3%-5% relative density foam core panels is made in Figure 48 through Figure 50. In Figure 48, the targets have been impacted by 2.0 mm diameter projectiles at  $6.58 \pm 0.06$  km/s with normal incidence. Although both targets were minimally perforated, significant differences in core damage can be observed in the figure. While damage to the  $\rho_{\text{rel}} = 3\%-5\%$  foam progresses through the to the rear facesheet of the panel, the 6%-8% foam arrests propagation of the primary fragment cloud at 80% of the total core thickness.

Figure 49 compares damage from 3.4 mm diameter projectiles at  $6.90 \pm 0.02$  km/s with oblique ( $60^\circ$ ) incidence. Again, the test results are the same for both panels (pass), yet damage to the foam core is more pronounced in the 3%-5% target. In addition to propagating through the thickness of the foam core along the projectile flight vector, the damage zone normal to the target surface is more pronounced. The cavity volumes of the 3%-5% and 6%-8% relative density foams is estimated at  $1722 \text{ mm}^3$  and  $1130 \text{ mm}^3$ , respectively.

For impact of 2.1 mm projectiles at low velocity ( $2.23 \pm 0.13$  km/s) with normal incidence, the 3%-5% panel was slightly below the failure limit, while the 6%-8% relative density foam panel was clearly perforated (see Figure 50). A comparison of core damage shows, similar to the previous tests, a larger damage volume in the lower density foam; however, damage propagates through to the rear facesheet in both panels. The 3%-5% relative density panel has a tempered rear facesheet, which is expected to result in improved ballistic resistance than the untempered material of the 6%-8% panel, particularly for impacts in which failure of the rear facesheet is not caused by a solid particle that penetrates beyond the primary foam damage volume.



**Figure 48:** Comparison of damages in HITF08263 ( $\rho_{\text{rel}} = 6\%-8\%$ ) and HITF08574 ( $\rho_{\text{rel}} = 3\%-5\%$ ).



**Figure 49:** Comparison of damages in HITF09007 ( $\rho_{\text{rel}} = 6\%-8\%$ ) and HITF08575 ( $\rho_{\text{rel}} = 3\%-5\%$ ).

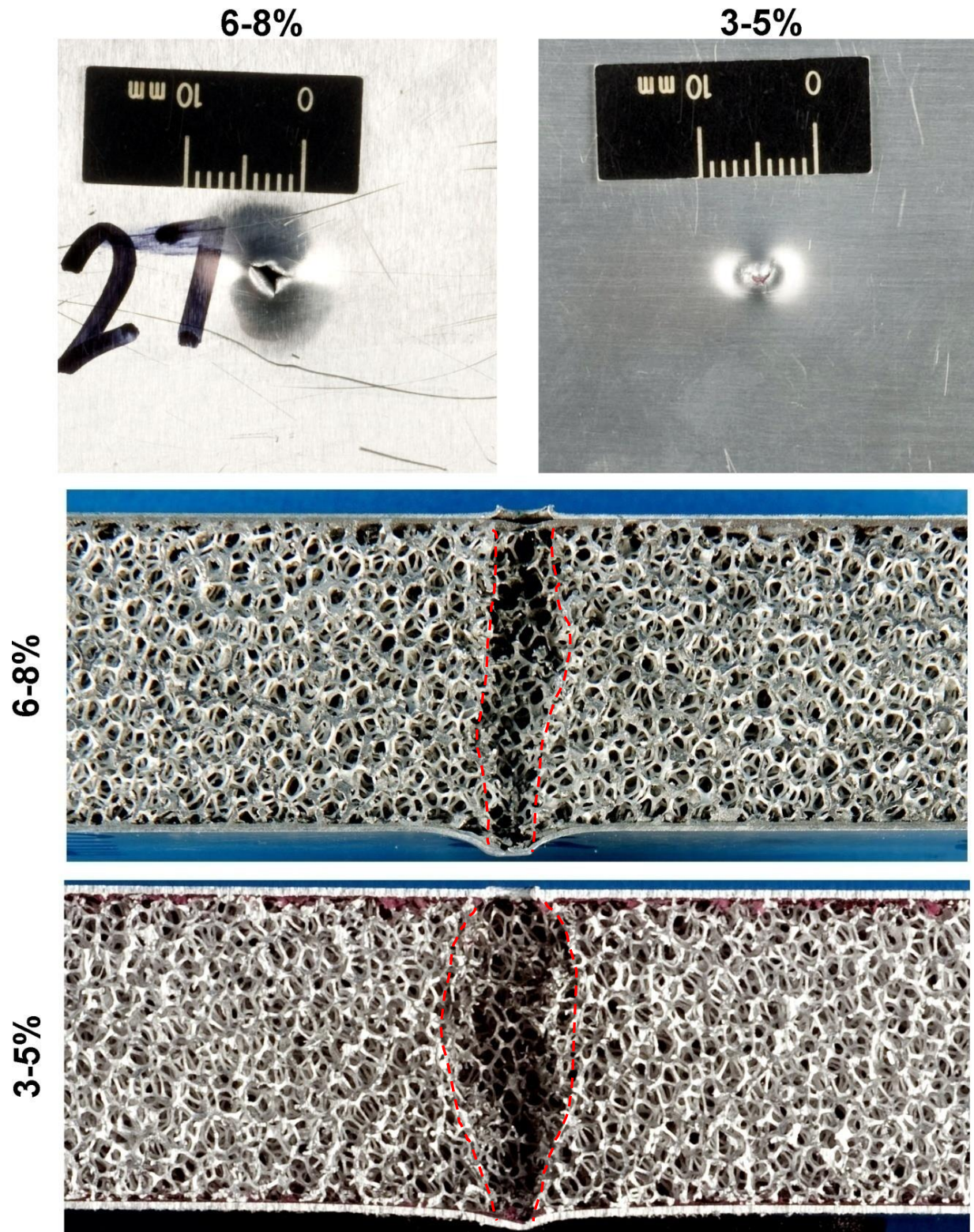


**Figure 50:** Comparison of damages in HITF08423 ( $\rho_{\text{rel}} = 6\%-8\%$ ) and HITF08583 ( $\rho_{\text{rel}} = 3\%-5\%$ ).

Although the gross results of the three comparison tests showed the performance of the reduced density panel to be superior to that of the baseline 6%-8% relative density configuration, this is not representative. Given the larger foam core damage volumes in the reduced-density foam, it is considered that increasing density improves the ability to arrest crater growth, resulting in higher protective capability.

### **Summary**

In Table 10, the failure limits of the 10/20/40 PPI foam core panels at ~6.8 km/s are summarized. Data from [10] are used to supplement the results from Table 7.

**Table 10:** Summary of 1.0" foam core panel failure limits ( $V \approx 6.8$  km/s).

Pore density (PPI)	Failure limit (projectile diameter, mm)		
	0°	45°	60°
10	< 2.0	2.5-2.7	< 3.2
20	1.9-2.0	2.3-2.5	3.0-3.2
40	≈ 2.0	≈ 2.7	> 3.4

In general, the protective capability of the foam core sandwich panels was found to increase with increasing PPI. The lower PPI foam core panels showed less lateral expansion of projectile fragments (i.e. less lateral damage extension in the foam core), and less densification (i.e. collapse of the foam cells) about the edges of the damaged area. These processes are expected to result in greater transitioning of projectile kinetic energy to plastic work in the higher PPI panels. Furthermore, smaller foam cells appear to reduce the occurrence of individual projectile fragments propagating through the foam core with few or no secondary impacts upon foam ligaments. This phenomenon can result in a significant reduction of the panel protective capability, and is a major contributor to uncertainty bounds of foam core sandwich panel failure limits.

## **Phase 2 Test Results**

A total of 12 successful tests were performed during Phase 2 to characterize the effect of core thickness on shielding performance. A summary of the tests is provided in Table 11.

**Table 11:** Phase 2 test results.

HITF No.	Target	Projectile Material (-)	Diameter (mm)	Impact conditions Angle (deg)	Velocity (km/s)	Result
1 08589	0.5" Al F40	Al2017-T4	1.3	0	2.43	Pass
2 08571	0.5" Al F40	Al2017-T4	1.4	45	6.68	Pass
3 08572	0.5" Al F40	Al2017-T4	2.0	60	6.70	Perforated
4 08580	0.5" Al F40	Al2017-T4	1.8	60	6.79	Pass
5 08581	0.5" Al F40	Al2017-T4	2.0	60	2.28	Pass
6 08582	0.5" Al F40	Al2017-T4	2.5	60	2.63	Perforated
7 08590	2.0" Al F40	Al2017-T4	4.0	0	2.70	Pass
8 08573	2.0" Al F40	Al2017-T4	5.2	45	6.98	Perforated
9 08591	2.0" Al F40	Al2017-T4	5.7	60	6.74	Pass
10 08614	2.0" Al F40	Al2017-T4	6.0	60	6.74	Pass
11 08613	2.0" Al F40	Al2017-T4	7.0	60	2.73	Perforated
12 09220	2.0" Al F40	Al2017-T4	6.0	60	2.74	Pass

The failure limits of the 0.5" Al F40, 1.0" Al F40, and 2.0" Al F40 targets have been characterized at approximately 6.8 km/s for multiple impact angles. These limits are expressed in Figure 51 in terms of the projectile kinetic energy normalized by the kinetic energy required to induce failure in the 1.0" panel; i.e.:  $KE/KE_{1.0" \text{ F40}}$ , and the kinetic energy required to induce failure of the panel at 0°, i.e.:  $KE/KE_{0=0^\circ}$ .

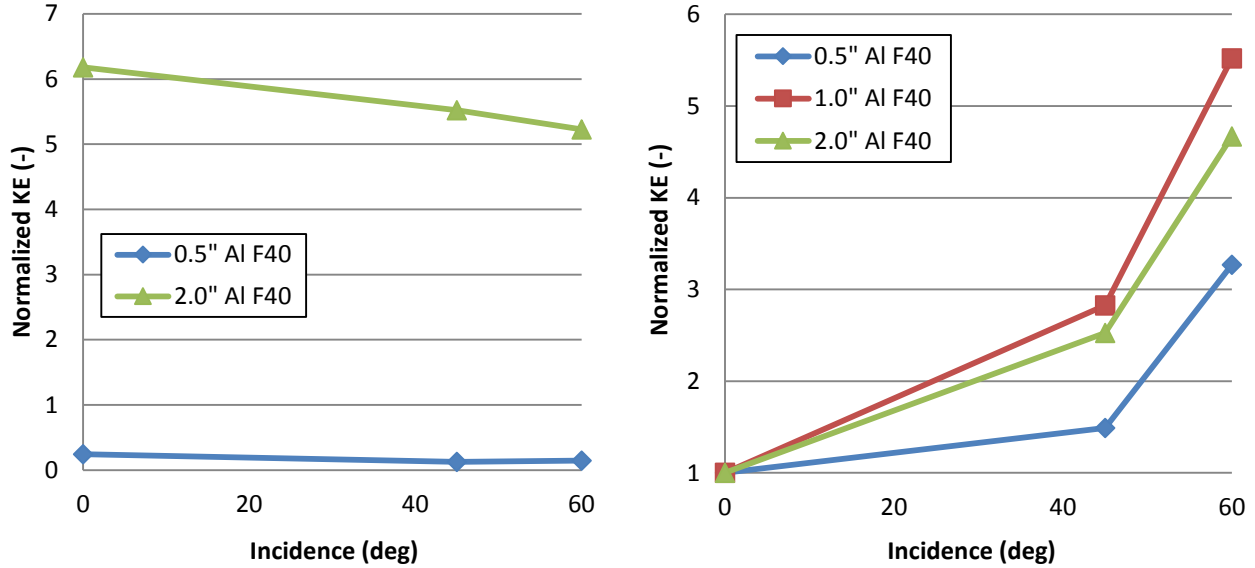


**Figure 51:** Failure limits of the 0.5", 1.0", and 2.0" thick Al F40 targets at approx. 6.8 km/s normalized in terms of:  
Left: 1.0" F40  $KE_{\text{crit}}$ ; right:  $KE_{\text{crit}}(\theta=0^\circ)$ .

The areal densities of the 0.5" Al F40 and 2.0" Al F40 panels are approximately 65% and 160% that of the 1.0" Al F40, respectively. At normal incidence, the ballistic limit of these two panels, in terms of kinetic energy at approx. 6.8 km/s, is 24% and 618% that of the 1.0" Al F40 panel, respectively. Therefore, by doubling the core thickness and increasing the areal density by approximately 50% (i.e. 0.5" Al F40 → 1.0" Al F40), the failure limit, in terms of kinetic energy, increases over 400% at normal incidence, and almost 700% at 60°. A further doubling of the core thickness and 60% increase in the areal density (i.e. 1.0" Al F40 → 2.0" Al F40) provides a further 600% increase in the kinetic energy required to perforate at normal incidence, and a further 525% increase for impact at 60°. In Figure 52, the kinetic energy required to perforate the panels at approx. 6.8 km/s is plotted in terms of target areal density. The failure limits have been normalized in terms of the 1.0" Al F40 failure limits. In the figure it is apparent that the performance gain with increasing target thickness and areal density is more pronounced for thicker (and heavier) targets. The effect on performance is shown to be relatively consistent for normal and oblique impacts.

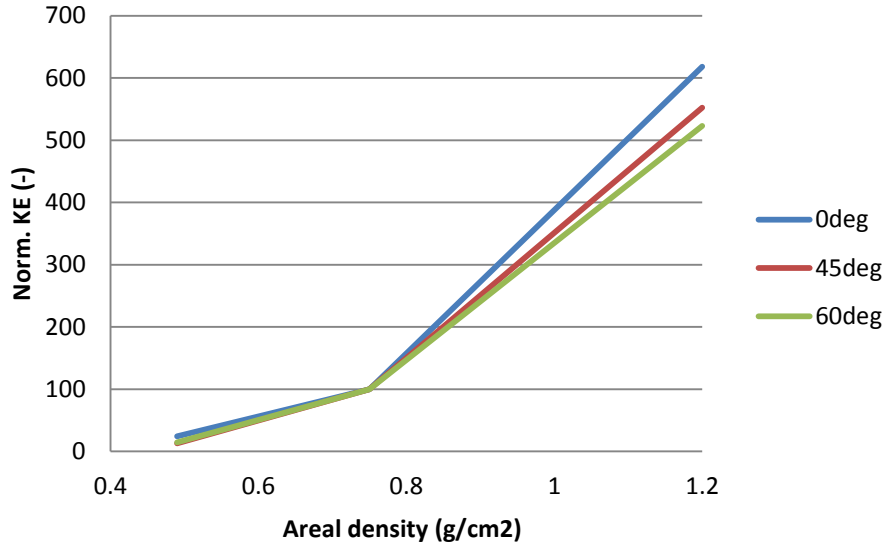


**Figure 52:** Variation of high-speed failure limits with increasing panel thickness and areal density.

### Phase 3 Test Results

Three variations of front facesheet thickness and rear facesheet thickness were considered in Phase 3 to evaluate their effect on shielding performance. A total of 12 successful hypervelocity impact tests were performed on the targets, a summary of which is given in Table 12.

**Table 12:** Phase 3 test results.

HITF No.	Target	Projectile		Impact conditions		Result
		Material	Diameter (-)	Angle (deg)	Velocity (km/s)	
1	09374	1.0" Al F40 B1W2	Al2017-T4	2.6	0	6.66 Pass
2	09375	1.0" Al F40 B1W2	Al2017-T4	2.8	0	6.64 Perforated
3	09376	1.0" Al F40 B1W2	Al2017-T4	3.4	45	6.72 Perforated
4	09377	1.0" Al F40 B1W2	Al2017-T4	3.3	45	6.85 Perforated
5	09320	1.0" Al F40 B2W2	Al2017-T4	3.0	0	7.00 Perforated
6	09321	1.0" Al F40 B2W2	Al2017-T4	2.7	0	6.94 Perforated
7	09322	1.0" Al F40 B3W2	Al2017-T4	2.8	0	6.59 Perforated
8	09323	1.0" Al F40 B3W2	Al2017-T4	2.6	0	5.88 Pass
9	09324	1.0" Al F40 B3W3	Al2017-T4	3.0	0	6.71 Perforated
10	09325	1.0" Al F40 B3W3	Al2017-T4	2.8	0	6.91 Perforated
11	09326	1.0" Al F40 B3W3	Al2017-T4	3.8	45	6.80 Perforated
12	09327	1.0" Al F40 B3W3	Al2017-T4	3.6	45	6.83 Perforated

Although the majority of phase three tests reported in Table 12 resulted in perforation of the rear facesheet, a number of these tests were considered equal to, or minimally above the failure limit and are therefore effective for definition of target ballistic limits. Two examples of minimal failure are shown in Figure 53.

The Phase 3 targets all displayed similar failure limits, with 2.7/2.8 mm diameter projectiles causing minimal failure at high velocity (~6.8 km/s) with normal incidence. Failure of the baseline 1.0" Al F40 target was induced by impact of a 2.0-mm diameter projectile at similar conditions in Phase 1. This represents a significant improvement in protective capability for a minimal increase in facesheet thickness (and therefore, weight); however the effect on performance was not constant – i.e. target B1W2 performance was similar to that of target B3W3. Two nominally identical impact tests were performed on

the 1.0" Al F40 target in Phase 1 with 2.0 mm diameter projectiles, nom. 6.8 km/s impact velocity, and normal incidence (HITF08263 and HITF08568). A comparison of damages in the two tests was made in Figure 41, and showed damage to the foam core extended through approximately 80% of the panel thickness. Failure of HITF08263, it was therefore concluded, was the result of a single solid fragment that was able to propagate beyond the primary damage cavity. The increase in facesheet thickness for targets in Phase 3 may reduce the panel's susceptibility to these types of failure, explaining the substantial improvement in failure limits for a marginal increase in target weight.

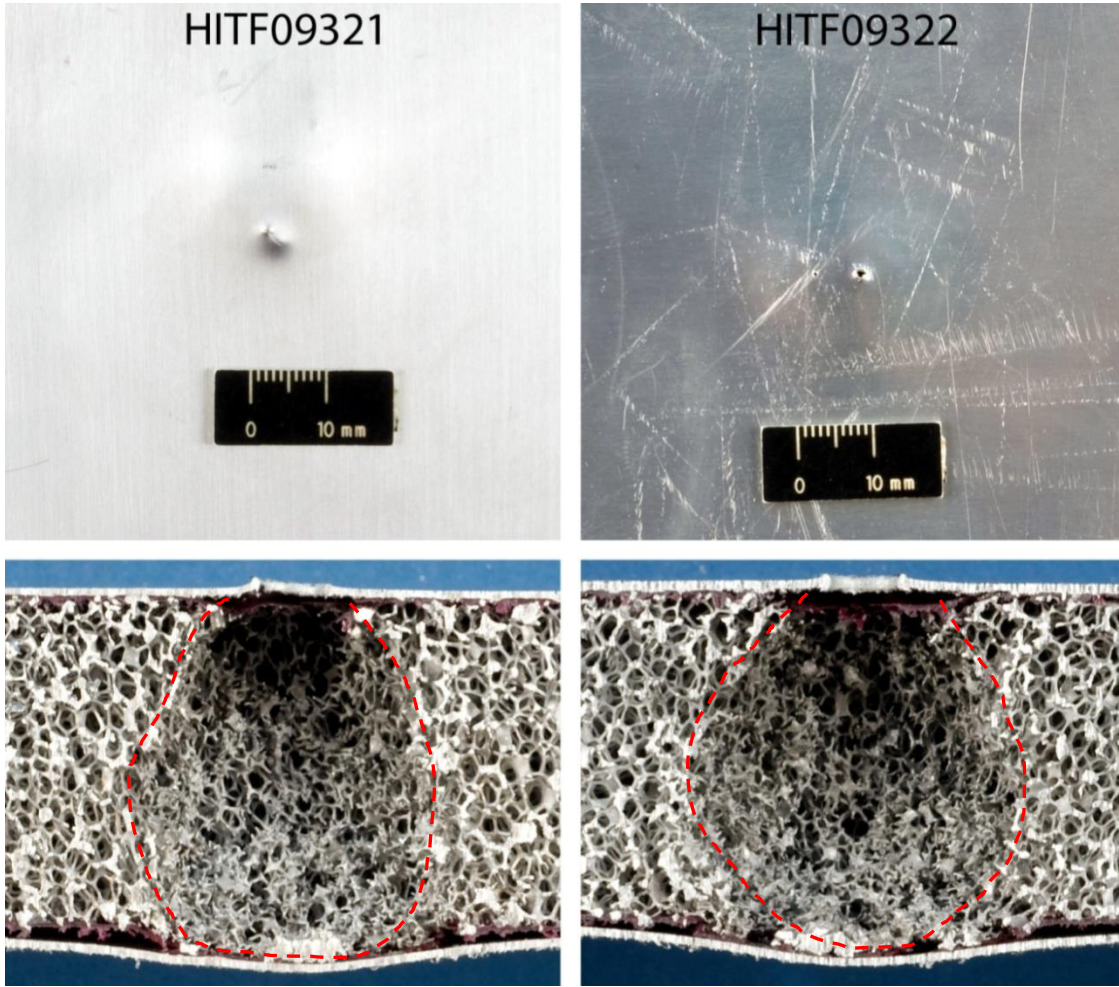


**Figure 53:** Two instances of minimal failure in Phase 3 tests useful for definition of ballistic limits.

#### Phase 4 Test Results

Six alternate sandwich panels were evaluated in 13 tests during Phase 4, including three advanced foam (2.0" Al F-var, 2.0" Al F-var (K/E), 2.0" Al F-var (N/E)) and three honeycomb (1.0" Trussgrid, 2.0" PN2 HC, 2.0" Al HC) configurations. The impact tests were performed at conditions nominally identical to select experiments on the baseline F40 foam targets, either from earlier phases of this study, or from Yasensky, Christiansen, and Prior [10]. The Phase 4 tests are summarized in Table 13.

In Figure 54 through Figure 56, a comparison of damage to the 1.0" Trussgrid panels is compared to that of the 1.0" Al F40 foam for three different impact conditions. Under impact of 2.0 mm diameter projectiles, the foam panel was minimally perforated, while the Trussgrid panel is shown to exhibit no damage on the rear facesheet. However, examination of the foam core shows that penetration depth of the

center cavity extended approxiamtely 80% through the thickness, and thus perforation of the rear facesheet is due an individual solid projectile fragment.

For impact at low velocity with normal incidence (Figure 55), similar damages are observed on both the foam and Trussgrid panels. This is also the case for impact at high velocity, with 60° obliquity (Figure 56). The Trussgrid panel used for the 60° test is shown to contain excessive amounts of facesheet adhesive, which fill portions of the 3-D honeycomb core. Although this is not expected to have a significant influence on the test result, it increases panel weight and introduces target variability to the performance comparison. For the three evaluation tests, the Trussgrid panel is considered to provide comparable performance to the F40 foam panel, and thus superior performance than standard honeycomb core sandwich panels.

**Table 13:** Phase 4 test results.

HITF No.	Target	Projectile Material (-)	Diameter (mm)	Impact conditions Angle (deg)	Velocity (km/s)	Result
1	8584 1.0" Trussgrid	Al2017-T4	2	0	6.72	Pass
2	9001 1.0" Trussgrid	Al2017-T4	3.4	60	6.75	Pass
3	9002 1.0" Trussgrid	Al2017-T4	2.1	0	2.61	Perforated
4	9003 2.0" PN2 HC	Al2017-T4	3.6	0	6.89	Perforated
5	9004 2.0" PN2 HC	Al2017-T4	6	60	6.96	Perforated
6	9005 2.0" Al HC	Al2017-T4	2.5	0	6.91	Perforated
7	9006 2.0" Al HC	Al2017-T4	6	60	6.81	Perforated
8	9365 2.0" Al F-var	Al2017-T4	4	0	6.96	Perforated
9	9366 2.0" Al F-var	Al2017-T4	4.5	0	2.79	Perforated
10	9368 2.0" Al Fvar (K/E)	Al2017-T4	4	0	6.89	Pass
11	9371 2.0" Al Fvar (N/E)	Al2017-T4	4	0	6.93	Perforated
12	9465 2.0" Al F-var*	Al2017-T4	4	0	6.9	Perforated
13	9466 2.0" Al Fvar (K/E)*	Al2017-T4	4	0	6.97	Pass

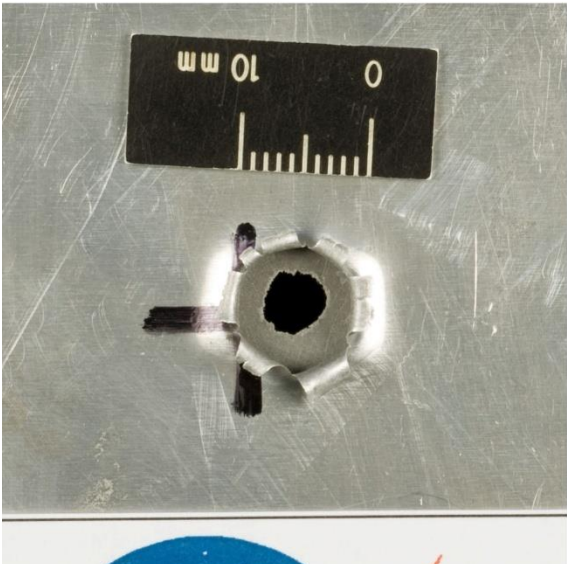
\* Reversed configuration

The performance of the alternate 2.0" foam-based panels is compared in Figure 32. Of the four panels, the F-var (K/E) is the only one not perforated. The baseline F40 and F-var targets are minimally perforated, while the F-var (N/E) panel is clearly ruptured. It is interesting to note that the F-var (N/E) panel is the first instance of rupture and rear wall petalling observed in this study. Failure of the unmodified foam core sandwich panels, in all cases, was due to perforation of small individual solid projectile fragments leading to pin-point perforations such as that observed for test HITF04163 in Figure 32. Although below the failure limit, the F-var (K/E) shows a much greater level of rear wall bulging than observed on the baseline foam core panels, and would be expected to fail catastrophically once the ballistic limit is exceeded (i.e. rupture). Another key feature of the Nextel/epoxy and Kevlar/epoxy reinforced panels is that the intermediate composite layers are shown to re-focus the debris cloud, which is observed as a reduction in lateral damage extension in the 5 PPI foam segment. This re-focusing effect is commonly observed on multi-layer shields such as the stuffed Whipple and Nextel multi-shock.

The F-var panel was intended to facilitate the maximum number of secondary impacts during the initial phase of penetration through the high PPI segments of the core, leading to fragmentation/melting/vaporization of the projectile and front facesheet material. As the penetration progressed, increased pore sizes were included to enable greater expansion of the (now optimally fragmented/molten) debris cloud, distributing the impulsive load over a larger area of the rear facesheet. Although increased expansion is visible in the 5 PPI segment of the F-var panel, the shielding performance is equal, if not inferior, to that of the baseline F40 foam. So, although the foam core is shown to limit lateral expansion of the debris cloud (compared to a standard Whipple shield), this mechanism is not considered to be critical to performance for this type of material.

Within multi-wall shields, Nextel fabric is used to break up solid projectile/bumper fragments by imparting strong secondary shocks, while Kevlar fabric is used to slow or capture solid particles. The performance of the K/E reinforced panel is shown in Figure 32 to be clearly superior to that of the N/E reinforced panel. This is not unexpected, as the key performance feature of the ceramic fabric (i.e. enhanced fragmentation/melting) is already produced by secondary impact of fragments on foam ligaments. Furthermore, the foam core panels have shown substantial sensitivity to perforation by small remnant solid projectile fragments, which is expected to be more effectively dealt with by the ballistic fabric.

HITF08263



HITF08584

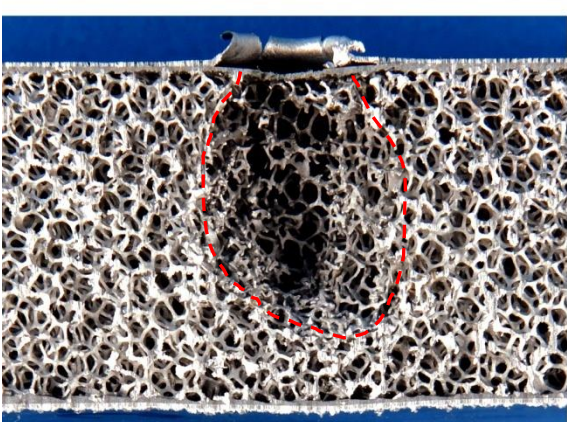
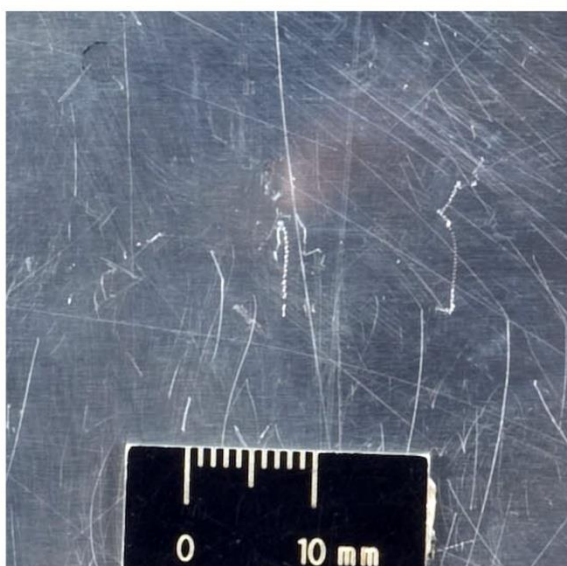
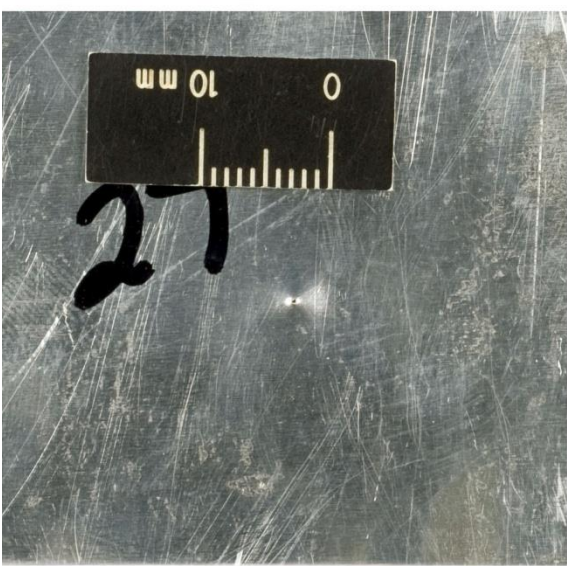
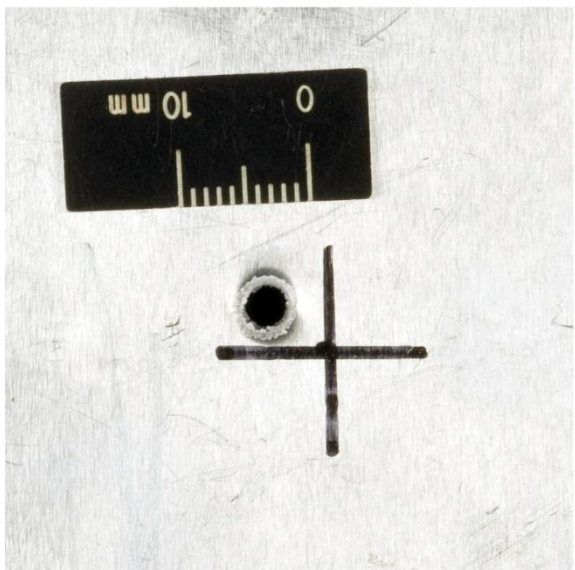


**Figure 54:** Comparison of impact damage in the 1.0" Al F40 (NASA) foam (left) and 1.0" Trussgrid (right) panels impacted by 2.0 mm diameter Al2017-T4 spheres at ~6.8 km/s with normal incidence.

# HITF08423



# HITF09002

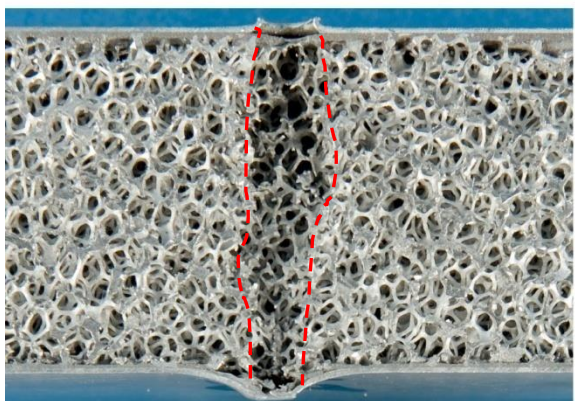
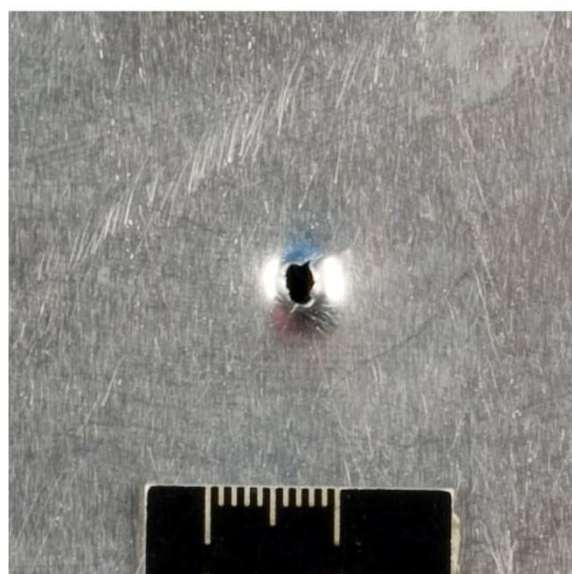
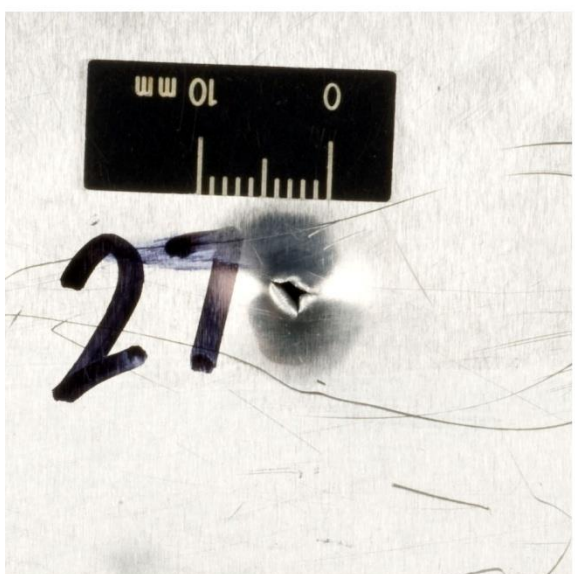
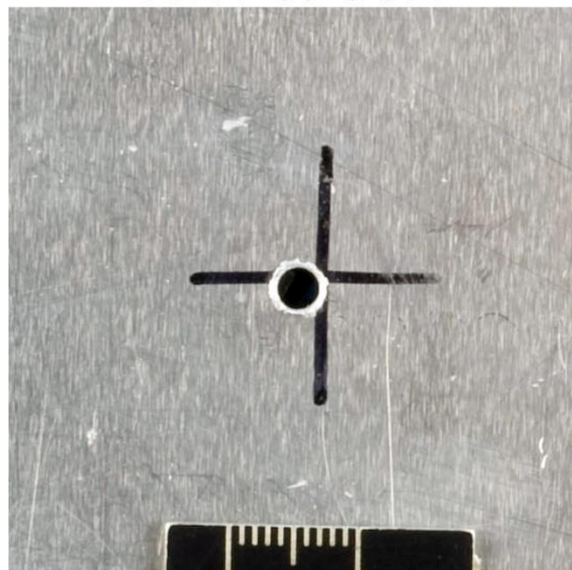


**Figure 55:** Comparison of impact damage in the 1.0" Al F40 (NASA) foam (left) and 1.0" Trussgrid (right) panels impacted by 2.1 mm diameter Al2017-T4 spheres at ~2.5 km/s with normal incidence.

HITF09007



HITF09001

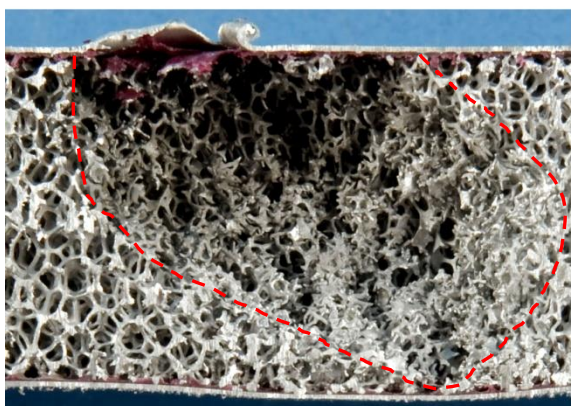
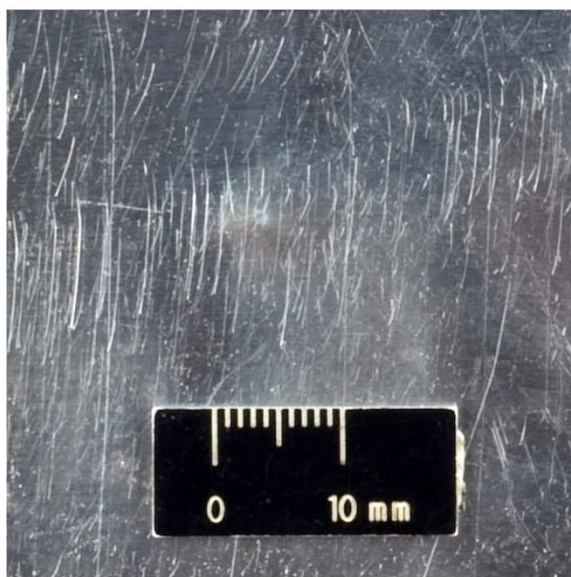
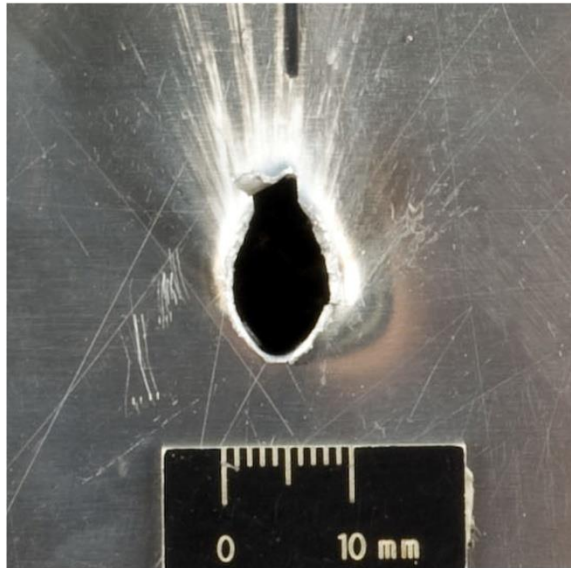


**Figure 56:** Comparison of impact damage in the 1.0" Al F40 (NASA) foam (left) and 1.0" Trussgrid (right) panels impacted by 3.4 mm diameter Al2017-T4 spheres at ~6.8 km/s with oblique incidence (60°).

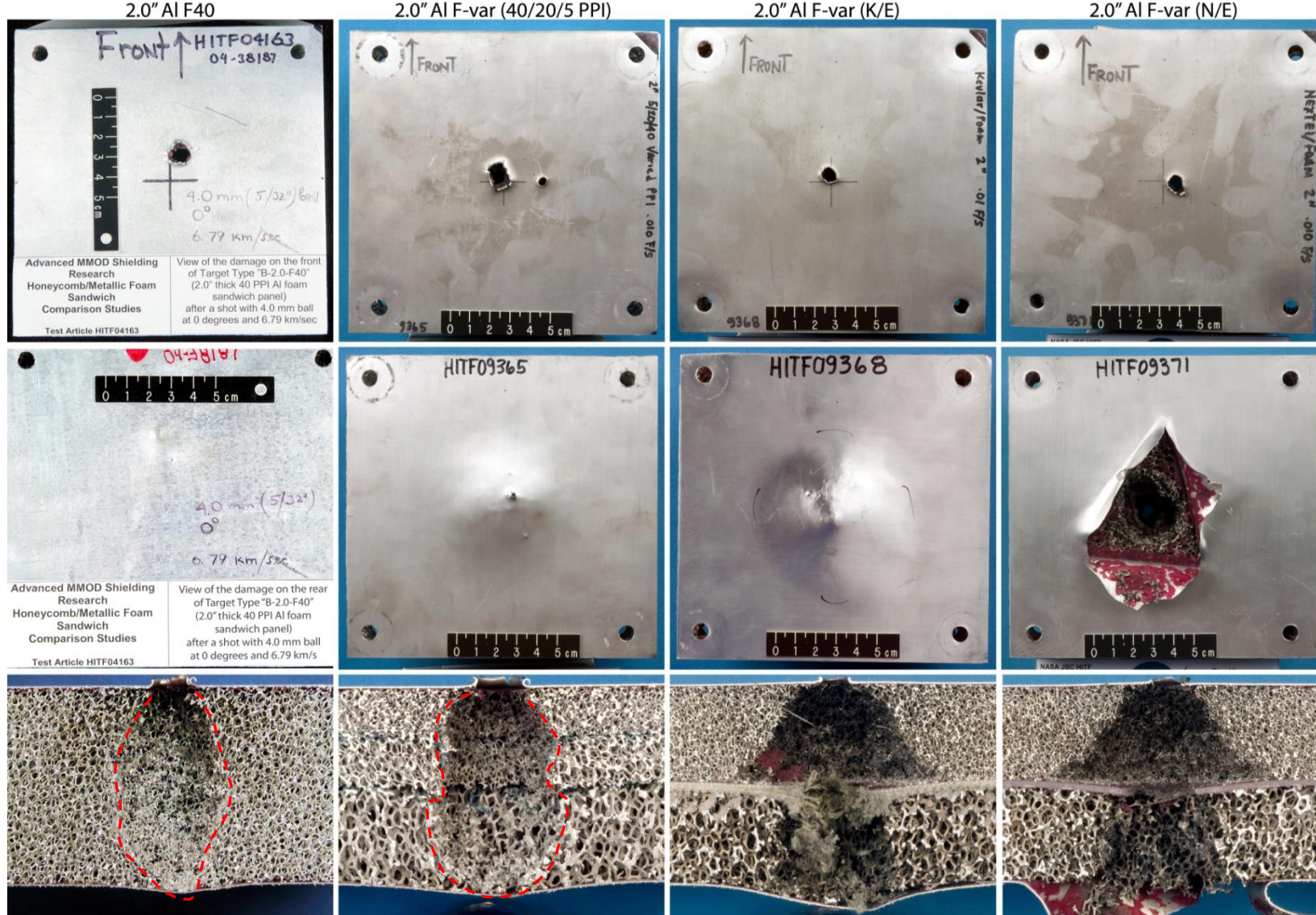


**Figure 57:** Comparison of the 2.0" Al F40 [10], F-var, F-var (K/E), and F-var (N/E) panels impacted by 4.0" mm diameter projectiles at ~6.8 km/s with 0°.

The performance of the alternate 2.0" honeycomb-based panels is compared to that of the baseline foam in Figure 59 and Figure 60. Under normal impact of 3.6 mm diameter projectiles at high velocity both honeycomb core panels are perforated, while no damage is observed on the rear of the foam panel. Indeed, the Al HC core panel was perforated by impact of a 2.5 mm diameter projectile at nominally identical conditions (see Figure 58). The lateral extension of damage within the panel cores is shown to be significantly greater in the Nomex (PN2) honeycomb than the aluminum, suggesting a lesser degree of channelling as predicted. Under impact of 6.0 mm diameter projectiles, both honeycomb core panels are again clearly perforated, while the rear facesheet of the foam core panel shows some bulging, but is not perforated. Examination of the foam core shows penetration through approximately 90% of the panel thickness. The PN2 panel is perforated in two places, corresponding to the normal and in-line fragment clouds. The panel rear facesheet was fully detached during the experiment. The Al HC panel is perforated in a location normal to the impact site on the front facesheet, and clear separation between the two fragment cloud components can be observed in the sectioned core. The in-line fragment cloud is shown to progress through to the rear facesheet, yet no corresponding damage is observed on the target rear side.

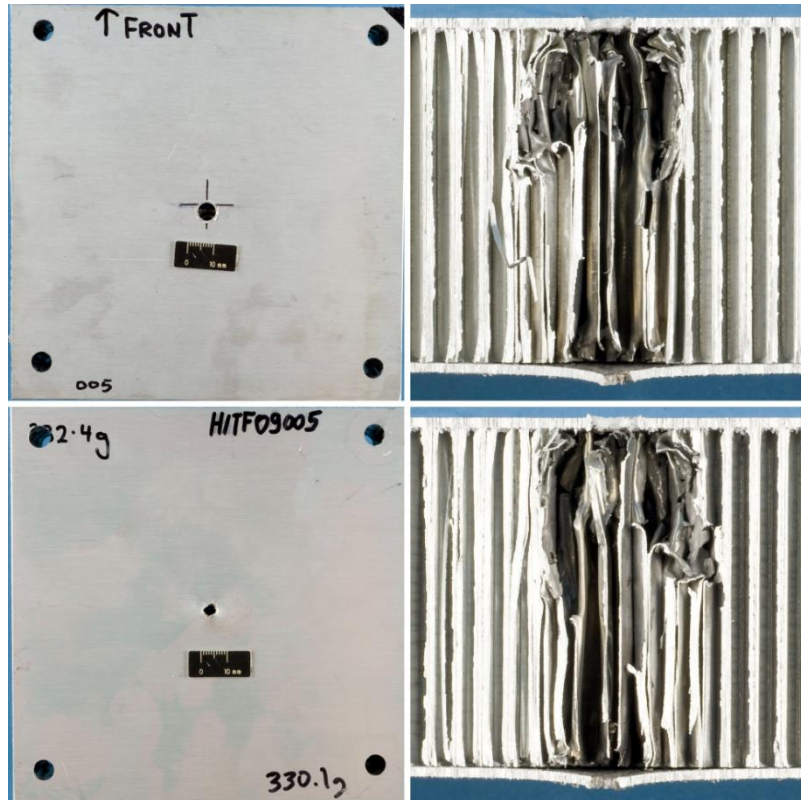


**Figure 58:** Al HC target damage following normal impact of a 2.5 mm diameter projectile at 6.91 km/s.

The performance of the Al HC and PN2 HC core panels is clearly inferior to that of the baseline F40 panel under both impact conditions investigated. Although the PN2 core was shown to reduce the degree of fragment channeling (compared to aluminum HC), this did not correspond to an improvement in shielding capability.

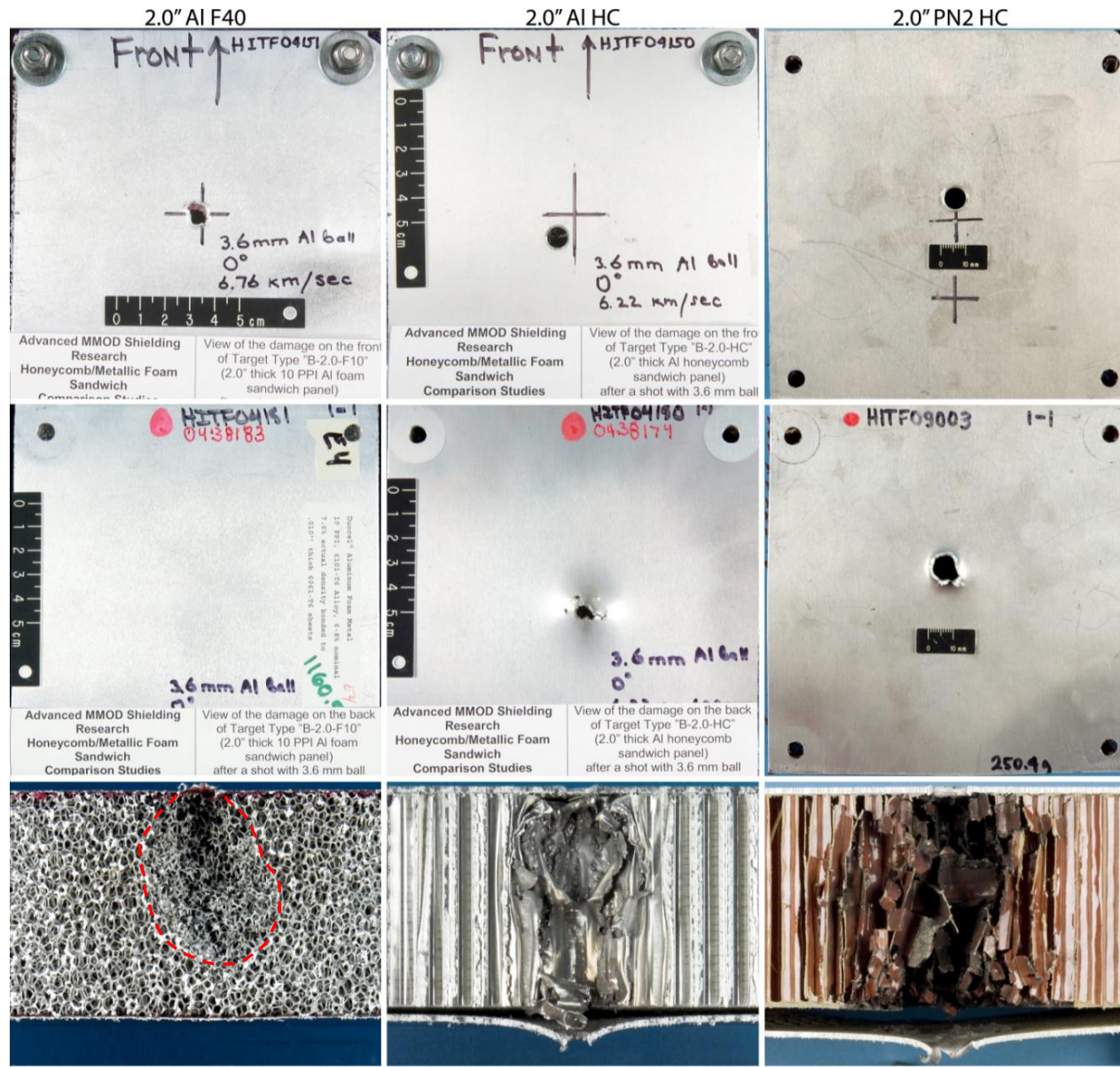


**Figure 59:** Comparison of the 2.0" Al F40 [10], Al HC [10], and PN2 HC panels impacted by 3.6 mm diameter projectiles at  $\sim 6.8$  km/s with  $0^\circ$ .

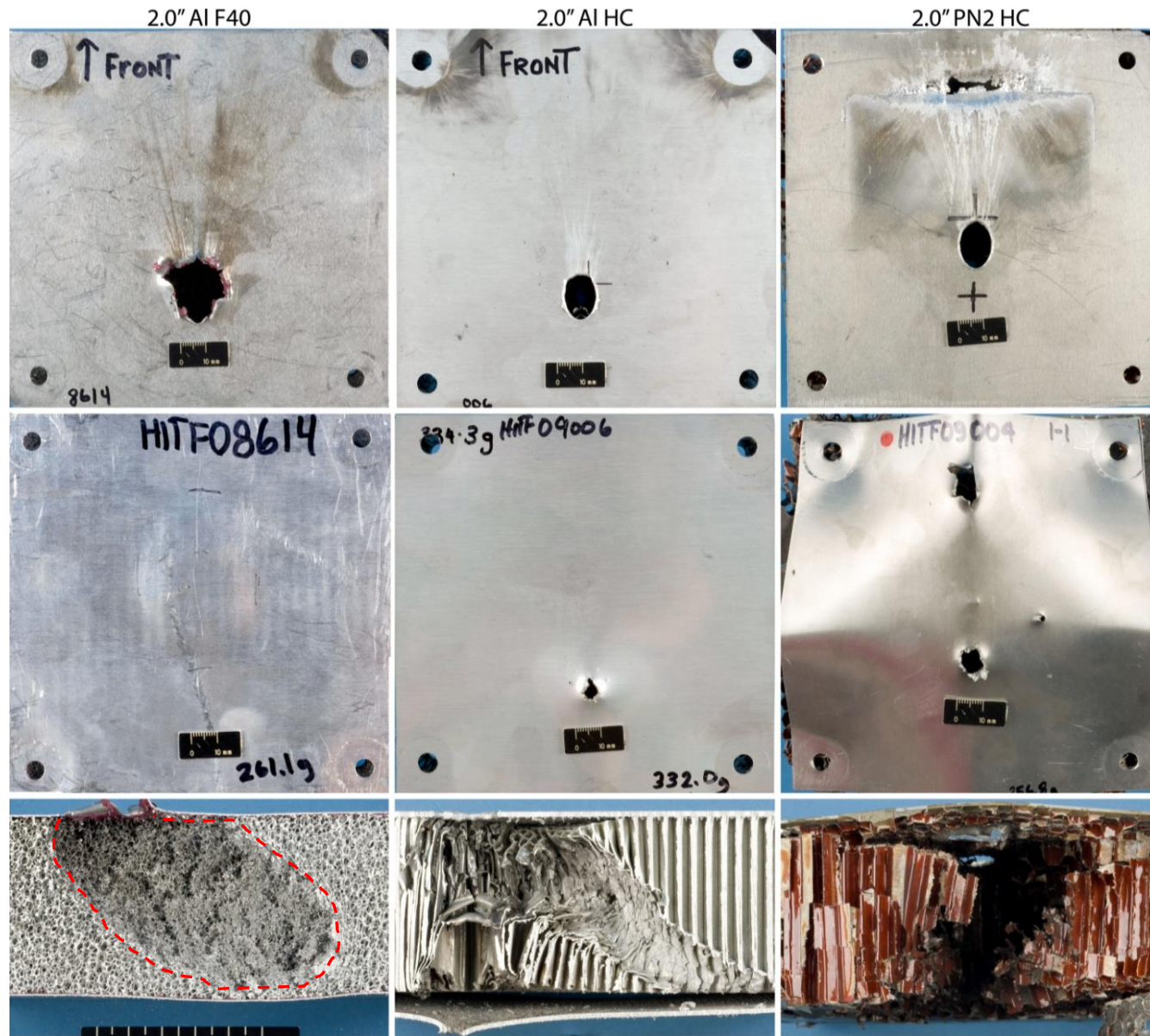


**Figure 60:** Comparison of the 2.0" Al F40, Al HC, and PN2 HC panels impacted by 6.0 mm diameter projectiles at  $\sim 6.8$  km/s with  $60^\circ$ .

The effect of reversing the variable pore density foams (F-var and F-var (K/E)) is evaluated in Figure 61 and Figure 62. In Figure 61, both F-var panels are shown to be perforated; however, the diameter of the exit hole in the reversed target (i.e. 5/20/40 PPI) is significantly larger than that in the panel impacted in the original orientation (i.e. 5/20/40 PPI). Examination of the core damage shows the open cavity extends through to the rear facesheet in the reversed configuration, while for the original orientation the cavity growth is arrested at approx. 95% of the core thickness.

Neither F-var (K/E) panels are found to be perforated in Figure 62; however, there is substantial rear facesheet bulging on both panels ( $b_{max} = 7.17$  and  $8.77$  mm for the original and reversed panels, respectively). Damage to the two panels is comparable, with greater lateral extension of damage in the 40 PPI segment of the original orientation panel than the corresponding 5 PPI segment of the reversed panel. Delamination of the composite reinforcement is more pronounced in the reversed configuration; however, this may be due to manufacturing induced voids rather than a manifest of the impact process.

For both the F-var and F-var (K/E) panels, a minimal improvement in protective capability is gained by orienting the panels such that the higher PPI segments are located toward the front facesheet.

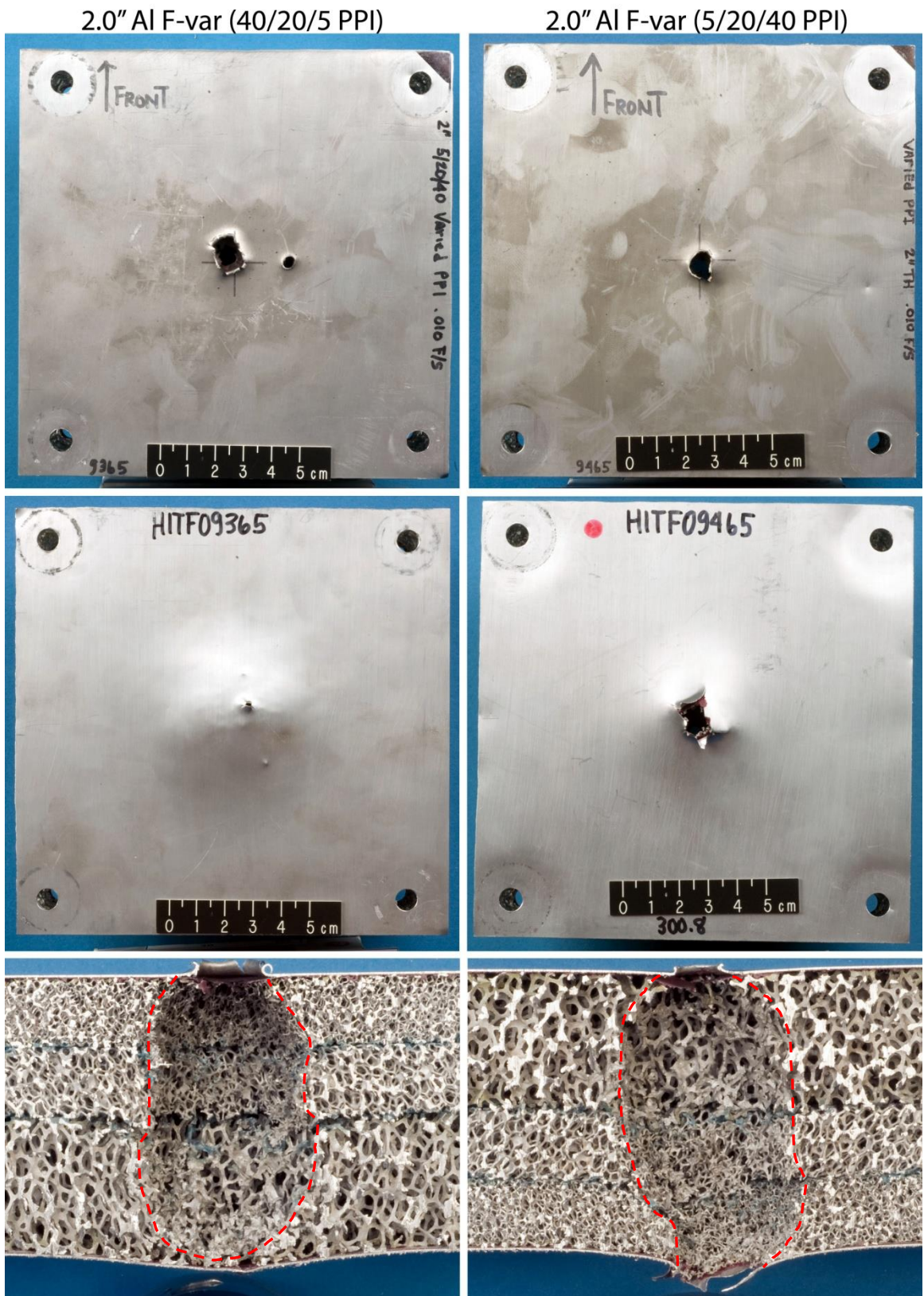


**Figure 61:** Comparison of the F-var original (left) and reversed (right) configurations impacted by 4.0 mm diameter projectiles at  $\sim 6.8$  km/s with normal incidence ( $0^\circ$ ).

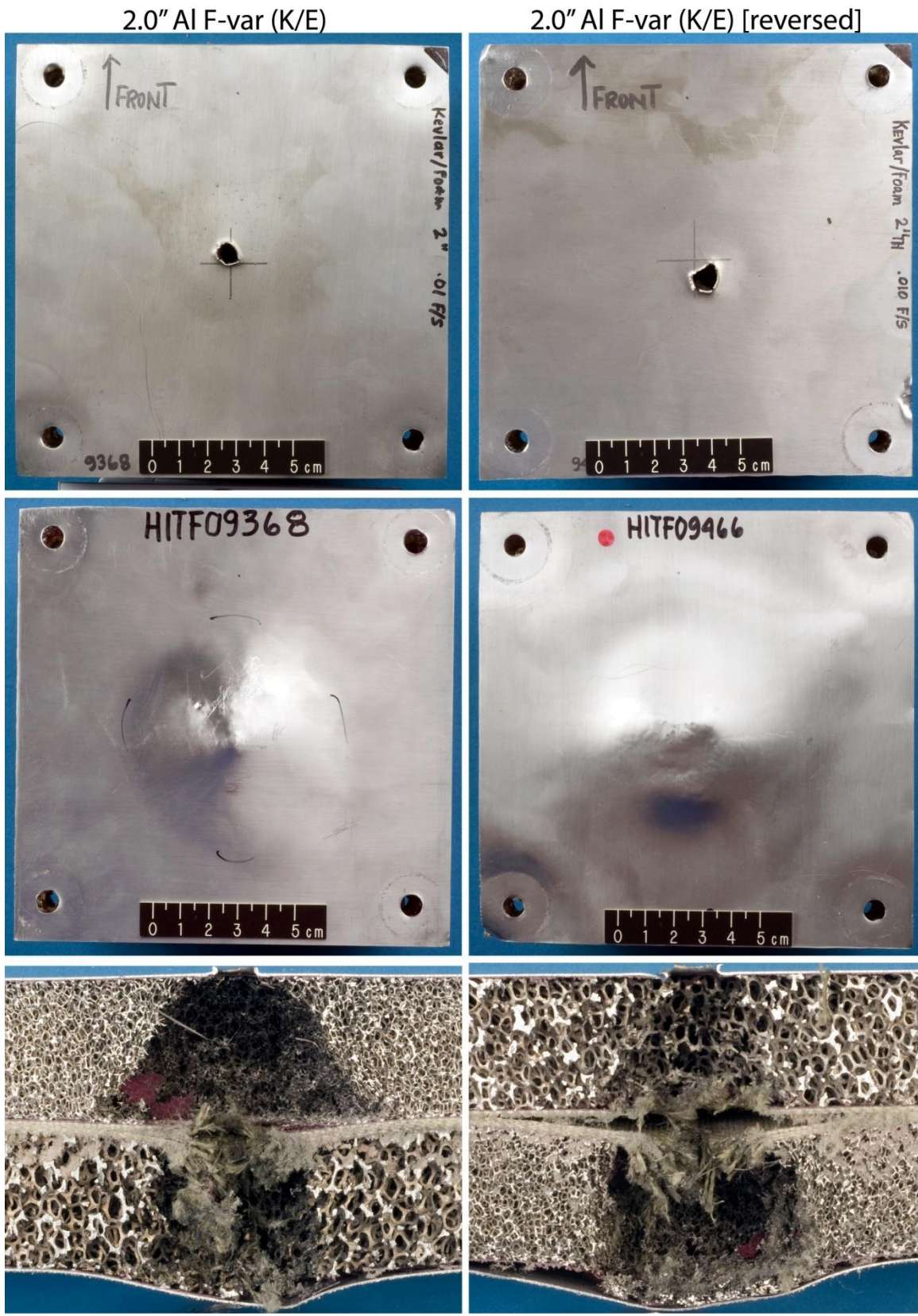


**Figure 62:** Comparison of the F-var (K/E) original (left) and reversed (right) configurations impacted by 4.0 mm diameter projectiles at  $\sim 6.8$  km/s with normal incidence ( $0^\circ$ ).

## A Ballistic Limit Equation for Foam Core Sandwich Panels

Ballistic limit equations define the threshold of perforation for a given structure or shielding configuration. They are generally based on analytical expressions, but use experimental data to empirically anchor them at the highest obtainable impact velocities. From the results presented in this report, it is possible to define a ballistic limit equation for aluminum sandwich panels with aluminum open-cell foam cores.

The penetration of porous media such as concrete, sandstone, and foams is generally described across the range of impact velocities relevant to spacecraft MMOD protection by a continuous relationship such as that in Cour-Palais [16]. However, clear evidence of increased performance with increasing velocity between 2.2 and 5.0 km/s was observed in the experiments (see Figure 63 and Figure 64), suggesting that the shield behavior is similar to that of a spaced multi-wall shield – i.e. performance enhancement following the onset of projectile fragmentation.

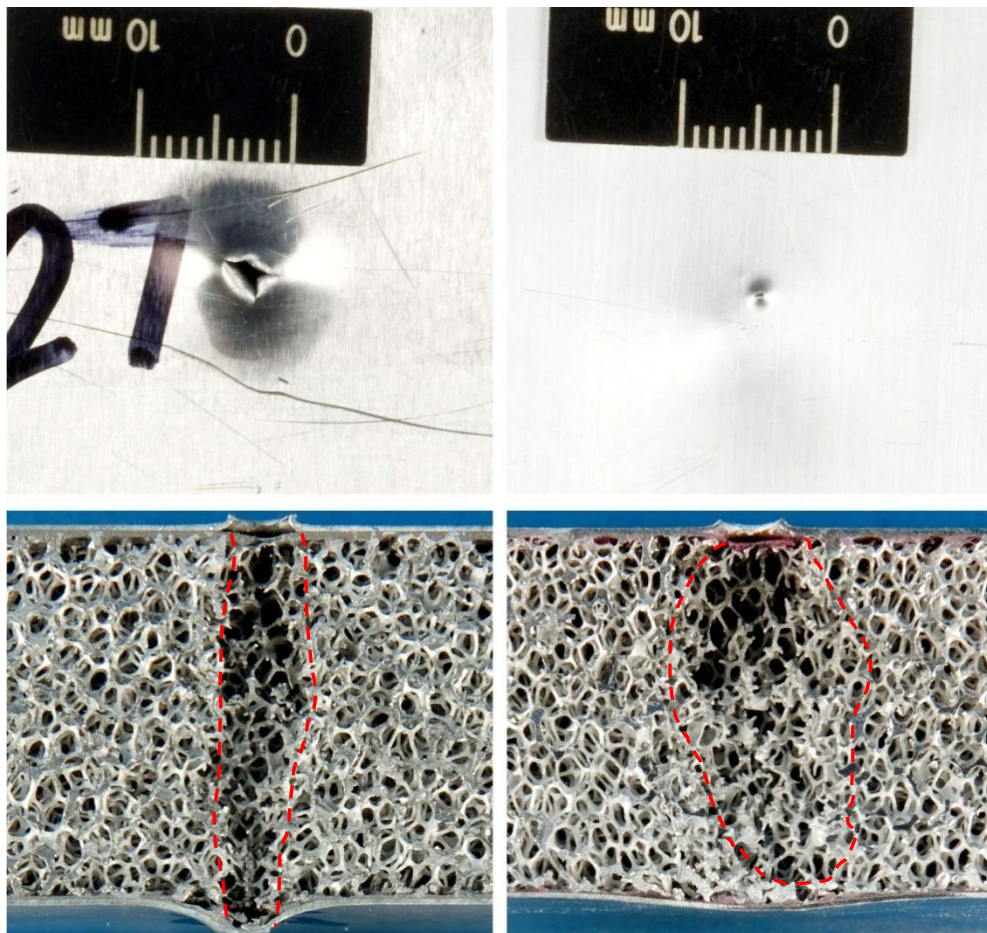


**Figure 63:** Evidence of decreased cratering depth with increasing velocity between 2.2 km/s and 5.0 km/s: HITF08423 (left) and HITF08424 (right).

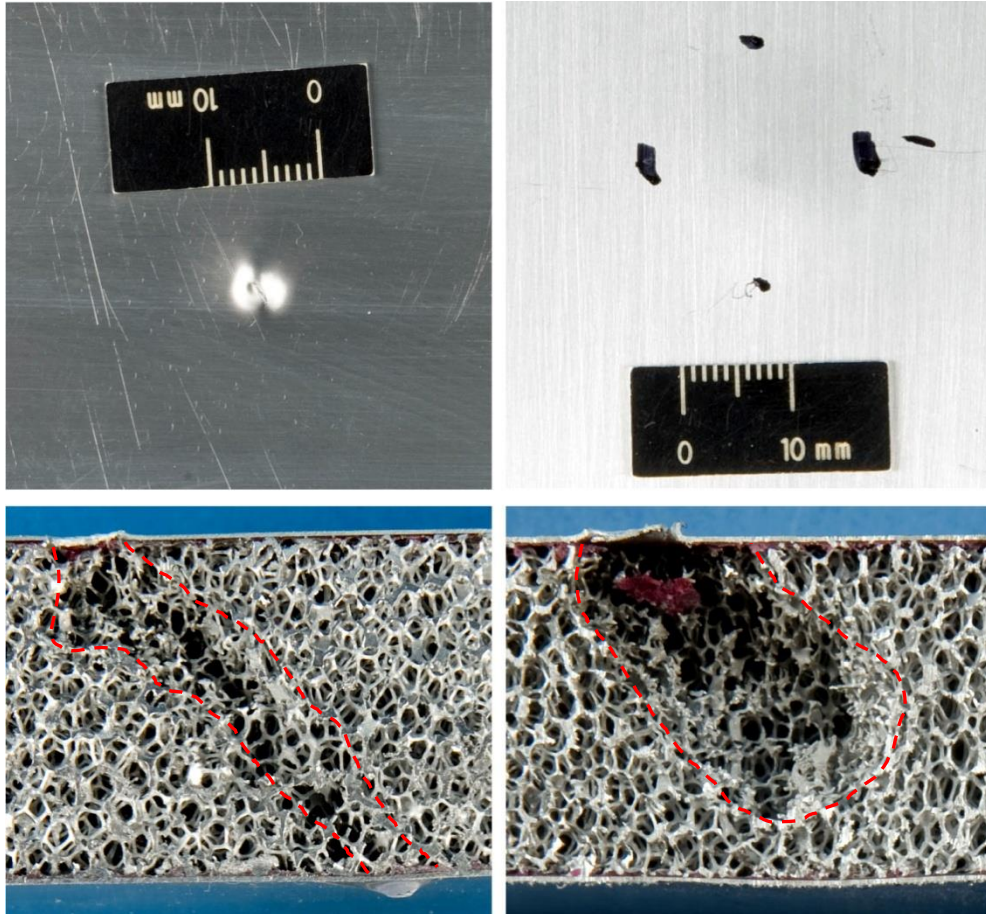


**Figure 64:** Evidence of decreased cratering depth with increasing velocity between 2.2 km/s and 5.0 km/s: HITF08420 (left) and HITF08427 (right).

As such, the derived ballistic limit equation is based on the NNO Whipple shield equation [2]. The ballistic limit equation is divided into three regimes: low velocity, transition (or shatter), and hypervelocity. The limits of these regimes are generally defined by physical processes that occur during impact of the projectile upon the bumper of a Whipple shield, or the front facesheet of a sandwich panel. However, considering the effect of secondary impacts upon individual foam ligaments, it is more reasonable for this type of configuration to define the ballistic limit equation limits according to the state of fragments when they impact upon the rear facesheet of the sandwich panel.

Secondary impacts on individual foam ligaments have been found to increase the thermal state of penetrating projectile and bumper fragments, leading to fragmentation, melt, and vaporization at lower impact velocities than traditional shields (e.g. Whipple shield). However, it is difficult to infer the state of the debris cloud upon impact with the foam core sandwich panel given the panel construction and failure mechanism observed in the majority of the experiments (i.e. single fragment perforation). The low-to-shatter regime velocity limit,  $V_{LV}$ , is defined as:

$$V_{LV} = 2.25 / (\cos \theta)^{1/3} \quad (1)$$

In the low-velocity regime (i.e.  $V \leq V_{LV}$ ), the ballistic limit of an open-cell foam core sandwich panel is calculated as:

$$d_c(v) = \frac{1.83 \left( t_b + t_w (\sigma/276)^{1/2} + t_f^{11/10} (\rho_f/\rho_w) \right)}{\left( \rho_p^{1/2} \cdot V^{2/3} \cdot (\cos \theta)^{4/5} \right)^{18/19}} \quad (2)$$

where  $t_b$  is the thickness of the front facesheet (cm)  
 $t_w$  is the thickness of the rear facesheet (cm)  
 $t_f$  is the thickness of the foam core (cm)  
 $\rho_w$  is the density of the rear facesheet ( $\text{g}/\text{cm}^3$ )  
 $\rho_f$  is the volumetric density of the foam core ( $\text{g}/\text{cm}^3$ )  
 $\rho_p$  is the projectile density ( $\text{g}/\text{cm}^3$ )  
 $\sigma$  is the yield strength of the rear facesheet material (MPa)

Eq. (2) is based on the Cour-Palais semi-infinite penetration relationship [16], and includes the foam core thickness in the maximum allowable penetration depth via determination of an equivalent-weight aluminum plate thickness. The effect of the foam on performance, compared to that of the equivalent aluminum plate, is included in the foam thickness exponential (1.1) and equation constant (1.83 vs. 1.62). Additionally, angle dependence is increased to  $(\cos \theta)^{4/5}$  from the original equation, indicating a more substantial performance increase with increasing obliquity.

For multi-wall shields, transition from the shatter regime to hypervelocity regime occurs when the rear wall failure mechanism changes from cratering/spallation to impulsive, indicating a completely (or near to) molten and gaseous debris cloud. Although the foam core is expected to enhance fragment melting and vaporization compared to a standard multi-wall shield, impulsive failure of the panel rear facesheet was not observed in any of the impact experiments on the baseline foam targets, even at velocities above 7 km/s. Rather, the failure threshold was defined by the perforation of individual solid fragments that often penetrated beyond the primary damage zone. Subsequently, not only is the failure limit of foam core sandwich panels subject to higher uncertainty than that of Whipple shields, the definition of the hypervelocity impact regime must be reconsidered. For this study, the transition from shatter regime to hypervelocity regime ( $V_{HV}$ ) is considered to occur once an increase in projectile velocity results in increased penetration depth and, therefore, increased rear facesheet damage. The transition velocity is defined as:

$$V_{HV} = 4.0 / (\cos \theta)^{1/3} \quad (3)$$

In the hypervelocity regime (i.e.  $V \geq V_{HV}$ ), the foam core sandwich panel ballistic limit equation is calculated as:

$$d_c(v) = 2.152 \frac{\left( t_w + 0.5 AD_f / \rho_w \right)^{2/3} 0.89 \cdot t_f^{9/20} (\sigma/483)^{1/3}}{\rho_p^{1/3} \cdot \rho_b^{1/9} \cdot V^{2/5} (\cos \theta)^{4/5}} \quad (4)$$

where  $AD_f$  is the foam core areal density ( $\text{g}/\text{cm}^2$ )  
 $\rho_b$  is the front facesheet density ( $\text{g}/\text{cm}^3$ )

The effect of the foam core is included in Eq. (4) as an increase in the Whipple shield rear wall thickness corresponding to 50% that of an equivalent weight plate, and an increase in the thickness/spacing dependence from 1/3 to 0.45. The original NNO equation is based on kinetic energy scaling in the hypervelocity regime. Although considered a conservative approach, limitations of experimental facilities prevent verification or adoption of proposed surrogate validation techniques (e.g.

numerical simulation, cadmium scaling, etc.). For the foam core sandwich panels, transition to hypervelocity regime is considered to occur at lower velocities, and as such, test data are available for empirical adjustment of the speed dependence ( $V^{-2/3} \rightarrow V^{-2/5}$ ). Additional modifications to the baseline equation are made for angle dependence and scaling constant.

In the intermediate regime (i.e.  $V_{LV} < V < V_{HV}$ ), linear interpolation is used:

$$d_c(v) = d_c(v_{LV}) + \frac{d_c(v_{HV}) - d_c(v_{LV})}{v_{HV} - v_{LV}} \cdot (v - v_{LV}) \quad (5)$$

The ballistic limit equation has been derived for application with 40 PPI foam core sandwich panels. In Phase 1 of the study, the 40 PPI panel was found to provide superior performance over the 10 PPI and 20 PPI panels; however, the variation was generally minimal (particularly when experimental scatter is considered). A nominal 5% decrease in the predicted critical projectile diameter in the hypervelocity regime should be applied for application of the ballistic limit equation to 10 and 20 PPI core panels.

In Figure 65 through Figure 73, the ballistic limit equation is expressed as a curve, demarcating between impact conditions expected to lead to failure of the structural panel, and those against which the shield is capable of defending. Test data are also included in the figures. Of the 99 impact tests performed in this study and in Yasensky, Christiansen, and Prior [10], 71 (72%) are predicted accurately. Twenty-five tests (25%) are slightly conservatively predicted (i.e.  $d_p/d_c < 1.2$ ), two (2%) are conservatively predicted (i.e.  $1.2 < d_p/d_c < 1.5$ ) and one (1%) is non-conservatively predicted. The single non-conservative prediction is within 1.0% of the experimental diameter (i.e.  $d_p/d_c \geq 0.99$ ), and as such is considered to lie well within the uncertainty bounds of the curve. In Figure 74, an evaluation of the ballistic limit equation's predictive accuracy is provided. In this figure, markers above unity are predicted failures, while those below are predicted pass events. Black markers below unity indicate non-conservative predictions, while white markers above indicate conservative predictions.

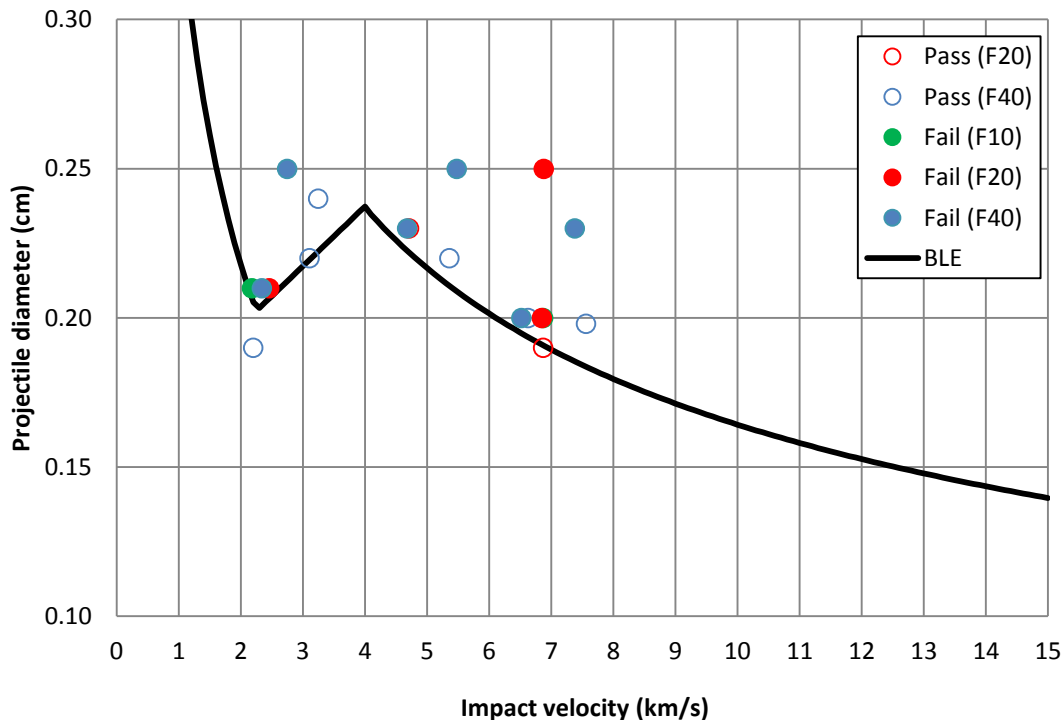


**Figure 65:** Ballistic limit curve for the baseline 1.0" Al foam sandwich panel at 0° plotted with test data.

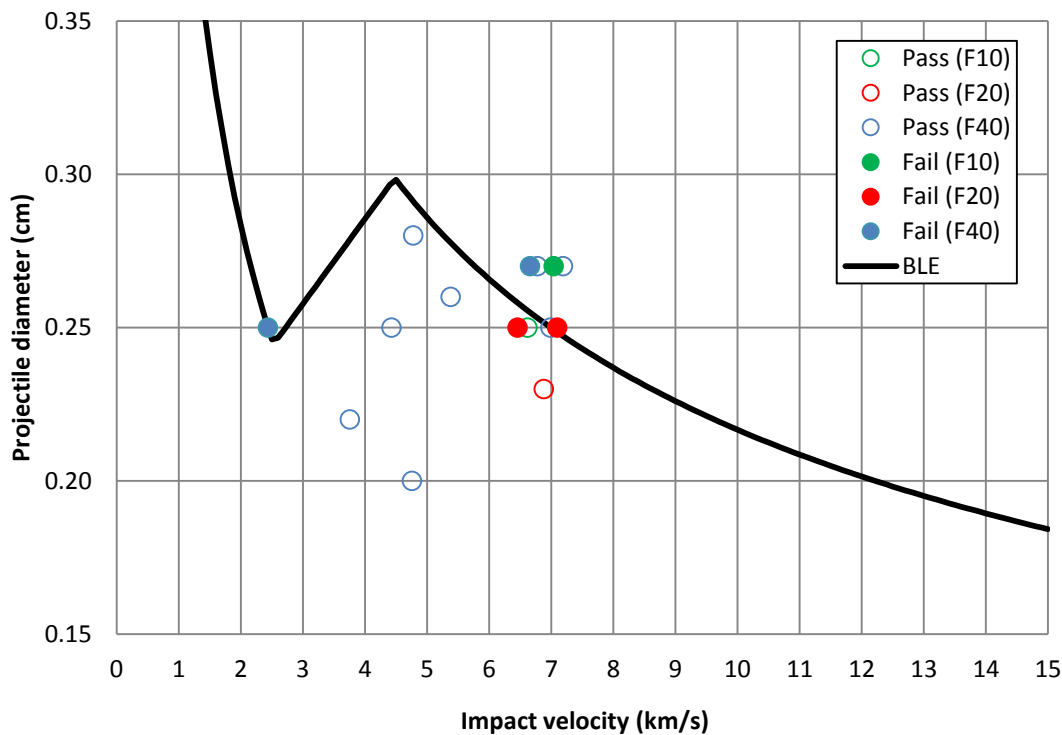


**Figure 66:** Ballistic limit curve for the baseline 1.0" Al foam sandwich panel at 45° plotted with test data.

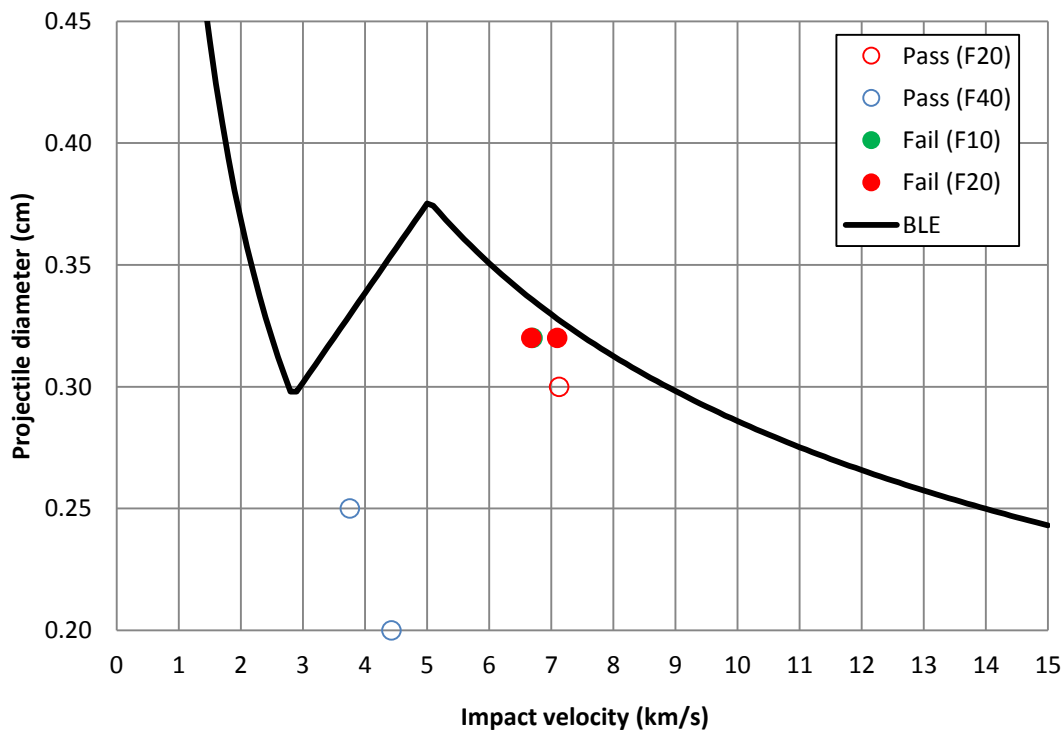


**Figure 67:** Ballistic limit curve for the baseline 1.0" Al foam sandwich panel at 60° plotted with test data.

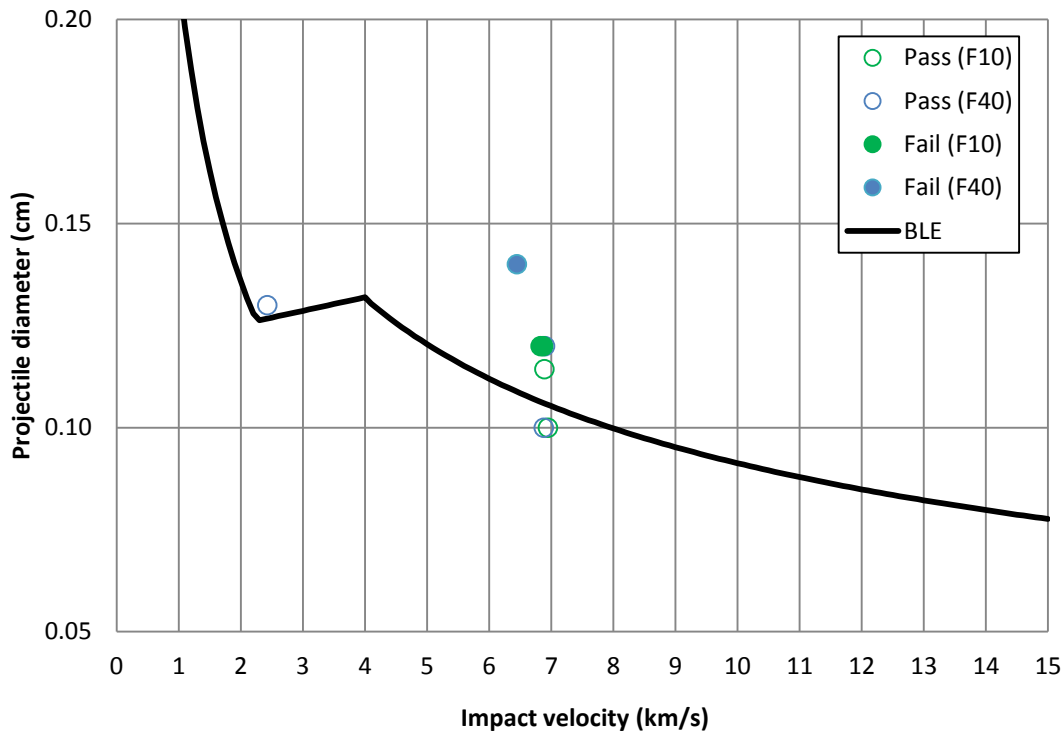


**Figure 68:** Ballistic limit curve for the 0.5" Al foam sandwich panel at 0° plotted against test data (including data from [10]).

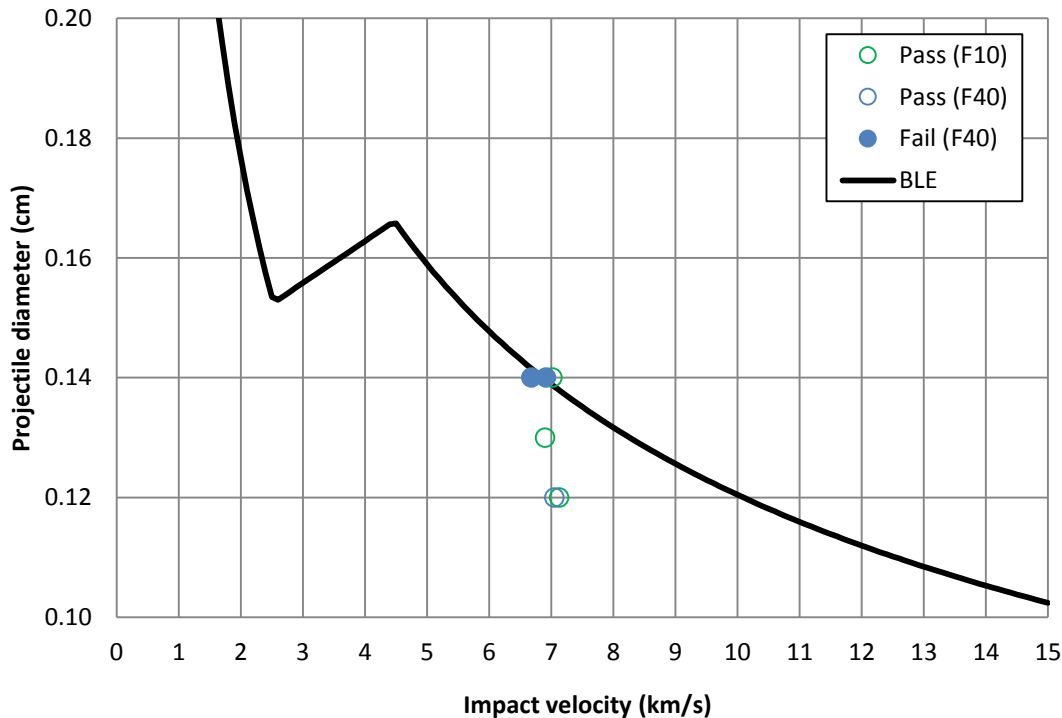


**Figure 69:** Ballistic limit curve for the 0.5" Al foam sandwich panel at 45° plotted against test data (including data from [10]).

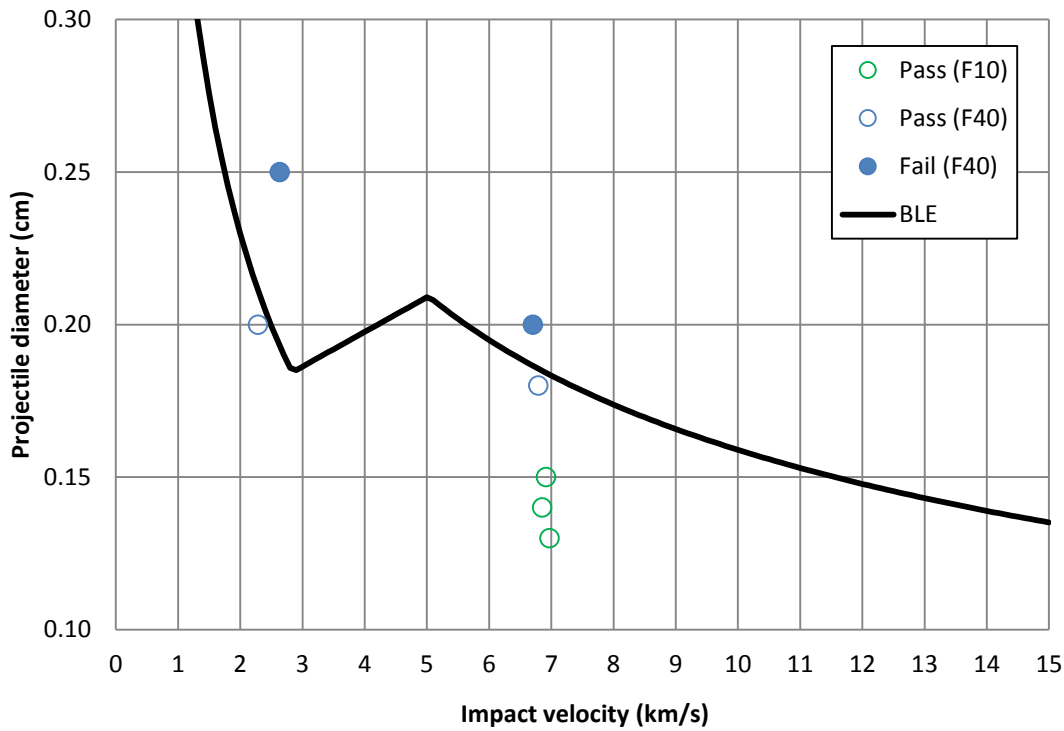


**Figure 70:** Ballistic limit curve for the 0.5" Al foam sandwich panel at 60° plotted against test data.

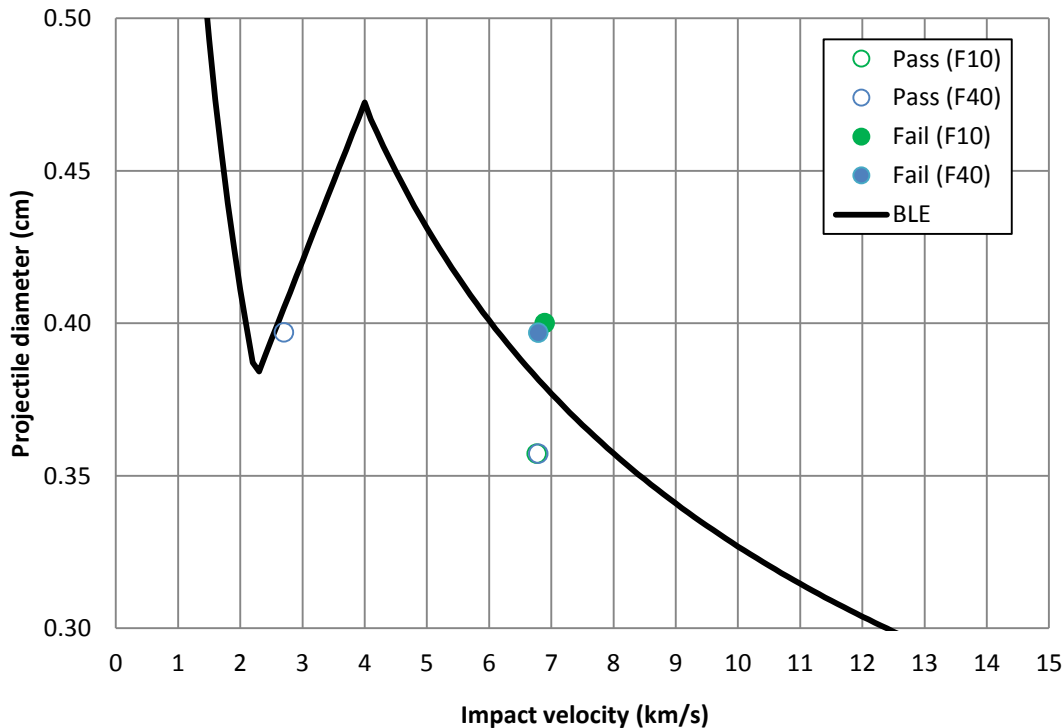


**Figure 71:** Ballistic limit curve for the 2.0" Al foam sandwich panel at 0° plotted against test data (including data from [10]).

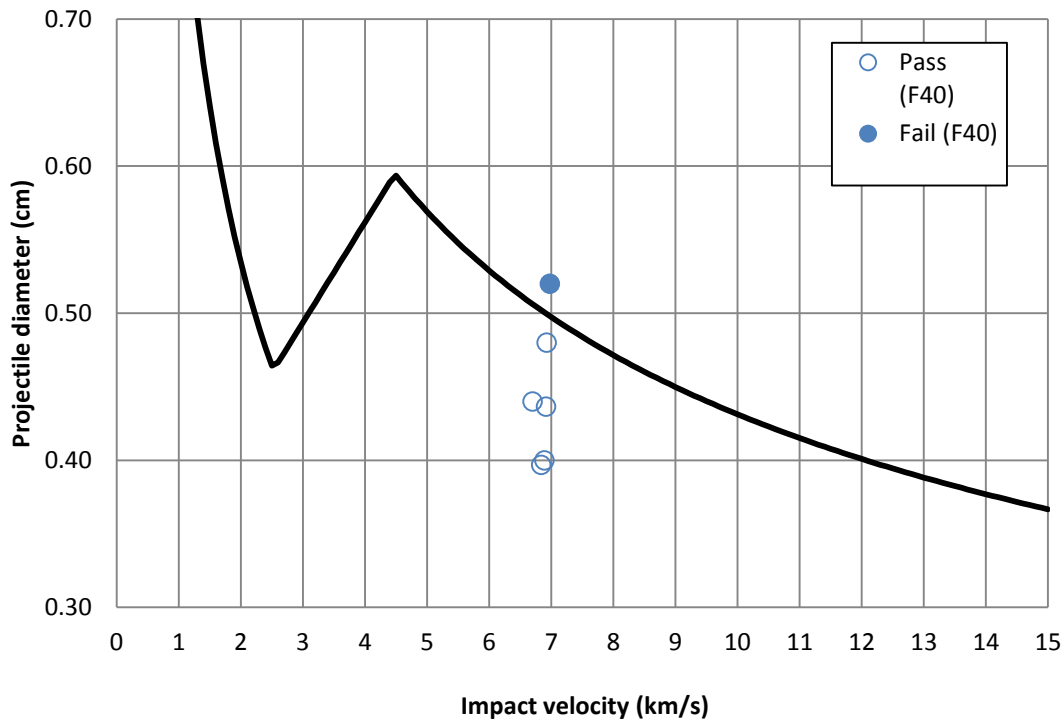


**Figure 72:** Ballistic limit curve for the 2.0" Al foam sandwich panel at 45° plotted against test data (including data from [10]).

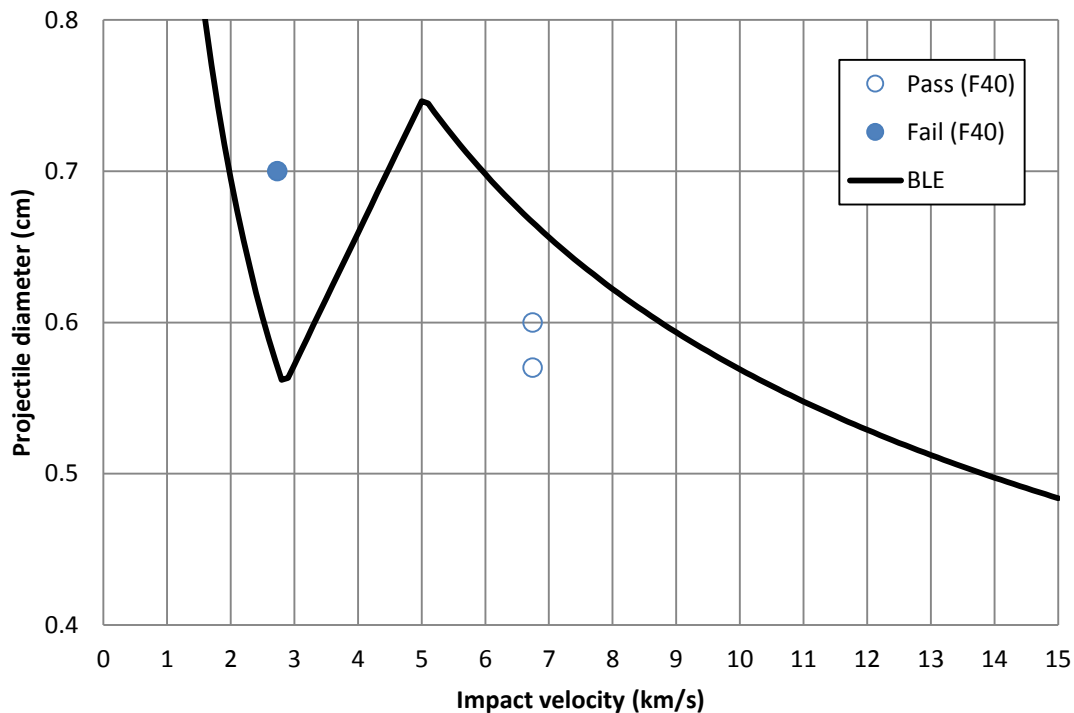


**Figure 73:** Ballistic limit curve for the 2.0" Al foam sandwich panel at 60° plotted against test data.

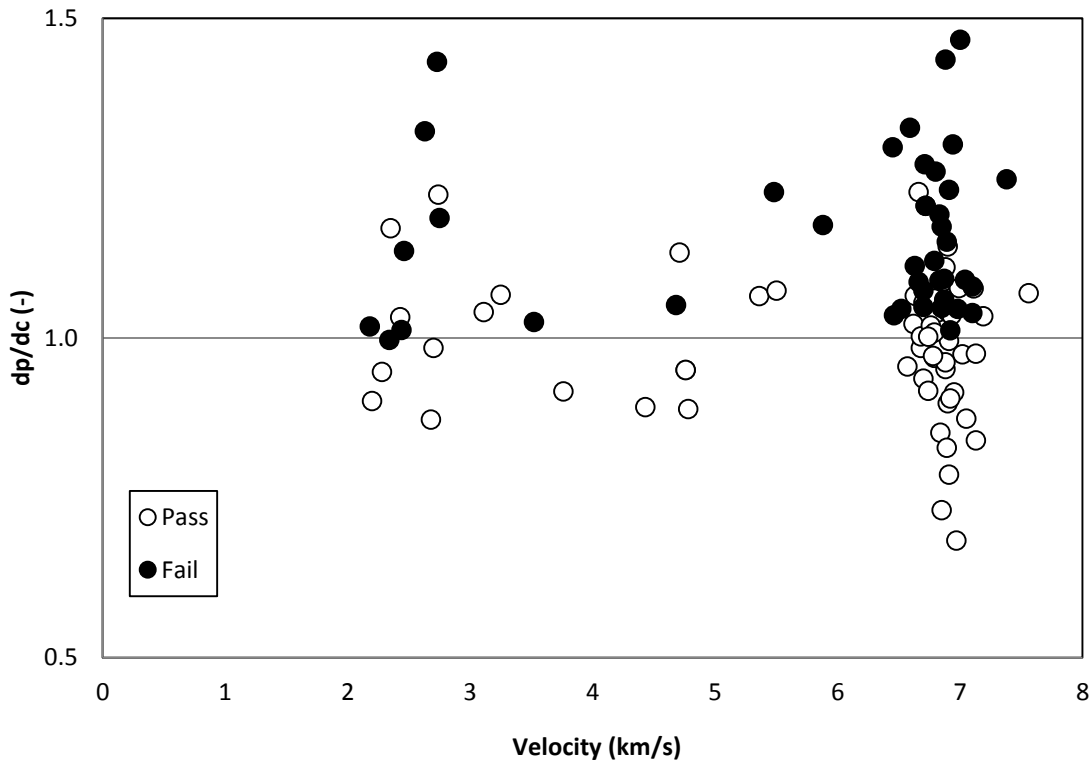


**Figure 74:** Evaluating the accuracy of the foam ballistic limit equation.

### Comparison with Other Shield Types

To understand the relative performance of foam core sandwich panels relative to other common low-weight shield types, the derived ballistic limit equation can be compared to those of a flight-representative Whipple shields (ballistic limit equation from Christiansen [2]) and aluminum honeycomb core sandwich panel (ballistic limit equation from Ryan, Schaefer, Destefanis, and Lambert [4]). As a Whipple shield requires non-ballistic mass for installation and support structure, 30% of the bumper mass is detracted from the weight budget. The selected Whipple shield consists of a 0.07 cm thick Al6061-T6 bumper and a 0.18 cm thick Al6061-T6 rear wall, with a standoff of 2.54 cm ( $AD_{total} = 0.69 \text{ g/cm}^2$ ). The honeycomb core sandwich panel has 0.105 cm thick Al6061-T6 facesheets, with a 2.54 cm thick type 1/8-5052-.001 honeycomb core ( $AD_{total} = 0.75 \text{ g/cm}^2$ ). A comparison of the ballistic limit curves is provided in Figure 75.

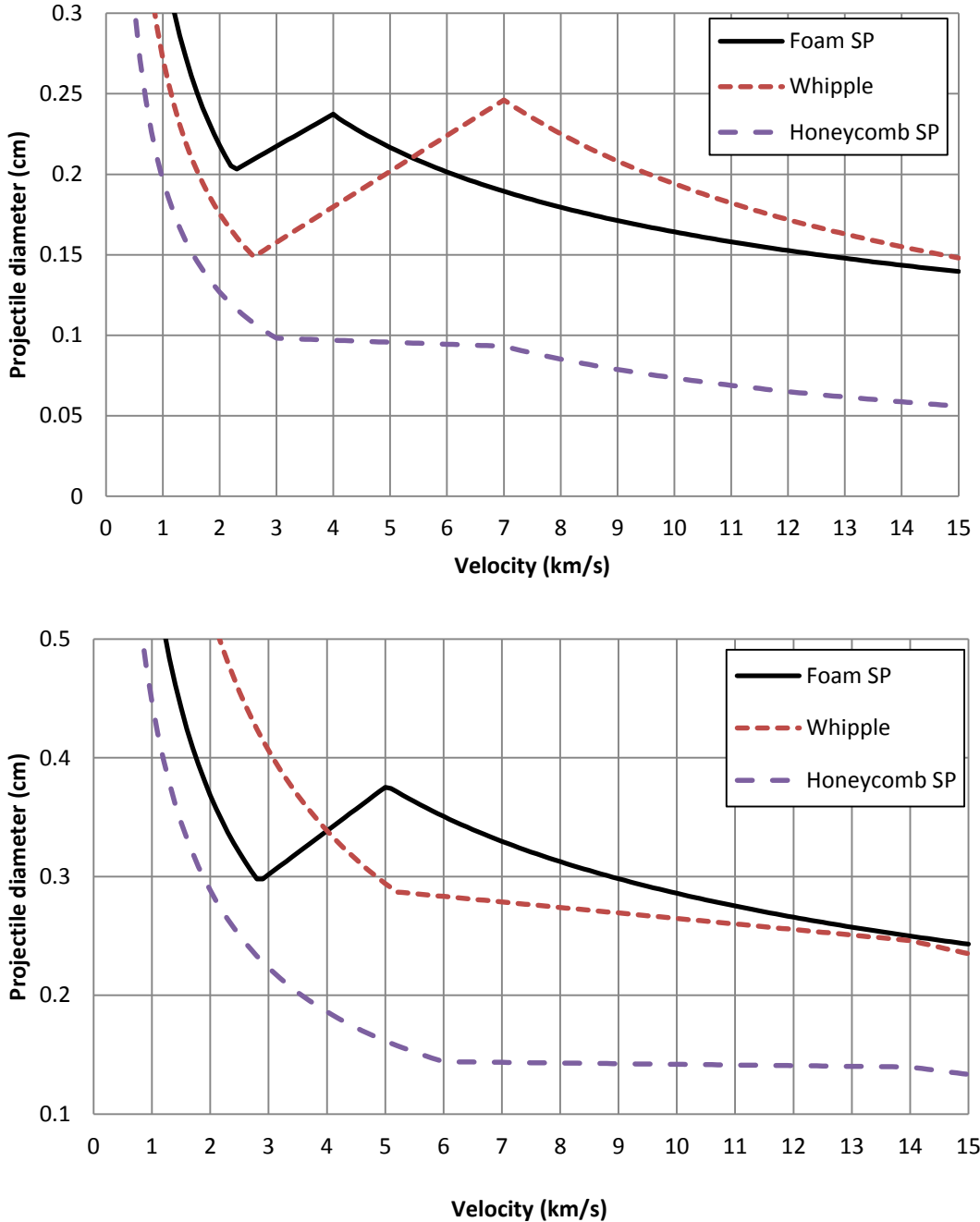


**Figure 75:** Comparison of ballistic limit curves for the 1.0" Al F40 foam panel, flight-representative Whipple shield, and honeycomb core sandwich panel (normal impact (top), 60° impact (bottom)).

The foam sandwich panel is shown to perform better than the aluminum honeycomb sandwich panel over the range of velocities considered. At velocities below 5 km/s, the performance of the foam panel is also superior to that of the metallic Whipple shield, yet poorer at higher velocities. The differing velocity dependence of the Whipple and foam ballistic limit equations is demonstrated by the decrease in performance variation between the two shields in the hypervelocity regime. It is expected that for mission risk assessment, the foam sandwich panel and Whipple shield configurations would provide comparable results.

## Concluding Remarks

Although unsuited to the task, honeycomb sandwich panels are amongst the most common structures used for shielding against the impact of micrometeoroids and orbital debris. Metallic open-cell foams provide a comparable level of mechanical and thermal performance to honeycomb core panels, and have been identified in a number of studies as a feasible component in multi-wall MMOD shields (e.g. [7][11]). Prior to this study, however, an extensive evaluation of their performance as a stand-alone protective structure has been lacking.

In this study, the performance of an open-cell aluminum foam (trade name Duocel®, manufactured by ERG Aerospace) has been evaluated through an extensive experimental impact program. The study was split into four phases, evaluating: the influence of core characteristics (i.e. pore density, relative density) on shielding performance; the effect of core thickness on shielding performance; the effect of facesheet thickness on shielding performance; and the performance of foam core panels relative to alternate, comparable weight, sandwich panel configurations.

In Phase 1 of the investigation, shielding performance was found to increase with increasing pore density; however, a definitive qualitative relationship was difficult to define due to sensitivity of the panels to experimental scatter. Secondary impacts of projectile and front facesheet fragments on individual foam ligaments is key to the shielding performance of foam structures, leading to enhanced fragmentation, melting, and vaporization at lower impact velocities than traditional dual-wall shields. However, for materials with large pore diameters relative to rear facesheet thicknesses, the non-homogeneity of the foam material can allow individual fragments to pass through the panel with few secondary impacts. These fragments are able to perforate the panel rear facesheet at conditions in which the main fragment cloud penetrates through only 40%-50% of the core thickness. The performance of 40 PPI foam core panels was defined as approximately 5% superior to 10 and 20 PPI foam structures, in terms of critical projectile diameter. The effect of relative material density, which influences the cross-sectional form of the foam ligaments, was also evaluated in Phase 1. Nominally identical impact tests were performed at three different conditions, for which the performance of the baseline 6%-8% relative density material was comparable to that of the 3%-5% relative density material. Examination of the core damage found that although the gross results of the tests were similar for the two materials, damage within the core of the 3%-5% relative density panel was significantly more pronounced than the heavier panel. As such, the performance of foam core sandwich panels is expected to increase with increasing relative density; however, the rate of performance increase is considerably less than would be gained through adding weight to the panel facesheets. From the findings in Phase 1, 40 PPI, 6%-8% relative density foam was selected for investigation in the remaining phases of the study.

In Phase 2, the thickness of the foam core was varied to evaluate its influence on failure limits. Two additional core thicknesses (1.27 cm and 5.08 cm) were evaluated over a series of 12 experiments. As expected, the performance of the foam core panels increased with increasing thickness; however, the panels remained sensitive to perforation by individual solid fragments that penetrated well beyond the primary damage cavity.

Phase 3 of the study investigated the influence of front and rear facesheet thickness on the failure limits of the core panel. Three variations of thickness for each facesheet were evaluated, and substantial improvements in protective capability were found for even minimal increases in the thickness of the rear facesheet. Changes in the front facesheet thickness were found to have minimal effect on the panel failure limits. The sandwich panels with increased rear wall thickness were found to be less susceptible to perforation by individual fragments penetrating beyond the primary damage cavity, which likely accounts for a majority of the performance gain found for small increases in rear facesheet thickness.

In Phase 4, a total of six alternate sandwich panel configurations were evaluated for comparison with the open-cell foam structure. Of the alternate configurations, three were modifications of the foam material, while the remaining three were variations of honeycomb core panels. A variable pore density panel (40/20/5 PPI) was designed to maximize secondary impacts during the initial penetration phase and

enable an increased degree of fragment cloud expansion toward the rear facesheet. The performance of the panel was similar to, if not slightly worse than, that of the baseline 40 PPI foam under normal impact at high velocity. The variable pore density foam configuration was reversed for a single test, such that the lower PPI sections were toward the outer edge of the panel (i.e. 5/20/40 PPI). This configuration results in larger foam ligament thickness to projectile fragment ratios during the initial penetration into the foam core. As the size of projectile and front facesheet fragments decrease (i.e. as they penetrate through the core thickness), the diameter of the foam cells is decreased, maximizing the potential for late-stage secondary impacts. This reversal was found to decrease the panel performance below that of the baseline 40 PPI foam. Two composite reinforced panels were constructed using Kevlar/epoxy and Nextel/epoxy laminates located in the middle of the foam core. The Nextel/epoxy reinforced panel was found to perform significantly worse than the baseline panel, while the Kevlar/epoxy reinforced panel provided a minimal improvement. However, both composite reinforced panels were found to limit the sensitivity of the foam core panels to perforation by individual fragments penetrating beyond the primary damage cavity. Used in conjunction with increased rear wall thickness, the Kevlar/epoxy reinforcement may provide a considerable increase in shielding capability while limiting variations in panel failure limits. The three honeycomb panels considered in Phase 4 included a Nomex honeycomb, 3-D aluminum honeycomb, and baseline aluminum honeycomb core. Use of Nomex honeycomb was intended to decrease the amount of fragment channeling commonly observed during impact on honeycomb core sandwich panels, due to a lower ricochet angle [13]. Although greater lateral expansion in the Nomex core was observed, compared to the aluminum honeycomb, the performance was substantially worse at both normal and oblique incidence. The 3-D aluminum honeycomb is constructed of foils rotated at +45°/-45°, thus eliminating the presence of shielding-detrimental through-thickness channeling cells. The performance of the 3-D honeycomb (trade name Trussgrid) was comparable to that of the 40 PPI foam over a variety of impact conditions, and should be evaluated further.

A ballistic limit equation was derived for the foam core sandwich panels, based on the new non-optimum Whipple shield equation [2]. The effect of repeated shocking, and its influence on projectile fragmentation and melting, is recognized in the transition velocities of the equation, which are defined at 2.25 and 4.0 km/s (normal), versus 3.0 and 7.0 km/s for a standard aluminum Whipple shield. The foam core is an active component in the shielding process, and as such is included in the ballistic limit equation as a scaled weight-equivalent increase in the facesheet thicknesses. Of the 99 new and existing experimental results, the equation correctly predicts 71 correctly, with 27 tests predicted conservatively, and one test predicted non-conservatively. The equation is validated for a variety of panel thicknesses, foam pore densities, relative density foams, facesheet thicknesses, impact angles, impact velocities, and projectile diameters, and is expressed in a form suitable for application in risk assessment codes.

The performance of the foam core panels predicted with the derived ballistic limit equation was compared to that of a flight-representative Whipple shield and honeycomb core sandwich panel. The foam panel was shown to be clearly superior to the predicted performance of the honeycomb core panel at both normal and oblique incidence, and is comparable to that predicted for the Whipple shield configuration. It is considered that for mission risk assessment, the foam panel and representative Whipple shield would provide comparable penetration probabilities.

## References

1. F.L. Whipple, “*Meteorites and Space Travels*”, Astronomical Journal; 1161: 131, 1947.
2. E.L. Christiansen, “*Design and Performance Equations for Advanced Meteoroid and Debris Shields*”, International Journal of Impact Engineering; 14: 145-156, 1993.
3. E Taylor, J. Glanville, R Clegg, R Turner, “*Hypervelocity Impact on Spacecraft Honeycomb: Hydrocode Simulation and Damage Laws*”, International Journal of Impact Engineering; 29: 691-702, 2003.
4. S. Ryan, F.K. Schaefer, R. Destefanis, M. Lambert. “A Ballistic Limit Equation for Hypervelocity Impacts on CFRP/Al HC Satellite Structures”, Advances In Space Research; 41: 1152-1166, 2008.
5. R Sennett, B Lathrop, “*Effects of Hypervelocity Impact on Honeycomb Structures*”, Journal of Spacecraft and Rockets; 5: 1496-1497, 1968.
6. M.F. Ashby, A.G. Evans, N.A. Fleck, L.J. Gibson, J.W. Hutchinson, H.N. Wadley, “*Metal Foams: A Design Guide*”, Butterworth Heinemann, Boston, ISBN: 0750672196, 2000.
7. R. Destefanis, F.K. Schaefer, M. Lambert, M. Farraud, E. Schneider, “*Enhanced Space Debris Shields for Manned Spacecraft*”, Int. J. of Impact Engineering; 29: 215-226, 2003.
8. R. Destefanis, “*Enhanced Space Debris Shields for Manned Spacecraft – Evaluation Report: Phase A and Phase B Tests*”, Alenia-Spazio, Turin, ESD-TN-Al-005, 2004.
9. F.K. Schaefer, T. Behner, C. Kurz, S. Ryan. “Enhanced Debris Shields for Manned Spacecraft – WP5000 Phase B Tests”, Fraunhofer Ernst-Mach-Institute (EMI), Freiburg, Report No. I-37/04 (ESA Contract 15512/01/NL/CK), 2004.
10. J. Yasensky, E.L. Christiansen, T. Prior, “*Hypervelocity Impact Evaluation of Metal Foam Core Sandwich Structures*”, GeoControl, Houston, NASA TP-2008-214776, 2008.
11. S. Ryan, T. Hedman, E.L. Christiansen. “Honeycomb vs. Foam: Evaluating a Potential Upgrade to International Space Station Module Shielding for Micrometeoroids and Orbital Debris”, NASA Johnson Space Center, Houston, NASA/TM-2009-214793, 2009.
12. S. Ryan, E.L. Christiansen. “Hypervelocity Impact Testing of Advanced Materials and Structures for Micrometeoroid and Orbital Debris Shielding”, NASA Johnson Space Center, Houston, NASA/TM-2010-XXXX, 2010.
13. C. Chu, Y. Chen, G. Hseu, D. Hwang D. The study of obliquity on the ballistic performance of basket fabric composite materials, *Journal of Composite Materials* 2007; **41**(13): 1539-1558.
14. J.C. Anderson, D.J. Henderson, K.M. Rodriguez. “*17-caliber Light Gas Gun Velocity Measurement Uncertainty Analysis*”, NASA JSC White Sands Test Facility, Las Cruces, WSTF-IR-1086-001-07, 2007.
15. J.C. Anderson, D.J. Henderson, K.M. Rodriguez. “*50-calider Light Gas Gun Velocity Measurement Uncertainty Analysis*”, NASA JSC White Sands Test Facility, Las Cruces, WSTF-IR-1103-001-07, 2007.
16. B. Cour-Palais. “Hypervelocity Impact Investigations and Meteoroid Shielding Experience Related to Apollo and Skylab”, Orbital Debris; 247-275, 1985.

## Appendix A

**Table A-1:** Phase 1 test results.

HITF No.	Result		Front facesheet				Rear facesheet				Core			WP Nh (-)
	Coarse [NP/SP/P]	Detailed [<,≤,=,≥,>]	d <sub>h</sub> (mm)	D <sub>dam</sub> (mm)	N <sub>h</sub> (-)	d <sub>h</sub> (mm)	D <sub>h</sub> (mm)	b <sub>d</sub> (mm)	b <sub>max</sub> (mm)	D <sub>HC</sub> (mm)	Δ <sub>HC</sub> (mm)			
1	08252	P	>	4.9×5.0	15.8×15.1	3	8.0×8.0	17.6×17.1	42.1×39.9	5.8	16.5×15.3	-	-	0
2	08253	P	≥	5.5×5.3	19.7×17.3	1	< 1.0	-	14.7×13.0	0.9	12.3×12.3	0.0×2.6	-	0
3	08254	NP	<<	4.4×5.3	19.4×20.6	0	-	-	0.0×0.0	0.0	12.8×12.5	-	-	-
4	08255	P	>	7.3×6.4	10.5×12.9	1	5.2×6.4	-	24.3×25.6	2.6	17.8×15.8	17.6×0.7	-	0
5	08256	NP	<	5.0×5.7	7.8×10.9	0	-	-	16.8×16.8	0.3	20.3×15.2	-	-	-
6	08257	P	≥	5.4×6.2	6.8×7.8	2	< 1.0	10.1×16.2	21.8×30.1	1.1	18.8×15.9	2.4×8.3	-	0
7	08258	NP	≤	6.8×11.0	11.1×14.8	0	-	-	20.1×25.8	0.6	26.0×20.4	-	-	-
8	08259	P	≥	6.3×9.4	10.8×15.0	1	< 1.0	-	28.0×35.1	1.0	31.3×20.8	25.7×5.5	-	0
9	08260	NP	<<	7.6×11.8	8.9×15.2	0	-	-	29.8×34.7	0.4	33.0×19.7	-	-	-
10	08261	P	≥	4.9×5.2	16.1×20.2	1	< 1.0	-	13.5×9.7	1.4	14.8×15.6	0.0×4.9	-	0
11	08263	P	≥	4.8×5.0	14.6×16.6	1	< 1.0	-	10.4×19.0	0.7	12.3×16.2	8.3×3.3	-	0
12	08268	NP	<<	4.9×6.8	13.4×12.3	0	-	-	16.8×12.9	0.5	13.0×14.1	-	-	-
13	08269	P	>	7.6×8.8	20.6×16.0	2	5.1×2.7	6.6×7.4	38.0×36.0	4.7	20.7×15.3	16.7×4.3	-	0
14	08270	NP	<<	5.3×6.7	16.9×18.0	0	-	-	22.2×23.5	0.8	20.0×13.1	-	-	-
15	08271	NP	<	7.3×9.2	21.2×17.5	0	-	-	24.9×26.0	2.0	22.0×15.9	-	-	-
16	08272	P	>	6.9×9.2	11.8×11.9	1	2.7×2.8	-	24.9×36.0	2.8	30.9×19.3	23.6×6.4	-	0
17	08267	NP	<<	7.5×12.7	18.9×25.7	0	-	-	21.3×26.2	0.9	30.9×21.8	-	-	-
18	09007	NP	<	6.6×12.9	12.5×13.7	0	-	-	33.0×34.7	1.7	31.0×21.4	-	-	-
19	08276	P	>	3.0×3.0	4.0×4.0	2	2.9×2.9	4.1×10.2	13.7×9.6	2.2	5.6×8.8	-	-	0
20	08279	P	>>	6.1×5.4	8.6×8.8	1	13.8×12.5	-	29.9×23.0	5.6	12.5×14.8	-	-	0
21	08280	P	>	8.1×8.4	8.4×8.4	1	7.3×8.3	-	13.0×14.3	2.2	6.6×5.4	3.2×1.9	-	0
22	08420	P	=	3.7×5.3	4.5×5.8	0	-	-	5.6×7.1	1.1	11.4×9.0	-	-	-
23	08421	NP	<	3.3×4.7	4.3×5.4	0	-	-	3.5×4.6	0.5	11.0×11.5	-	-	-
24	08422	P	>	3.9×3.9	5.4×5.4	1	3.4×3.0	-	18.5×20.9	3.5	13.8×15.0	1.2×0.3	-	0
25	08424	P	=	3.9×3.8	5.1×5.2	1	0.2×0.4	-	19.4×20.4	0.9	13.3×12.1	2.0×0.7	-	0
26	08425	NP	<	4.9×3.9	5.8×5.1	0	-	-	23.6×29.2	0.8	13.9×10.1	-	-	-
27	08427	NP	<<	5.4×6.3	6.6×7.8	0	-	-	18.9×21.7	0.4	21.0×16.3	-	-	-
28	08428	NP	<<	6.0×6.9	9.3×11.6	0	-	-	19.8×22.9	0.5	14.4×14.0	-	-	-
29	08423	P	>	3.3×2.7	5.0×5.0	1	2.9×2.4	-	12.3×14.4	2.1	6.0×6.4	0.9×0.9	-	0
30	08567	NP	<<	3.8×3.8	5.4×5.4	0	-	-	0.0×0.0	0.0	4.1×6.9	-	-	-
31	08568	NP	<<	4.3×5.1	6.2×10.5	0	-	-	15.8×17.8	0.4	14.2×14.3	-	-	-

HITF No.	Result		Front facesheet				Rear facesheet				Core			WP
	Coarse [NP/SP/P]	Detailed [<,≤,=,≥,>]	d <sub>h</sub> (mm)	D <sub>dam</sub> (mm)	N <sub>h</sub> (-)	d <sub>h</sub> (mm)	D <sub>h</sub> (mm)	b <sub>d</sub> (mm)	b <sub>max</sub> (mm)	D <sub>HC</sub> (mm)	Δ <sub>HC</sub> (mm)	N <sub>h</sub> (-)		
32	08569	P	>	6.6×7.5	10.2×8.4	1	1.8×2.2	3.7×4.7	27.4×26.2	3.1	26.8×17.5	12.4×0.0	0	
33	08585	NP	<<	4.5×4.8	5.5×5.7	0	-	-	0.0×0.0	0.0	13.2×10.0	-	-	
34	09072	NP	<	3.1×3.2	4.0×4.3	0	-	-	15.2×14.1	0.3	6.8×9.8	-	-	
35	09357	NP	≤	3.7×3.9	4.6×5.1	0	-	-	36.3×34.8	1.6	nm	-	-	
36	09073	NP	<	4.2×4.4	5.8×6.0	0	-	-	15.6×15.2	0.5	13.5×15.1	-	-	
37	09358	P	≥	4.2×4.5	6.0×5.6	2	< 1.0	< 1.0	57.1×56.5	3.5	nm	nm	nm	
38	09074	NP	<	5.1×5.5	6.0×6.9	0	-	-	9.2×18.7	0.4	13.1×14.6	-	-	
39	09359	P	>	5.2×6.4	7.2×7.7	1	5.5×4.6	7.9×12.9	51.9×55.2	5.5	nm	nm	nm	
40	09075	NP	<	3.9×6.0	5.2×6.8	0	-	-	8.2×12.8	0.06	16.5×8.9	-	-	
41	09360	P	>	5.9×6.9	6.2×8.1	1	< 1.0	2.9×4.1	54.6×43.2	2.6	nm	nm	nm	
42	09362	NP	≤	10.7×10.3	12.8×14.4	0	-	-	62.1×62.1	2.7	nm	-	-	
43	09363	NP	<	7.6×8.8	10.1×10.1	0	-	-	53.6×52.0	1.6	nm	-	-	
44	09364	NP	≤	10.3×9.5	12.3×11.1	0	-	-	61.8×62.5	2.8	nm	-	-	
45	08574	P	≥	4.4×4.4	5.7×5.6	2	< 1.0	6.9×7.3	nm	1.12	14.1×14.6	nm	nm	
46	08575	NP	<	6.8×10.1	8.4×10.8	0	-	-	nm	1.63	42.3×31.1	-	nm	
47	08583	NP	≤	3.1×3.1	4.0×4.1	0	-	-	nm	1.42	8.2×9.45	-	nm	

**Table A-2:** Phase 2 test results.

HITF No.	Result		Front facesheet				Rear facesheet				Core		WP N <sub>h</sub> (-)
	Coarse [NP/SP/P]	Detailed [<,≤,=,≥,>]	d <sub>h</sub> (mm)	D <sub>dam</sub> (mm)	N <sub>h</sub> (-)	d <sub>h</sub> (mm)	D <sub>h</sub> (mm)	b <sub>d</sub> (mm)	b <sub>max</sub> (mm)	D <sub>HC</sub> (mm)	Δ <sub>HC</sub> (mm)		
1	08589	NP	=	1.9×1.9	2.5×2.5	0	-	-	5.3×3.3	< 1.0	1.7×5.2	-	nm
2	08571	NP	<	4.2×3.6	5.5×4.5	0	-	-	15.9×19.2	< 1.0	11.0×8.1	-	nm
3	08572	P	≥	5.6×6.5	6.9×9.4	1	0.4×0.4	0.5×0.5	18.8×24.3	< 1.0	16.8×12.1	nm	nm
4	08580	NP	≤	3.7×6.2	4.8×8.1	0	-	-	18.3×25.2	< 1.0	13.1×12.2	-	nm
5	08581	NP	<	3.0×5.0	3.0×5.0	0	-	-	0.8×0.8	< 1.0	9.3×5.2	-	nm
6	08582	P	≥	3.5×7.2	3.5×7.2	1	0.8×3.9	5.0×7.6	10.5×22.1	1.8	15.3×7.7	1.0×20.9	nm
7	08590	NP	<	4.7×4.9	5.8×6.0	0	-	-	10.6×11.6	1.1	15.2×14.5	-	nm
8	08573	P	≥	12.5×14.5	13.0×17.2	1	1.1×1.1	1.1×1.1	43.0×52.6	2.0	47.7×39.2	49.6×12.4	nm
9	08591	NP	<	15.3×25.6	19.4×26.8	0	-	-	38.8×50.3	1.2	58.1×44.8	-	nm
10	08614	NP	<	19.4×26.6	27.1×28.0	0	-	-	45.1×68.8	2.1	62.4×46.5	-	nm
11	08613	P	>	10.4×18.8	13.9×22.4	1	12.7×14.5	12.7×14.5	nm	7.1	44.5×26.8	81.7×3.1	nm
12	09220	NP	≤	7.6×15.5	8.8×17.1	0	-	-	17.5×17.5	1.9	59.1×28.8	-	nm

**Table A-3:** Phase 3 test results.

HITF No.	Result		Front facesheet				Rear facesheet				Core		WP N <sub>h</sub> (-)
	Coarse [NP/SP/P]	Detailed [<,≤,=,≥,>]	d <sub>h</sub> (mm)	D <sub>dam</sub> (mm)	N <sub>h</sub> (-)	d <sub>h</sub> (mm)	D <sub>h</sub> (mm)	b <sub>d</sub> (mm)	b <sub>max</sub> (mm)	D <sub>HC</sub> (mm)	Δ <sub>HC</sub> (mm)		
1	9374	NP	<	4.9×5.2	7.6×7.4	0	-	-	66.9×56.3	nm	nm	nm	nm
2	9375	P	≥	5.9×4.8	6.9×6.0	1	< 1.0	< 1.0	79.9×71.5	nm	nm	nm	nm
3	9376	P	≥	10.1×13.3	13.3×12.4	2	< 1.0	< 1.0	73.2×73.1	nm	nm	nm	nm
4	9377	P	>	11.2×8.2	8.2×14.6	2	1.6×2.3	2.7×3.7	78.7×73.3	nm	nm	nm	nm
5	9320	P	>	4.9×5.0	5.0×6.1	1	17.8×8.0	19.3×11.2	nm	9.1	21.6×22.8	1.1×1.0	nm
6	9321	P	=	5.2×4.8	4.8×6.4	0	-	-	nm	3.0	20.2×17.6	nm	nm
7	9322	P	≥	5.2×5.3	5.3×6.6	2	< 1.0	7.1×1.6	nm	2.5	22.2×23.5	nm	nm
8	9323	NP	≤	5.2×5.0	5.0×6.7	1	< 1.0	< 1.0	nm	1.9	22.0×20.9	nm	nm
9	9324	P	≥	5.8×5.7	5.7×7.4	2	< 1.0	< 1.0	nm	nm	nm	nm	nm
10	9325	P	≥	5.4×5.2	5.2×7.2	1	< 1.0	< 1.0	40.1×46.3	nm	nm	nm	nm
11	9326	P	≥	nm	nm	nm	nm	nm	nm	nm	nm	nm	nm
12	9327	P	>	nm	nm	nm	nm	nm	nm	nm	nm	nm	nm

**Table A-4:** Phase 4 test results.

HITF No.	Result		Front facesheet				Rear facesheet				Core		WP N <sub>h</sub> (-)
	Coarse [NP/SP/P]	Detailed [<,≤,=,≥,>]	d <sub>h</sub> (mm)	D <sub>dam</sub> (mm)	N <sub>h</sub> (-)	d <sub>h</sub> (mm)	D <sub>h</sub> (mm)	b <sub>d</sub> (mm)	b <sub>max</sub> (mm)	D <sub>HC</sub> (mm)	Δ <sub>HC</sub> (mm)	WP N <sub>h</sub> (-)	
1	8584	NP	<	3.9×4.3	5.7×5.4	0	-	-	nm	0.5	19.6×24.1	-	nm
2	9001	NP	<	7.5×14.0	9.3×15.1	0	-	-	nm	0.7	38.1×32.4	-	nm
3	9002	P	>	3.2×3.2	4.3×4.3	1	2.3×3.3	2.7×3.8	nm	2.9	9.8×12.0	0.0×0.0	nm
4	9003	P	>>	8.7×8.7	10.8×10.8	1	9.7×9.7	12.2×13.4	nm	10.3	59.2×52.3	1.2×0.0	nm
5	9004	P	>>	12.5×18.5	14.5×20.1	3	7.6×11.7	11.3×16.1	nm	27.4	102.1×74.6	nm	nm
6	9005	P	>	7.0×6.8	8.6×7.8	1	4.7×4.2	5.5×5.6	nm	2.2	23.4×22.0	0.0×0.0	nm
7	9006	P	>>	12.5×17.5	16.7×19.2	2	5.4×8.0	8.2×9.9	nm	5.8	62.1×57.2	nm	nm
8	9365	P	≥	6.0×7.8	12.0×15.4	1	1.0×1.3	2.6×3.3	nm	nm	31.1×32.1	0.0×1.8	nm
9	9366	P	>>	6.0×5.9	7.2×7.1	1	3.9×4.1	5.2×18.8	nm	nm	18.3×24.1	2.8×5.1	nm
10	9368	NP	≤	6.7×7.2	8.9×8.8	0	-	-	nm	nm	49.7×49.2	-	nm
11	9371	P	>>	7.1×6.3	8.6×9.9	1	29.8×33.8	58.5×73.3	nm	nm	52.3×49.7	0.0×0.0	nm
12	9465	P	>>	7.0×7.0	8.8×11.6	1	7.5×7.3	20.3×20.5	nm	nm	27.2×31.8	0.0×0.0	nm
13	9466	NP	≤	8.2×8.4	9.9×10.1	1	nm	nm	nm	8.8	34.3×35.2	nm	nm



REPORT DOCUMENTATION PAGE			Form Approved OMB No. 0704-0188
<p>Public reporting burden for this collection of information is estimated to average 1 hour per response, including the time for reviewing instructions, searching existing data sources, gathering and maintaining the data needed, and completing and reviewing the collection of information. Send comments regarding this burden estimate or any other aspect of this collection of information, including suggestions for reducing this burden, to Washington Headquarters Services, Directorate for Information Operations and Reports, 1215 Jefferson Davis Highway, Suite 1204, Arlington, VA 22202-4302, and to the Office of Management and Budget, Paperwork Reduction Project (0704-0188), Washington, DC 20503.</p>			
1. AGENCY USE ONLY (Leave Blank)	2. REPORT DATE November 2015	3. REPORT TYPE AND DATES COVERED Technical Memorandum	
4. TITLE AND SUBTITLE Hypervelocity Impact Testing of Aluminum Foam Core Sandwich Panels		5. FUNDING NUMBERS	
6. AUTHOR(S) Shannon Ryan; Eric L. Christiansen			
7. PERFORMING ORGANIZATION NAME(S) AND ADDRESS(ES) Lyndon B. Johnson Space Center Houston, Texas 77058		8. PERFORMING ORGANIZATION REPORT NUMBERS S-1210	
9. SPONSORING/MONITORING AGENCY NAME(S) AND ADDRESS(ES) National Aeronautics and Space Administration Washington, DC 20546-0001		10. SPONSORING/MONITORING AGENCY REPORT NUMBER TM-2015-218593	
11. SUPPLEMENTARY NOTES			
12a. DISTRIBUTION/AVAILABILITY STATEMENT Unclassified/Unlimited Available from the NASA Center for AeroSpace Information (CASI) 7115 Standard Hanover, MD 21076-1320		12b. DISTRIBUTION CODE Category: 18	
<p><b>13. ABSTRACT (Maximum 200 words)</b>          Spacecraft weight and/or volume restrictions often prevent the inclusion of a dedicated shield for protection against the impact of micrometeoroids and orbital debris (MMOD). In such circumstances, shielding is provided by the vehicle's primary structure – commonly constructed of honeycomb core sandwich panels (HC SPs). Although their high specific strength and stiffness are ideal for structural requirements, the protective capability of HC SPs is rather poor. For the majority of impact conditions relevant to MMOD, pressures generated during impact are sufficient to induce projectile fragmentation. Common MMOD shielding configurations utilize this effect by locating a thin, sacrificial plate (aka bumper plate) ahead of the vehicle pressure hull. Expanding projectile and bumper fragments disperse as they propagate through the shield, spreading the load over an area of the pressure hull significantly larger than that of the original projectile. Metallic foams are a promising new material for spacecraft primary structures as they provide comparative mechanical performance to metallic honeycombs without the presence of channeling cells detrimental to MMOD shielding. The objective of this study was to characterize the shielding performance of sandwich panel structures with open-cell metallic foam cores. The test program was divided into four phases, each with a different objective.       </p>			
14. SUBJECT TERMS micrometeoroids; hypervelocity impact; shielding; protection; honeycomb structures; space debris; spacecraft design		15. NUMBER OF PAGES 96	16. PRICE CODE
17. SECURITY CLASSIFICATION OF REPORT Unclassified	18. SECURITY CLASSIFICATION OF THIS PAGE Unclassified	19. SECURITY CLASSIFICATION OF ABSTRACT Unclassified	20. LIMITATION OF ABSTRACT Unlimited



---